AN INFRARED STUDY OF SMALL MOLECULES IN INERT MATRICES

by

HERBERT F. SHURVELL

B.Sc. Exeter, 1959,
M.Sc. British Columbia, 1962.

A THESIS SUBMITTED IN PARTIAL FULFILMENT OF

THE REQUIREMENTS FOR THE DEGREE OF

DOCTOR OF PHILOSOPHY

in the Department
of
Chemistry

We accept this thesis as conforming to the
required standard

THE UNIVERSITY OF BRITISH COLUMBIA

January, 1964.

In presenting this thesis in partial fulfilment of the requirements for an advanced degree at the University of British Columbia, I agree that the Library shall make it freely available for reference and study. I further agree that permission for extensive copying of this thesis for scholarly purposes may be granted by the Head of my Department or by his representatives. It is understood that copying or publication of this thesis for financial gain shall not be allowed without my written permission.

Department of CHEMISTRY

The University of British Columbia,
Vancouver 8, Canada.

Date March 18, 1964

The University of British Columbia

FACULTY OF GRADUATE STUDIES

PROGRAMME OF THE

FINAL ORAL EXAMINATION

FOR THE DEGREE OF

DOCTOR OF PHILOSOPHY

of

HERBERT FRANCIS SHURVELL

B.Sc., Exeter University, 1959
M.Sc., The University of British Columbia, 1962

FRIDAY, MARCH 13, 1964, AT 2:30 P.M.
IN ROOM 261, CHEMISTRY BUILDING

COMMITTEE IN CHARGE

Chairman: F.H. Soward

W.A. Bryce	E.A. Ogryzlo
F.W. Dalby	C. Reid
K.B. Harvey	R.F. Snider

External Examiner: D.F. Eggers Jr.

University of Washington

AN INFRARED STUDY OF SMALL MOLECULES IN INERT MATRICES

ABSTRACT

Infrared absorption spectra of HCl and HBr, suspended in solid argon, krypton and nitrogen, were recorded in order to obtain information on intermolecular forces. SO_2 in argon and nitrogen, and CO in argon were also studied. The spectra were observed in the temperature range from liquid helium temperatures up to the melting point of the matrix.

The halogen acids gave more complicated spectra in the noble gas matrices than in nitrogen. This has been correlated with the different thermal properties of the matrix materials. Matrix to solute ratios from 100 to 800 to 1 were used and evidence was found for solute-solute interactions. arising from incomplete isolation of solute molecules at the lower ratios. During the warm-up period at the end of an experiment, additional peaks appeared in the spectra. It is suggested that these new peaks were due to clusters of solute molecules produced by diffusion of the solute through the lattice.

Semi-empirical calculations were carried out to estimate shifts of vibrational frequencies of the trapped molecules. From these calculations it was concluded that repulsive intermolecular forces play an important part in determining the magnitude and direction of the shifts. A first order perturbation calculation was made, using a Lennard-Jones' potential, to determine the effect of the matrix on the rotational energy levels of a trapped molecule.

Spectra of the clathrate-hydrates of SO_2, H_2S and krypton were recorded at liquid nitrogen temperatures, and the SO_2 hydrate was studied in the temperature range from 4° to 120° K. The spectrum of the water skeletal vibrations exhibited several interesting features. The assignment of the 1600 cm^{-1} and 2200 cm^{-1} peaks to ν_2 and $\nu_2 + \nu_R$ was confirmed and a new peak at 2410 cm^{-1} was observed. A lattice mode in the spectrum of the SO_2 hydrate was observed in combination with ν_3 of SO_2.

GRADUATE STUDIES

Field of Study: Chemistry

Topics in Physical Chemistry	J.A.R. Coope R.F. Snider
Seminar in Physical Chemistry	J.N. Butler
Quantum Chemistry	J.A.R. Coope
Chemical Thermodynamics	J.N. Butler
Spectroscopy and Molecular Structure	C. Reid A.N. Bree L.W. Reeves K.B. Harvey

Related Topics

Differential Equations	S.A. Jennings
Computer Programming	Charlotte Froese
Group Theoretical Methods	W. Opechowski
Elementary Quantum Mechanics	W. Opechowski

Unrelated Topics

Topics in Inorganic Chemistry	N. Bartlett W.R. Cullen
Topics in Organic Chemistry	R. Stewart J.P. Kutney

PUBLICATIONS

The infrared absorption of some crystalline inorganic formates.
K.B. Harvey, B.A. Morrow and H.F. Shurvell, Can.J. Chem. 41, 1181 (1963)

Statistical probabilities of some arrangements of solute molecules on substitutional sites.
K.B. Harvey, J.R. Henderson and H.F. Shurvell, Can. J.Chem. 42, (in press)

Infrared absorption of the SO_2 clathrate-hydrate. motion of the SO_2 molecule.
K.B. Harvey, F.R. McCourt and H.F. Shurvell, Can.J. Chem. 42, (in press)

A B S T R A C T

Infrared absorption spectra of HCl and HBr, suspended in solid argon, krypton and nitrogen, were recorded in order to obtain information on intermolecular forces. SO_2 in argon and nitrogen, and CO in argon were also studied. The spectra were observed in the temperature range from liquid helium temperature up to the melting point of the matrix.

The halogen acids gave more complicated spectra in the noble gas matrices than in nitrogen. This has been correlated with the different thermal properties of the matrix materials. Matrix to solute ratios from 100 to 800 to 1 were used and evidence was found for solute-solute interactions arising from incomplete isolation of solute molecules at the lower ratios. During the warm-up period at the end of an experiment, additional peaks appeared in the spectra. It is suggested that these new peaks were due to clusters of solute molecules, produced by diffusion of the solute through the lattice.

Semi-empirical calculations were carried out to estimate shifts of vibrational frequencies of the trapped molecules. From these calculations it was concluded that repulsive intermolecular forces play an important part in determining the magnitude and direction of the shifts. A first order perturbation calculation was made, using a Lennard-Jones' potential, to determine the effect of the matrix on the rotational energy levels of a trapped molecule.

Spectra of the clathrate-hydrates of SO_2, H_2S and krypton were recorded at liquid nitrogen temperatures, and the SO_2 hydrate was studied in the temperature range from 4° to $120^{\circ}K$. The spectrum of the water skeletal vibrations exhibited several interesting features. The assignment of the 1600 cm^{-1} and 2200 cm^{-1} peaks to ν_2 and $\nu_2 + \nu_R$ was confirmed and a new peak at 2410 cm^{-1} was observed. A lattice mode in the spectrum of the SO_2 hydrate was observed in combination with ν_3 of SO_2.

K.B. Harvey

ACKNOWLEDGMENT.

I would like to express my gratitude to Dr. K. B. Harvey for his help and guidance during the course of this work. Many helpful discussions with Dr. R. F. Snider are also appreciated, and thanks are due to Mr. R. Muehlchen for assistance with the construction and maintenance of the apparatus.

Financial assistance from the Shell Oil Company and the National Research Council of Canada is gratefully acknowledged.

TABLE OF CONTENTS.

LIST OF TABLES.

LIST OF FIGURES.

CHAPTER 1. INTRODUCTION.

1-1 Preliminary Remarks.

The bulk of the work for this thesis was carried out on small molecules in inert matrices. The emphasis throughout has been on the effects of environment on the infrared spectra, which naturally leads to a discussion of intermolecular forces. In this light the work on gas-hydrates becomes directly related to the matrix work, since we are effectively studying small molecules in a water "matrix".

The spectroscopic studies of small molecules in high pressure gas, liquid, solution and solid states, which are reviewed in section 1-4, correlate with the present matrix and gas hydrate work, since in these environments intermolecular forces determine the shapes, widths, shifts and splitting of infrared bands. The present work attempts to extend this information and apply it to the interpretation of spectra of molecules in matrix and gas hydrate environments.

1-2 Studies of Molecular Interactions by the Matrix Isolation Method.

The matrix isolation technique in conjunction with infrared spectroscopy, offers a unique approach to the problem of interactions between molecules. The technique consists of dispersing the substance (solute) of interest in an inert frozen matrix at a temperature low enough to permit separation and isolation of single solute molecules. This is usually achieved by condensing gas mixtures on a plate cooled by liquid hydrogen, or liquid helium, as in the present work. Materials most commonly used for matrices are nitrogen and the rare gases.

Under conditions of perfect isolation, the molecule under examination is subject only to solute-matrix interactions. Such ideal conditions occur, with proper deposition conditions, at very high matrix to solute ratios. Interactions between solute molecules become important at low matrix to solute ratios, and the method can be employed to study intermolecular forces which manifest themselves in changes in the infrared spectrum of the isolated molecule.

The matrix isolation method, initially employed for trapping and retention of very reactive species such as free radicals, has been widely used in recent years for the study of small molecules in a matrix environment. For example, Pimentel et al (1,2,3) have recorded spectra of several small molecules in solid nitrogen at 20^{o}K, and Milligan and co-workers (4,5,6) have carried out many investigations with small molecules using matrix isolation methods.

Of particular interest is the work carried out on water by these two groups, both of which reported complex spectra in the regions of the three fundamentals of the water molecule. Pimentel (2) interpreted the spectra in terms of isolated monomers, hydrogen-bonded dimers and higher polymers. Milligan and his co-workers (4,5) put forward evidence for free rotation of the trapped molecules in the solid matrix; the latter view was supported by Glasel (7) on the basis of results from similar work. A disagreement in interpretation of results from matrix-isolation studies of ammonia, between Pimentel et al and Milligan et al, is found in references (3) and (6).

Previous matrix studies on HBr and HCl were carried out by Becker and Pimentel (1) who recorded survey spectra under low

resolution of HBr and HCl in solid nitrogen as a test of the matrix isolation technique. Since this work was started, a note by Schoen et al (8) has been published, reporting the rotation-vibration spectrum of matrix-isolated hydrogen chloride. These workers used high matrix to solute ratios and observed a simple spectrum, which they interpreted using a hindered rotator model.

Maki (9) reported infrared spectra of CO as a solid and in solid matrices. The spectra observed were complicated only by weak shoulders and peaks due to isotopic CO molecules.

Recent work in this laboratory (10) indicated that straightforward explanations based on molecular association or free rotation, were inadequate and that a more detailed study of intermolecular forces should be considered in the interpretation of results obtained at low matrix to solute ratios. With this in mind, and in view of the relatively small attention which has been given to matrix isolation studies of the simple molecules HCl, HBr and CO, a detailed investigation on these molecules was undertaken. It was hoped that such a study would provide information which could be applied to the interpretation of results obtained from more complex systems.

Infrared spectra of HCl, HBr and CO in nitrogen and argon matrices were recorded at various matrix-to-solute ratios. Change in environment was also studied during warming of the deposit from 4°K up to the melting point of the matrix. By addition of other solute impurities to the gas mixtures, it was hoped to demonstrate the extent of solute-solute interactions, and thus simplify the interpretation of the matrix-solute spectra.

Several theoretical treatments (11-14) have been carried out

on molecular rotation in solids and solid matrices, using various hindered rotator models. These calculations predict shifts of band centres and splitting of degenerate rotational levels. Calculations of shifts of vibrational fundamentals due to solute-matrix interactions have been made with some success. One of the earliest calculations due to Kirkwood, Bauer and Magat (15,16) was based on a simple dielectric theory. This approach was used more recently by Pullin (17), who developed an improved theory. Buckingham (18), in a quantum mechanical calculation, derived a useful formula which has been tested successfully by Maki (9) and Ewing and Pimentel (19). A third approach, based on classical electrostatic forces, was used by Linevsky (20) in his matrix work on lithium fluoride.

In Chapter 4 of this thesis, calculations of hindered rotator energy levels for the hydrogen halides, using a Lennard-Jones' (6-12) potential are carried out. In addition, intermolecular forces between solute molecules in nearest neighbour, next-nearest neighbour, etc., positions are considered and the corresponding vibrational shifts calculated.

1-3 Molecular Interactions in the Gas Hydrates.

Directly related to the matrix isolation studies from the point of view of molecular interactions is the present work on the infrared spectra of gas hydrates. The gas hydrates are interesting compounds because of their unusual clathrate, or cage structure. Von Stackelberg (21) is responsible for much of our present knowledge of the structure and properties of the gas hydrates. The compounds studied in the present work all belong to the $M \cdot 6H_2O$ class with the

structure designated as Type I by Von Stackelberg.

A preliminary infrared study on SO_2, argon and krypton hydrates, was made in this laboratory by McCourt (22). Shifts in frequency of certain peaks in the skeletal water spectrum and the appearance of a new peak, not present in the spectrum of ice, were the main features observed in this work. It was felt that a more detailed study might reveal information on intermolecular interactions and molecular motion in the cage.

A comprehensive study of SO_2-hydrates, using both normal and heavy water was undertaken at liquid nitrogen temperatures. Spectra of krypton and H_2S hydrates were also recorded. The skeletal water vibrations and the vibrations of the enclathrated molecules were examined under high resolution, using the Perkin Elmer 421 spectrometer. In one series of experiments with the SO_2- hydrate, the region of SO_2 was studied under high resolution at various temperatures from 4° up to 120°K using the Perkin Elmer 112G spectrometer.

1-4 A Summary of Related Work on the Hydrogen Halides and Carbon Monoxide.

Intermolecular forces, as manifested in infrared spectra of the hydrogen halides and Carbon monoxide, in gas, liquid and solid phases, have been the subject of a great deal of work in recent years. The appearance of a Q-branch produced by high pressures of foreign gas in the 1-0 bands of HCl and HBr has been observed by Vodar and his co-workers (23). Similar studies were made by Rank et al (24), who suggested that the formation of a molecular complex between the hydrogen halide and the rare-gas atoms used as pressurizing

agents occurred. Pressure-induced shifts of HCl caused by noble gases have been measured by Ben-Reuven et al (25) and a theory developed which accounts for the main features of the observed shifts.

Among the earliest workers in the field, West and Edwards (15) examined the spectra of HCl in solutions of various solvents, and interpreted their results using the Kirkwood-Bauer-Magat formula (16). Recently, Kwok and Robinson (26) studied HCl in liquid Xenon and observed a broad band with two shoulders in the region of the fundamental. They attribute their results to unresolved P and R branches combined with solvent-induced O, Q and S branches. The infrared spectra of HCl and HBr in solution in various inert solvents have been recorded by Lascomb et al (27) who report gas to solution shifts varying from -40 to -142 cm^{-1}, depending on the polarity of the solvent. In similar studies, other workers (28,29) conclude from the shapes of the absorption bands that there is some degree of rotation of solute molecules.

A very recent study of the overtone bands of pure solid CO and its solution in nitrogen and argon in the gaseous liquid and solid states has been made by Vu, Atwood and Vodar (30). These workers concluded that the anharmonicity constant was virtually unchanged in the liquid and solid states, compared with the gaseous state, and the observed small band shift was due only to the change of vibration frequency. In similar experiments on HCl and HBr (31) the same workers found that the anharmonicity constant for these molecules decreases considerably in the solid state. The spectrum of solid CO has also been reported by Ewing and Pimentel (19).

Straightforward assignments of peaks to the fundamentals of various isotopic CO molecules were made, and a broad feature +70 cm^{-1} from the main peak was assigned to combinations of the vibrational mode with both rotational and translational lattice modes.

Solid HCl and HBr at low temperatures have been studied by Hornig and Osberg (32). In the region of the fundamental, sharp doublets were observed with splittings of 42 cm^{-1} for HCl and 34 cm^{-1} for HBr. The gas to solid shifts were large, -161 cm^{-1} for HCl and -137 cm^{-1} for HBr, and it was concluded that these molecules form hydrogen-bonded chains in their low temperature crystalline phases. In a latter paper, Hornig and Hiebert (33) reported the spectra of mixed HCl-DCl and HBr-DBr crystals over the entire composition range. At low concentrations of DCl in HCl a single peak due to isolated DCl molecules was found. More complex spectra observed for higher DCl concentrations were attributed to superposition of peaks arising from hydrogen-bonded chains of varying length.

CHAPTER 2. EXPERIMENTAL.

2-1 Experimental Methods.

The matrix isolation technique has been described by Pimentel et al (1,34), by several authors in the book edited by Bass and Broida (35), and was outlined in section 1-1 of this thesis.

In the present matrix work, a gaseous mixture of a hydrogen halide or carbon monoxide with argon or nitrogen, was prepared in a 4 litre storage bulb several days before an experiment. A convection current in the gaseous mixture was produced by heating the bottom of the storage bulb. This ensured thorough mixing of the gases prior to deposition.

A schematic diagram of the apparatus is given in Fig. 1 and a diagram of the low temperature cell, in Fig. 2. During a run, the mixture was passed through a deposition tube into the low temperature cell where the gas stream was allowed to impinge on a caesium iodide plate cooled by liquid helium. A needle valve was used to control the deposition rate which was indicated by the pressure reading of a thermocouple gauge. Deposition was continued until a film of condensed material suitable for infrared study had been produced. This often required deposition times of several hours since the mixture must be deposited slowly to prevent temperature rise of the deposit, with subsequent diffusion of the trapped species.

High matrix to solute ratios ($\sim$ 500 : 1) were used to study isolated molecules, whereas low ratios ($\sim$ 100 : 1) were employed when it was desired to observe the effects of molecular interactions on the infrared spectra. In some experiments, conditions such as

fig 1. THE APPARATUS
vacuum system and low temperature cell.

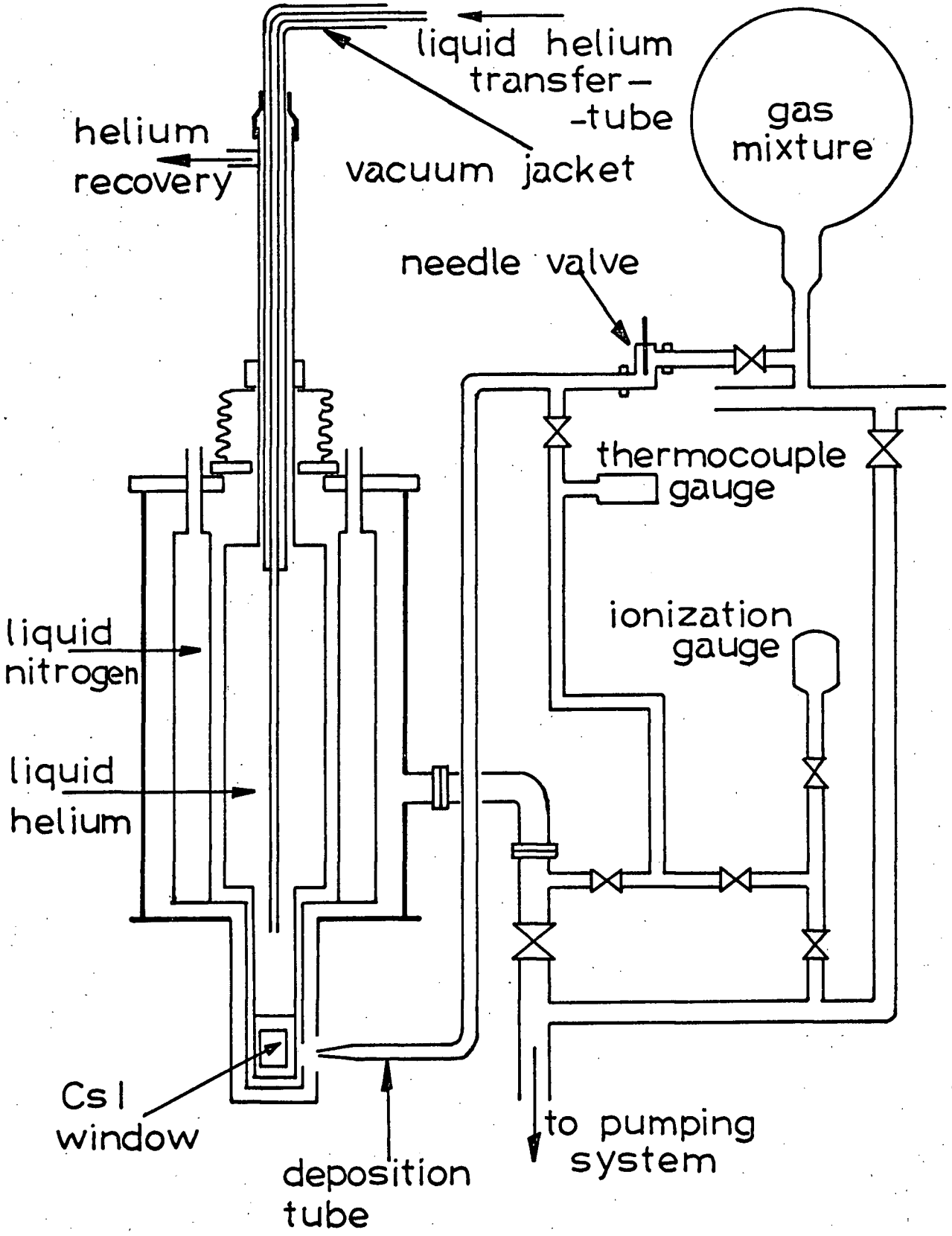

fig 2. THE LOW TEMPERATURE CELL

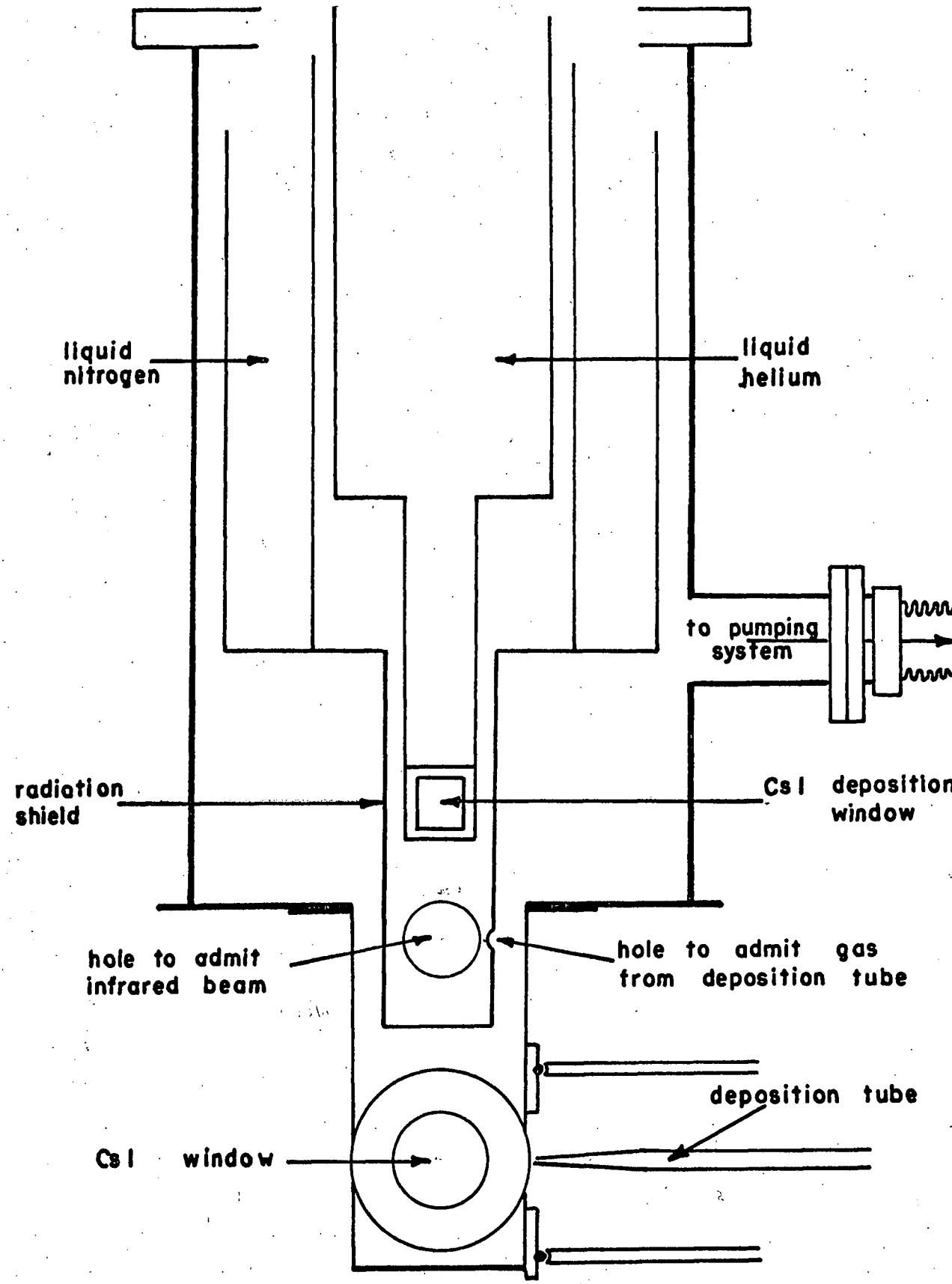

rapid deposition, or formation of the deposit at temperatures well above liquid helium temperatures, were utilized to ensure that diffusion occurred during deposition. In addition, several experiments were carried out in which a third polar molecule, SO_2 or CO was added to the gas mixture.

The gas hydrate studies were made mostly at liquid nitrogen temperatures in a low temperature cell (Fig.4). A few experiments were carried out at liquid helium temperatures using the same apparatus used for the matrix isolation work. Mixtures of water vapour and the hydrate former were prepared by a procedure similar to that used in the matrix work, and deposited on a caesium iodide plate cooled by liquid nitrogen. Short deposition times, of the order of seconds, were necessary because ice absorbs strongly in the infrared, and very thin films were essential to produce satisfactory spectra.

When it was desired to examine the skeletal water vibrations, a mixture was prepared containing a slight excess over the stoichiometric ratio of the hydrate former. This ensured that all the water was tied up as hydrate. Conversely, when the vibrations of the enclathrated molecule were studied, a slight excess of water was used to eliminate the formation of solid hydrate former.

2-2 Details of the Low Temperature Cells.

The cell used for the matrix isolation studies is of the Duerig-Mador (36) type and is illustrated in Fig.2. It consists essentially of a central liquid helium container surrounded by a radiation shield and an outer vessel equipped with optical windows

of caesium iodide. The cell is connected to a vacuum system of the conventional type.

The liquid helium container is made of copper and is suspended by a stainless steel neck to minimize heat inflow by conduction, which would accelerate the evaporation of liquid helium. To improve the efficiency of the radiation shield, it is usually filled with a liquid refrigerant such as liquid nitrogen. A copper block at the bottom of the helium container holds a caesium iodide plate on which the deposit forms. After several unsuccessful runs during the early part of the present work, the window holder was modified to improve thermal contact between the window and the copper block. A larger block was machined (see Fig. 3) with a recess to support the caesium iodide plate which is tightly held against the block by means of a copper gasket secured with four copper screws. All space between the edges of the window, the gasket and the copper block is filled with silver conductive paint.

The cold junction of a gold-silver/gold-cobalt thermocouple is attached to the copper block and the "hot" junction is maintained at liquid nitrogen temperature. The E.M.F. from this thermocouple is amplified and recorded as a trace on the same chart paper as the spectrum, thus giving a record of the temperature at which the spectrum was observed. No attempt was made to calibrate the thermocouple at points between 4° and 77°K; intermediate temperatures were estimated by linear interpolation.

The liquid helium container with the attached window holder may be turned through 90° so that the caesium iodide plate can face either the deposition tube or the windows of the outer vessel.

fig 3.

DETAIL OF WINDOW HOLDER IN THE LIQUID HELIUM CELL

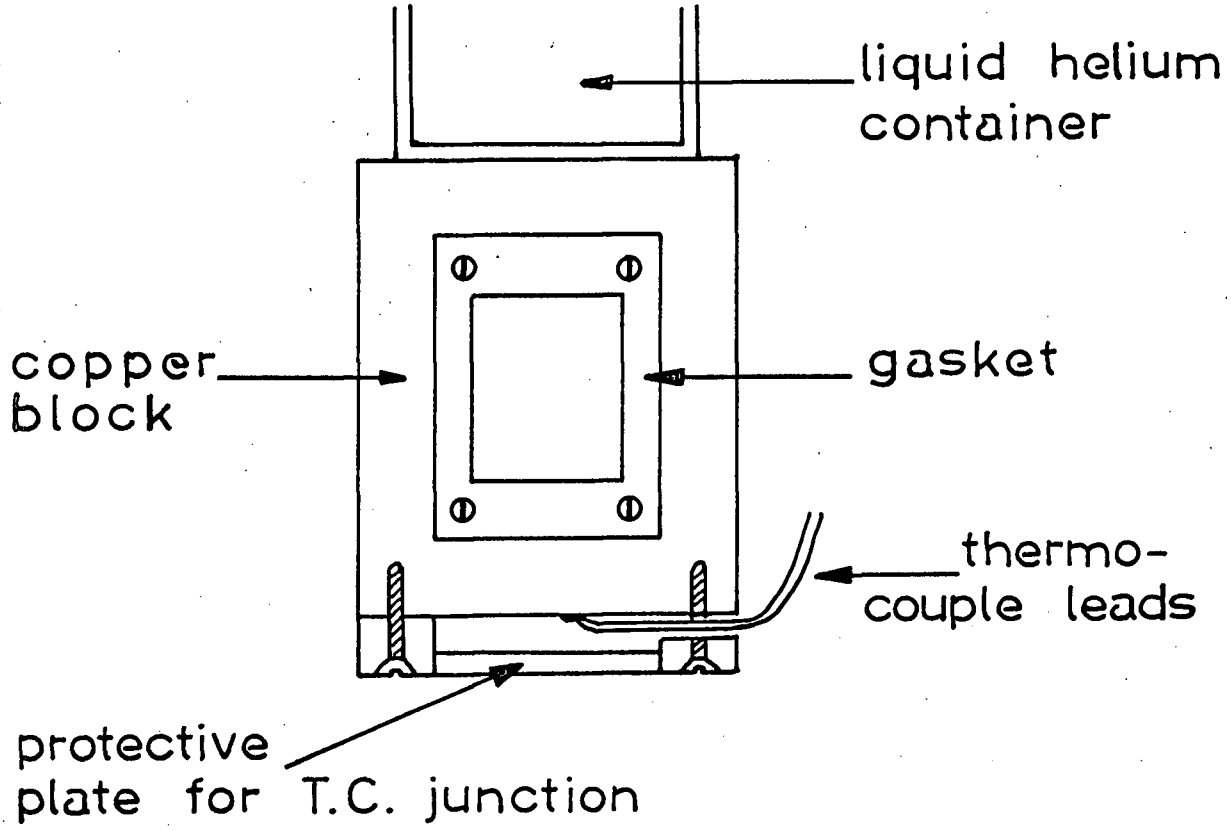

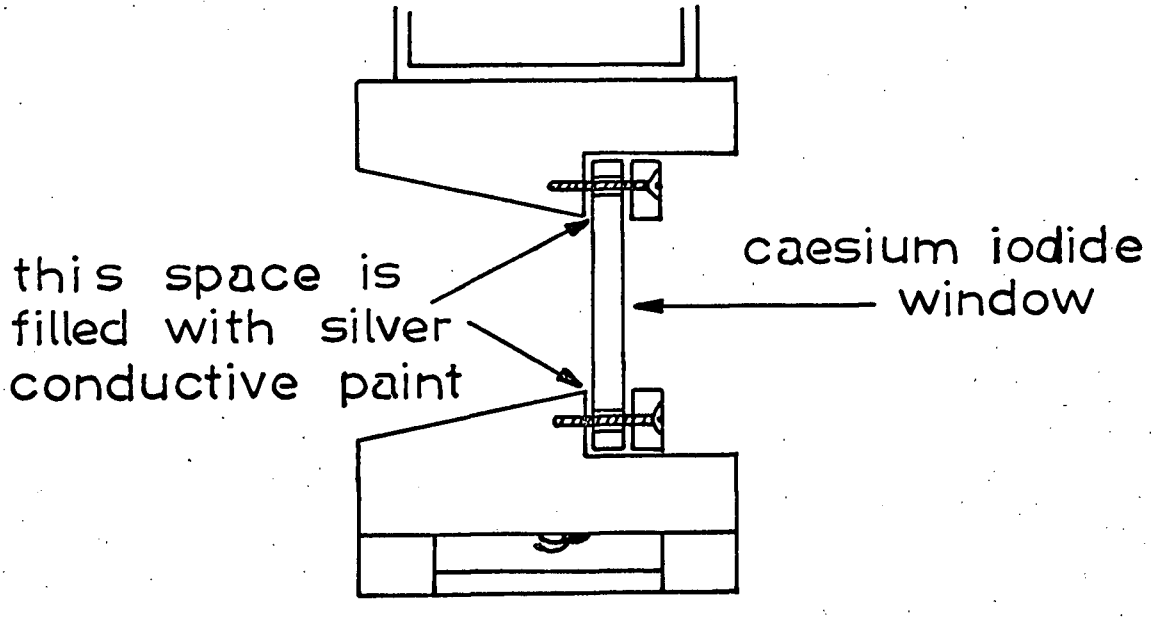

fig 4.

CELL FOR STUDIES AT LIQUID NITROGEN TEMPERATURES

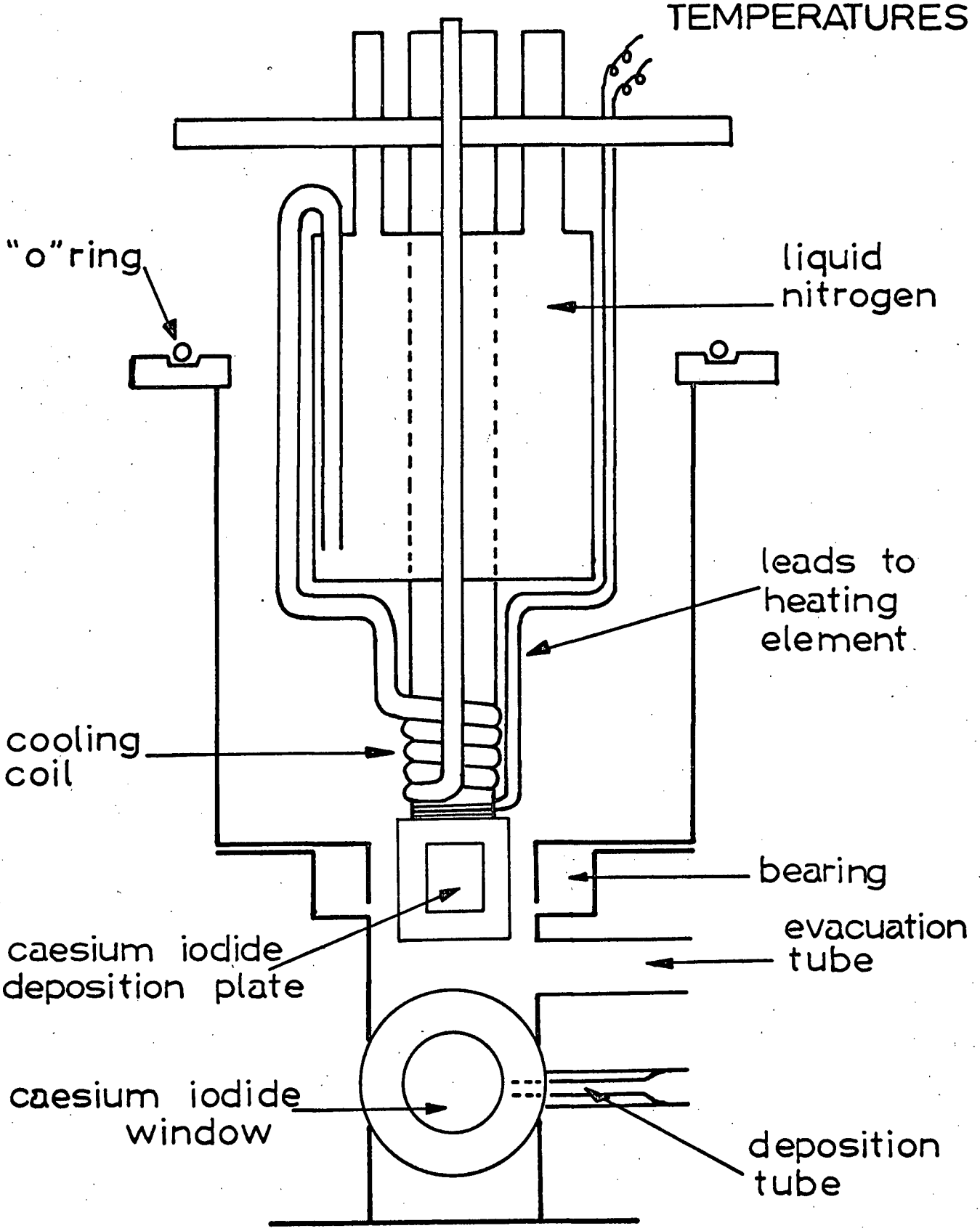

The cell used for the gas-hydrate work is shown in Fig.4. This cell retains the salient characteristics of the Duerig-Mador cell just described but is smaller and has no radiation shield. Other notable features are the heating and cooling devices by means of which the temperature may be varied from 77°K to well above room temperature, as required. The heating is effected by passing a controlled electric current through a coil of pyrotenax wire. The cooling is regulated by a flow of cold nitrogen gas or liquid nitrogen through a coiled copper tube. Both heating and cooling coils are wound close to the window holder. It has been found expedient when working at 77°K to keep the central tube filled with liquid nitrogen in addition to circulating liquid nitrogen through the cooling coil.

There is also a difference in the device for rotating the window through 90°. In the liquid helium cell, only the innermost container is rotated, by means of a bearing located at the neck of the container. In the liquid nitrogen cell, both the outer vessel and the liquid nitrogen container move through 90° on a bearing situated at the base of the outer vessel.

The cold junction of a copper-constantan thermocouple is attached to the bottom of the window holder and the hot junction is maintained at room temperature. The thermocouple E.M.F. is observed by means of a Leeds and Northrup millivolt potentiometer and the corresponding temperature obtained from tables.

2-3 Diffusion in Solid Matrices.

In the present study, some early matrix experiments and some

later runs in which the deposit was rapidly formed, gave results which indicated that diffusion of the trapped species had occurred during deposition. The problem of diffusion in solid matrices has been discussed by Pimentel in Chapter 4 of reference (35). It was found that small molecules diffuse rapidly at 0.4 - 0.6 of the melting point of the matrix. During deposition the film temperature may rise well above that of the cold plate if the deposition rate is rapid. This effect is serious because of the poor thermal conductivity of most of the common matrix materials. For example, during the deposition of nitrogen at 4°K, Fontana (37) observed a temperature rise of approximately 10°K at a deposition rate of 30 cc/min. (S.T.P.) The deposition rate in this work during a typical two hour run was 12.5 cc/min., so one might expect a maximum temperature rise of 4°K. Such a rise would bring the temperature of the film up to 0.14 and 0.11 of the melting point of argon and nitrogen respectively, which should be well below the temperature at which rapid diffusion sets in.

There is another factor which must be considered in addition to the temperature rise of the solid matrix film. It is possible that in certain cases thermal contact deteriorates between the caesium iodide window and the window holder, resulting in warming of the window and consequently also of the deposit. Evidence for this was obtained in early experiments before the new window holder was designed. In these experiments, either no isolation of the solute molecule was achieved, or peaks were observed which were not normally present at 4°K, but which had been observed at higher temperatures during warm-up studies. However, with the modified

cell and using slow deposition rates, reasonable isolation was always achieved.

2-4 Materials.

Regular grade argon and prepurified nitrogen for matrix work were obtained from Matheson Co. Inc. Anhydrous SO_2, HBr and HCl, purified H_2S and C.P. grade CO were also obtained from the Matheson Company. High purity Krypton was supplied by Air Reduction Corporation. D_2O of 99.8% purity, supplied by General Dynamics Corporation, Liquid Carbonic Division, and double distilled water were used in the gas hydrate work. The rare gases and nitrogen were used without further purification. All other materials were treated by freezing and pumping on the solid to remove traces of non-condensable gas. Mass spectroscopic analyses of argon, krypton and nitrogen indicated an upper limit of impurity for argon and nitrogen of 5-10 parts per million, and 50-60 p.p.m. for krypton. Minimum purities stated by the manufacturer for the other gases were as follows: SO_2 - 99.98%; HBr - 99.8%; HCl - 99.0%; H_2S - 99.5%; and CO - 99.5%.

2-5 The Spectrometers.

The Perkin Elmer 112G Spectrometer is a high resolution single beam, double pass instrument. The main features are: a 60° Potassium bromide fore-prism, which acts as a filter to eliminate the energy of unwanted orders, and a 75 lines per millimeter echelette grating, blazed for maximum intensity at 12 μ (850 cm^{-1}) in the first order. The instrument was calibrated using the accurately known lines of the vibration-rotation spectra of HCl (38), HBr (39), CO (40), and

other molecules (41).

The optical path length in the 112 G instrument is about 5 metres and atmospheric water and CO_2 show strong absorption in the neighbourhood of 4μ and 6μ . This interferes seriously with spectra recorded in these regions and it is very desirable to remove these vapours by passing a current of dry nitrogen gas through the instrument housing for some time before a spectrum is recorded.

The Perkin Elmer 421 spectrometer is a double beam instrument capable of high resolution. The dispersion unit comprises two gratings, each used in the first order only. Interference filters are used to reject unwanted orders of radiation diffracted by each grating; these replace the customary fore-prism. The standard instrument operates in the range 4000 - 650 cm^{-1}, but a grating interchange is available which extends the accessible long wavelength region out to 300 cm^{-1}.

In an infrared spectrometer, the resolution obtained under given conditions depends on the frequency interval passed by the exit slit. For a particular frequency ν_o this interval may be expressed as:

$$\nu_o \pm \Delta \nu_s$$

where: $\Delta \nu_s$ is the spectral slit width.

The spectral slit width, which depends on the mechanical slit width and on the optical design of the instrument is approximately equal to the separation of two lines which are just resolved. Using formulae given by Siegler (42) for the model 112-G spectrometer, and tables given by Roche (43) for the model 421 spectrometer, spectral slit widths have been estimated for the instrument settings

used in the present work and have been included on the spectra reproduced in Chapter 3.

CHAPTER 3 RESULTS.

3-1 Infrared Spectra of HCl in Solid Argon.

Gas mixtures containing one part of HCl to 100, 200, 500 and 800 parts of argon were deposited at 4°K. The spectra obtained from these deposits are shown in Fig. 5 and the frequencies and relative intensities of the observed peaks are tabulated in Table I. The spectrum of HCl in argon at high matrix to solute ratios consists of a strong peak at 2889 cm^{-1}, a peak of medium intensity at 2853 cm^{-1}, and a weak shoulder at 2900 cm^{-1}. These peaks correspond to those reported by Schoen et al (8). However, several additional features are observed at all matrix ratios used in this work, and at low ratios certain of these new peaks are more important than the trio mentioned above. An interesting feature of this dilution study is the change in relative intensity of the peaks in the spectrum as the matrix to HCl ratio increases from 100:1 to 800:1.

In Fig. 6 a warm-up study is depicted for an argon to HCl ratio of 500:1. Some of the new peaks which appear in the spectrum as the temperature rises correspond to certain peaks previously observed in experiments conducted at low matrix to HCl ratios. Furthermore, the peaks which appear during warm-up do not disappear or decrease in intensity on recooling the deposit to 4°K. During warm-up studies it was found necessary to increase the monochromator slit widths as the temperature rose because light scattering by the deposit increased considerably. This may indicate the formation of microcrystals of the solute.

TABLE 1.

Infrared absorption of HCl in argon at 4°K. Line intensities (log I_o/I) relative to the peak at 2889 cm^{-1}.

Frequency cm^{-1}	Argon to HCl ratio 100:1	200:1	500:1	800:1
2787.5	1.11	.16	-	-
2817	1.59	.82	.07	.15
2853	.40	.37	.22	.29
2863	-	.13	.05	.10
2867.5	.33	.13	.05	.05
2889	1.00	1.00	1.00	1.00
2900	sh	sh	.07	-

sh = shoulder

To illustrate the effect of solute-solute intermolecular interactions on the spectrum of HCl in argon, mixtures containing CO or SO_2 with HCl and argon were prepared. The spectra obtained from deposits of these mixtures are shown in Fig. 7. For the HCl/CO/argon mixture, the intensities of the peaks were changed relative to the HCl/argon case, but the main features of the spectrum were unaltered. When SO_2 was added to the HCl/argon mixture several new features were observed in the HCl spectrum. Three new peaks were found: a very strong peak at 2808 cm^{-1}, a shoulder at 2821 cm^{-1} and a weak peak at 2829 cm^{-1}.

3-2 Infrared Spectra of HCl in Solid Nitrogen and Krypton.

At 4°K the spectrum of HCl in a nitrogen matrix consists of one strong peak with two very weak satellites (see Fig.8). During the warm-up, however, many changes occur in the spectrum. (See Fig. 9). Several peaks appear and disappear before the solid nitrogen sublimes away from the window leaving solid HCl. Figure 10 shows the spectrum of solid HCl deposited at 4°K and warmed slowly to 55 K. Comparison of Figures 9 and 10 indicates that the final form of the spectrum of HCl in nitrogen is indeed identical with that of solid HCl at the same temperature. The observed frequencies for HCl in nitrogen are compared with the spectra of HCl in argon and krypton in Table 2.

Solid HCl deposited at 4°K gives a broad band centred at 2762 cm^{-1}, but as the temperature rises this band resolves into three peaks at 2712, 2753 and 2780 cm^{-1}. The changes in relative intensity of the peaks in the spectrum of solid HCl are shown in Fig.10.

TABLE 2.

Infrared Absorption of HCl in Argon, Krypton and Nitrogen at 4°K. (Frequencies in cm^{-1}).

Argon 500:1	Krypton 300:1	Nitrogen 200:1	HCl gas
2787.5 (m)	-	-	-
2817 (s)	2800 (s)	-	-
2853 (m)	2838 (m)	2814 (vw)	2864 P(1)
2863 (w)	-	-	-
2867.5 (w)	2854 (w)	2842 (vw)	-
2889 (vs)	2874 (vs)	2852 (vs)	2905 R(0)
2900 sh	-	2875 (vw)	2925 R(1)

In this and subsequent tables the following abreviations for intensities are used: vs = very strong, s = strong, m = medium, w = weak, vw = very weak, and sh = shoulder.

fig 5.

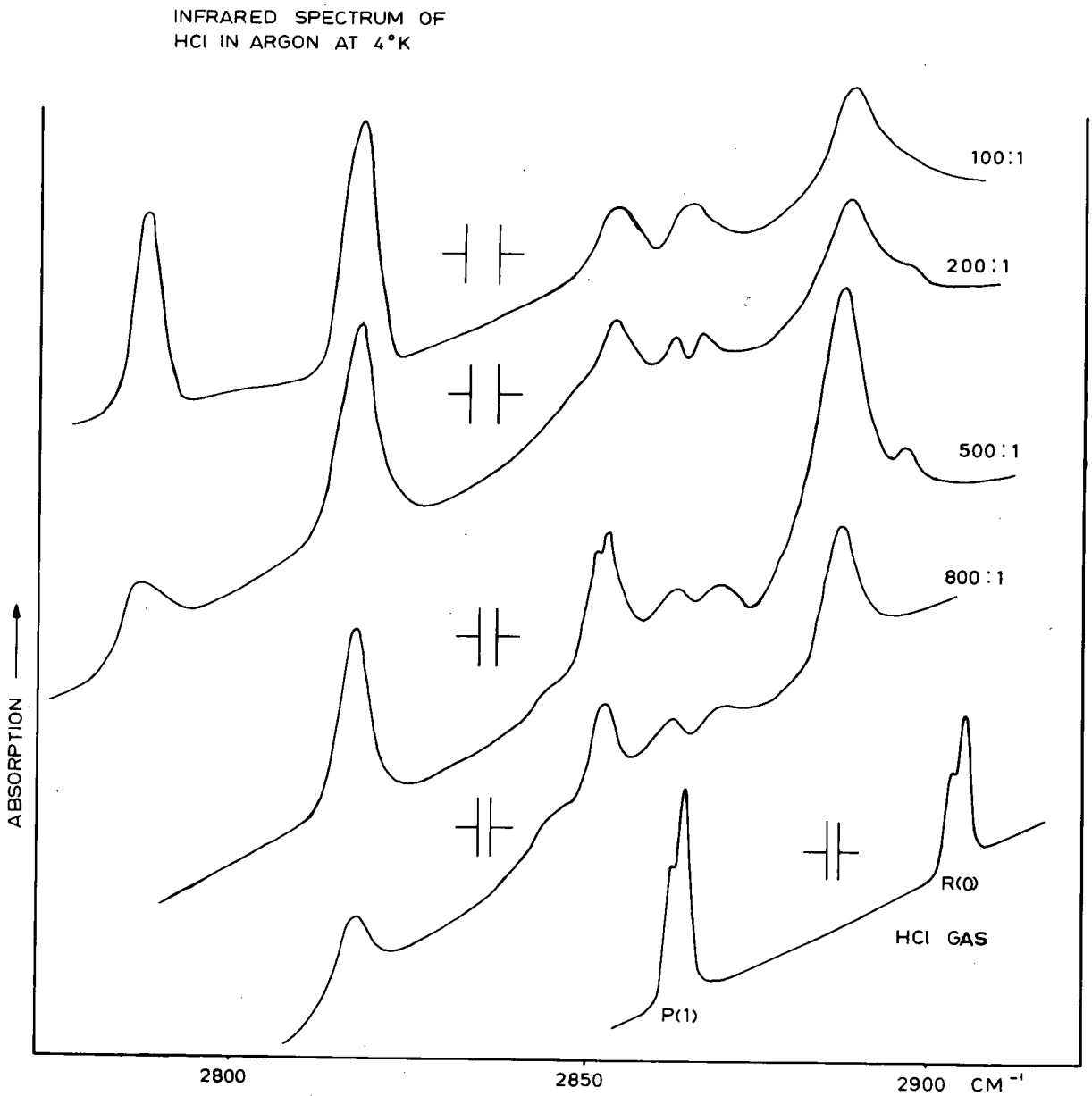
INFRARED SPECTRUM OF
HCl IN ARGON AT 4°K
100:1
200:1
500:1
800:1
ABSORPTION
R(0)
HCl GAS
P(1)
2800
2850
2900 CM⁻¹

fig 6.

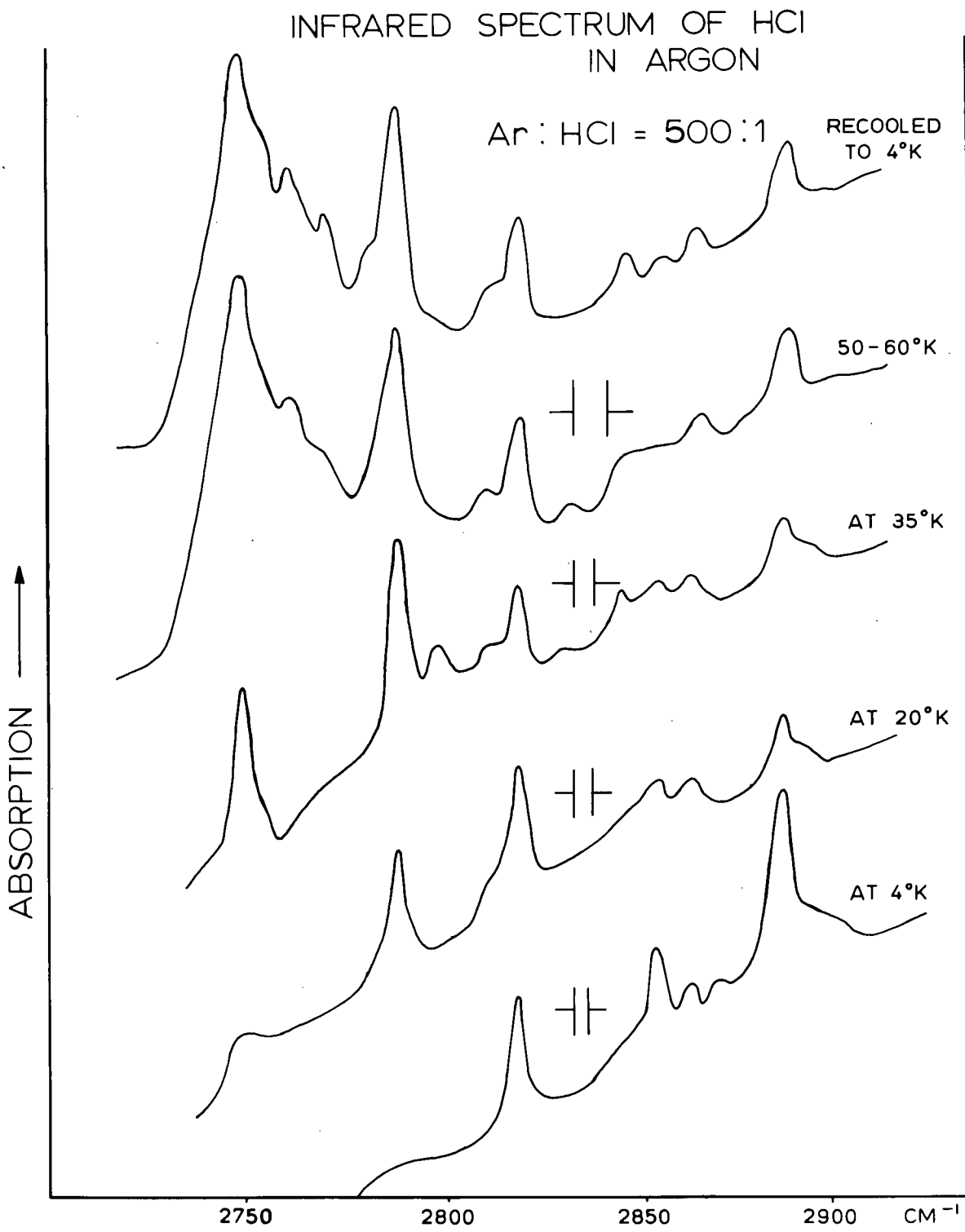
INFRARED SPECTRUM OF HCl
IN ARGON
Ar : HCl = 500 : 1
RECOOLED
TO 4°K
50-60°K
AT 35°K
AT 20°K
AT 4°K
ABSORPTION
2750
2800
2850
2900
CM⁻¹

fig 7.

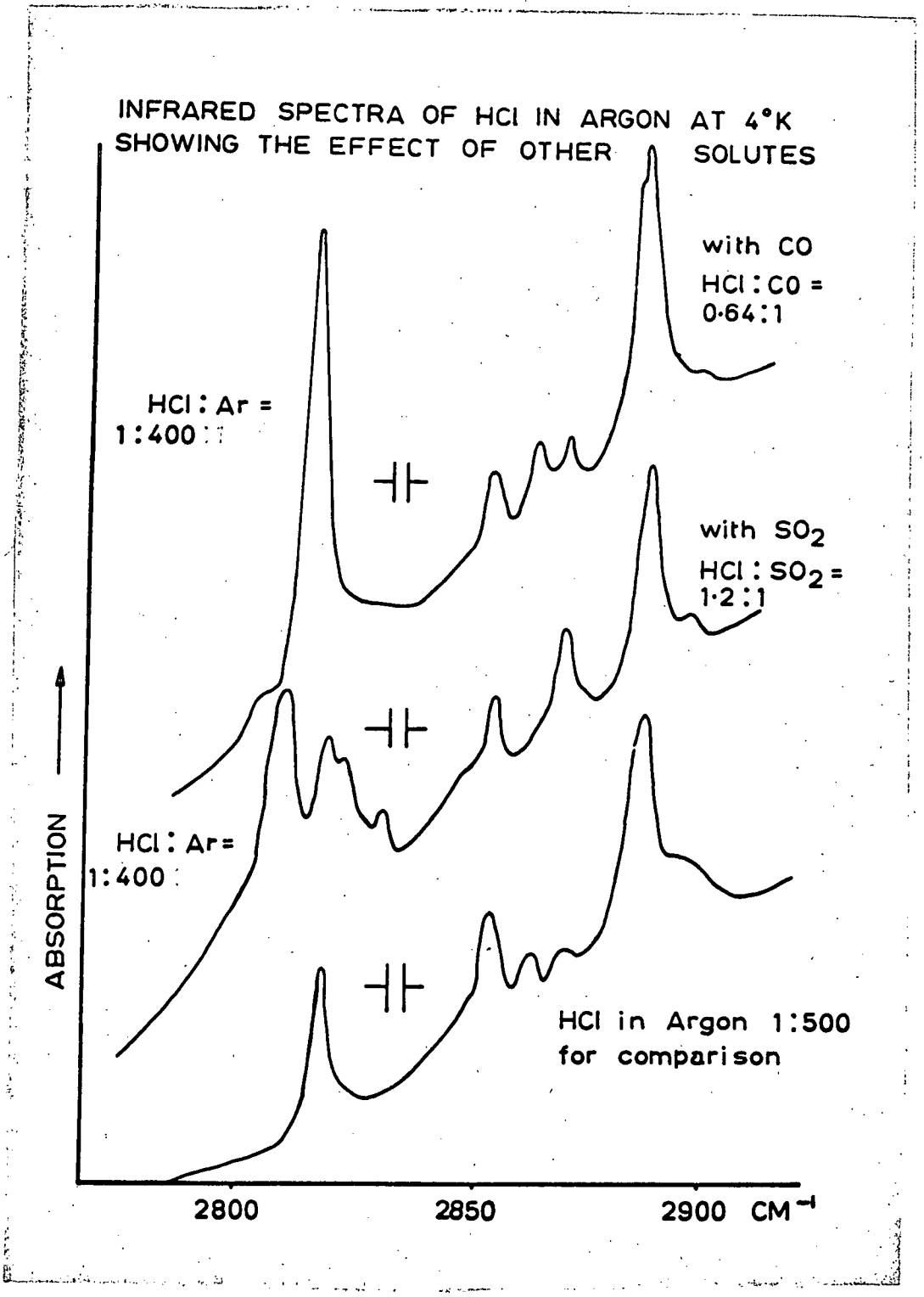
INFRARED SPECTRA OF HCl IN ARGON AT 4°K
SHOWING THE EFFECT OF OTHER SOLUTES
with CO
HCl : CO =
0·64 : 1
HCl : Ar =
1 : 400 : 1
with SO_2
HCl : SO_2 =
1·2 : 1
HCl : Ar =
1 : 400
HCl in Argon 1 : 500
for comparison
ABSORPTION
2800
2850
2900 CM^{-1}

fig 8.

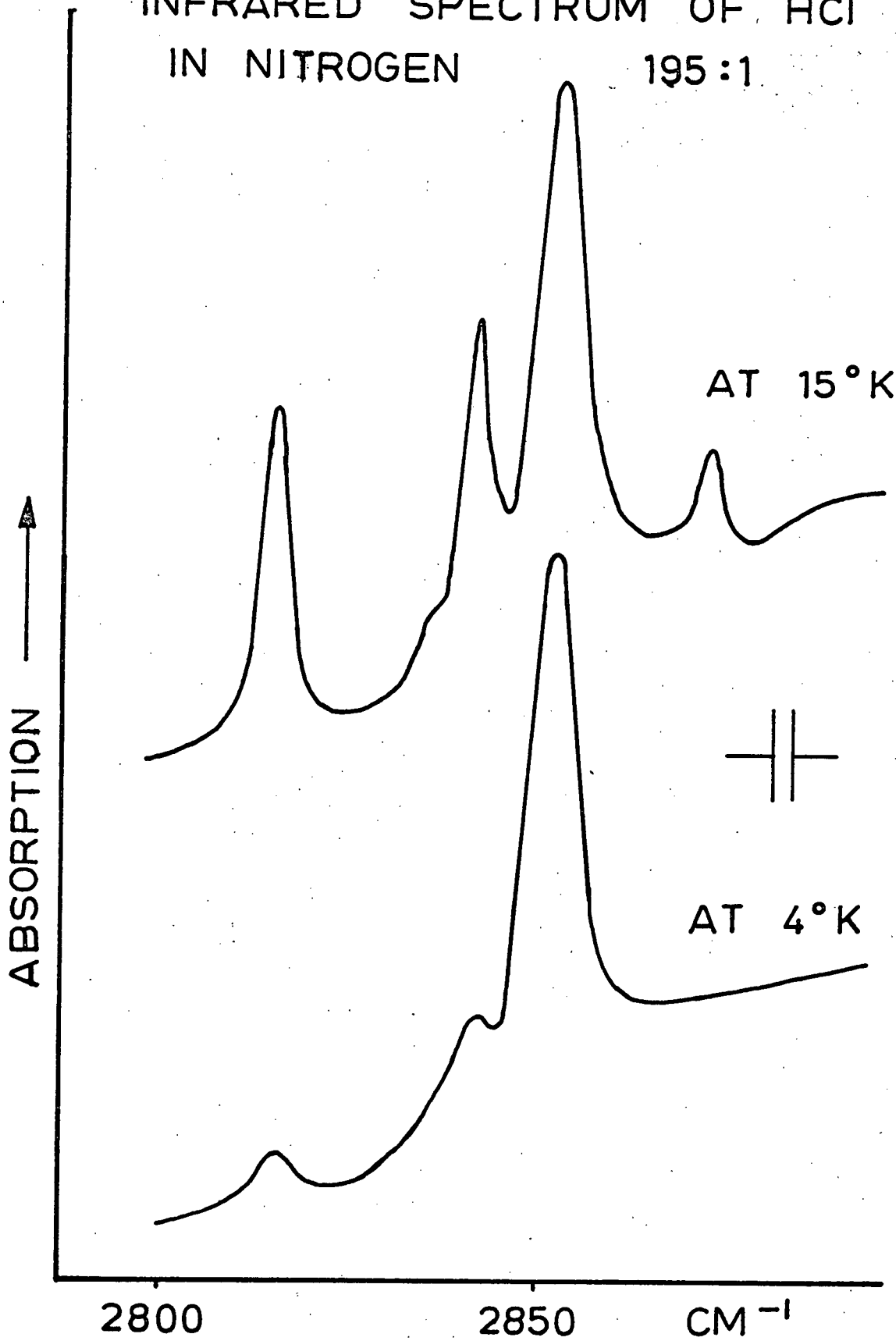
INFRARED SPECTRUM OF HCl
IN NITROGEN 195:1
AT 15°K
AT 4°K
ABSORPTION
2800
2850
CM⁻¹

fig 9.

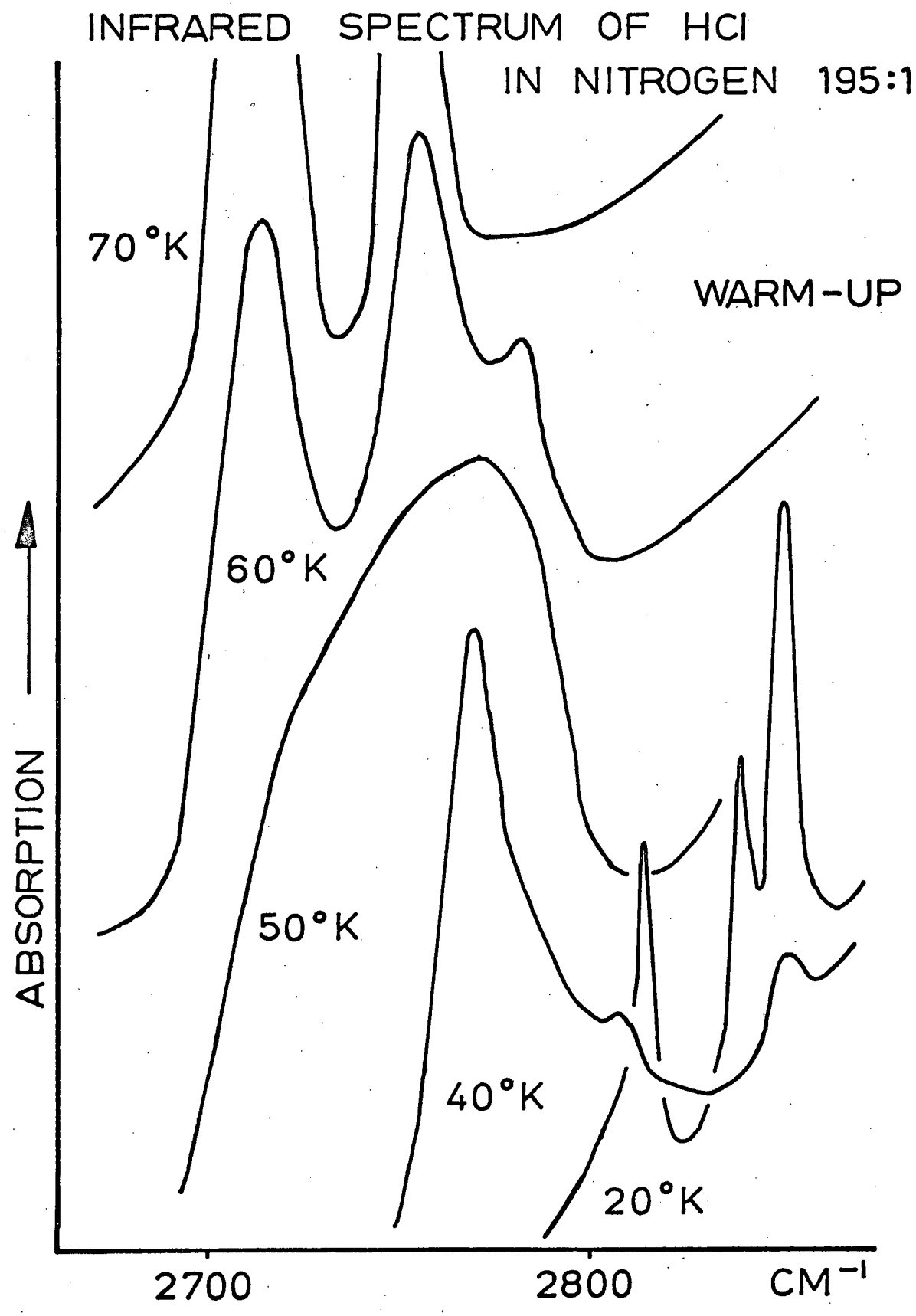
INFRARED SPECTRUM OF HCl
IN NITROGEN 195:1
70°K
WARM-UP
60°K
50°K
40°K
20°K
ABSORPTION
2700
2800
CM⁻¹

fig 10.

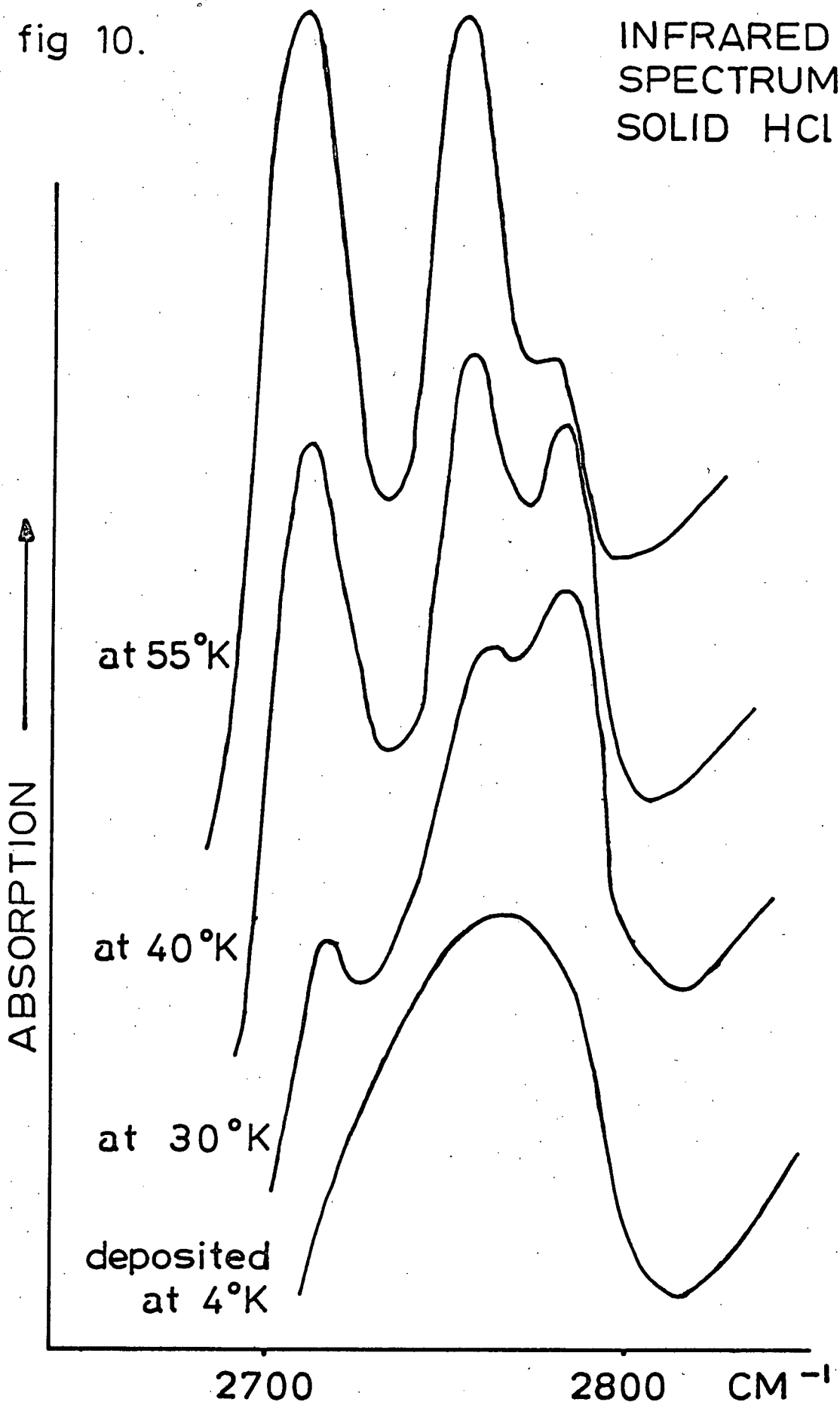
INFRARED SPECTRUM OF SOLID HCl
ABSORPTION
at 55°K
at 40°K
at 30°K
deposited at 4°K
2700
2800
CM⁻¹

3-3 Infrared Spectra of HBr in Argon, Krypton and Nitrogen Matrices.

The spectra of HBr in argon, krypton and nitrogen are compared in Fig. 11, and the observed frequencies tabulated in Table 3. The spectrum of HBr in krypton at a matrix to solute ratio of 320:1 is seen to be very similar to that of HBr in argon at a ratio of 500:1. The main difference is a shift of the whole spectrum to lower wave numbers in the krypton matrix. In solid nitrogen, a simple spectrum consisting of one main peak with three very weak subsidiaries is observed. The subsidiary peaks increase in intensity during warm-up (see Fig. 12), in a way similar to that observed for HCl in nitrogen.

A dilution study of HBr in argon at matrix ratios of 100, 300 and 500 to 1 was carried out, and the resulting spectra are shown in Fig. 13. The frequencies, with intensities at the various argon to HBr ratios, are given in Table 4. A variation in the number and relative intensities of peaks with dilution is evident in this series of experiments.

A typical warm-up study is illustrated by Fig. 14, where variations in the spectrum of HBr in argon at a matrix to solute ratio of 300:1 are shown. New peaks which appear during warm-up do not disappear on recooling to 4°K., and further deposit at this temperature adds only to the intensity of the peaks originally observed at 4°K. Spectra of HBr, perturbed by other solute molecules in an argon matrix, were recorded as in the work with HCl. These spectra are reproduced in Fig. 15. The main features of the HBr spectrum remain unchanged, but when CO is present a new,

very strong peak is observed at 2520 cm^{-1} and with SO_2, three new peaks are found at 2484, 2517 and 2524 cm^{-1}.

TABLE 3.

Infrared absorption of HBr in various matrices at 4°K. (Frequencies in cm^{-1}).

Ar (505:1)	Kr (320:1)	N_2(175:1)	HBr (gas)
2465 w	-	-	-
2496 m	2491 s	2493 vw	-
2550 m	2531 s	2506 vw	2542 P(1)
2558 vw	2541 w	2535 w	-
2569 s	2551 vs	2545 vs	2575 R(0)
2575 sh	-	-	2591 R(1)

TABLE 4

Infrared absorption of HBr in argon at 4°K. Line intensities (log I_o/I) relative to the peak at 2569 cm^{-1}.

Frequency cm^{-1}	Argon to HBr ratio 110:1	215:1	300:1	505:1
2465	-	1.60	.50	.21
2496	1.24	1.15	.98	.71
2550	.41	.36	.40	.36
2558	.18	.09	.20	.14
2569	1.00	1.00	1.00	1.00
2575	sh	sh	sh	sh

fig 11.

INFRARED SPECTRA OF HBr IN VARIOUS MATRICES AT 4°K

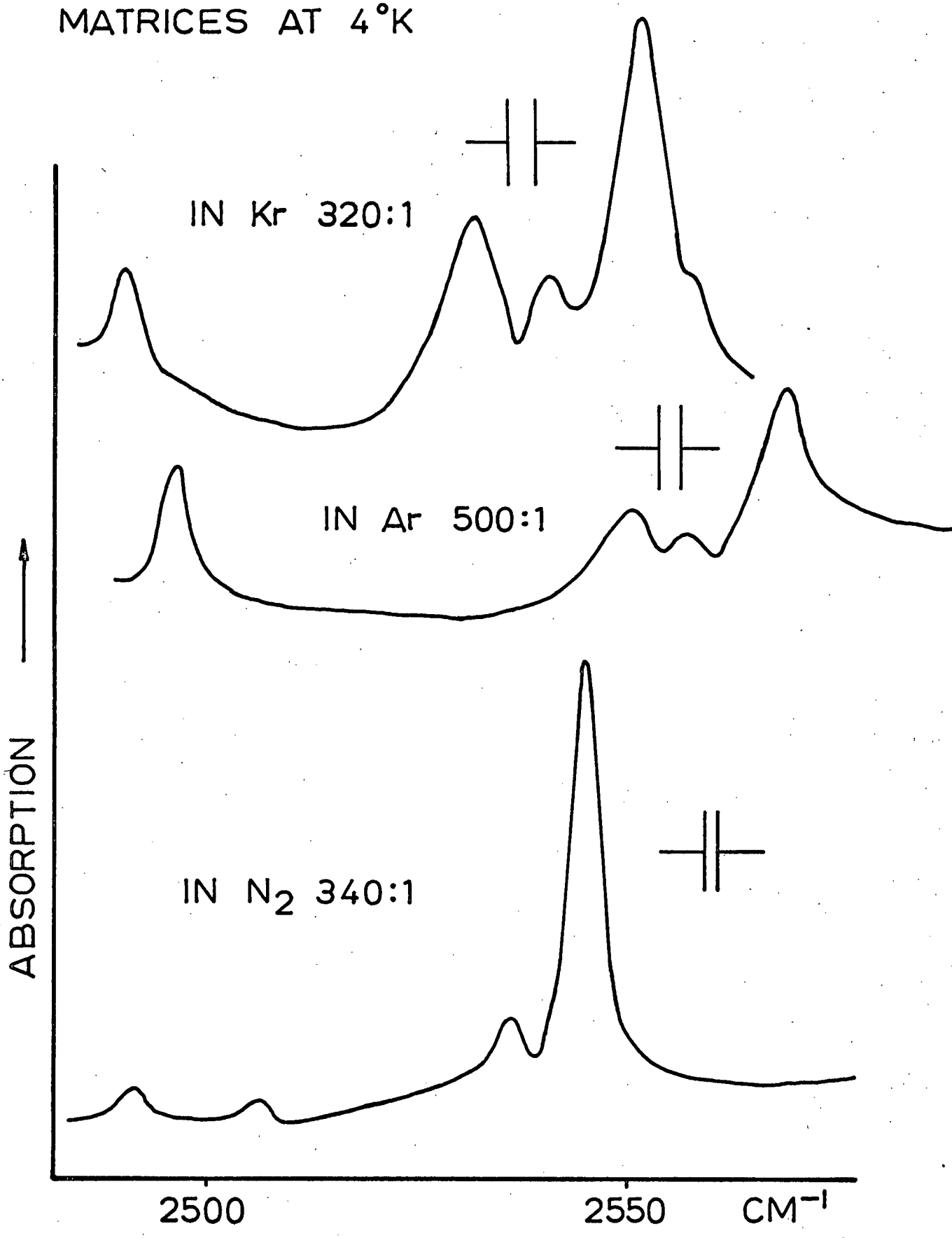

fig 12.

INFRARED SPECTRUM OF HBr IN NITROGEN

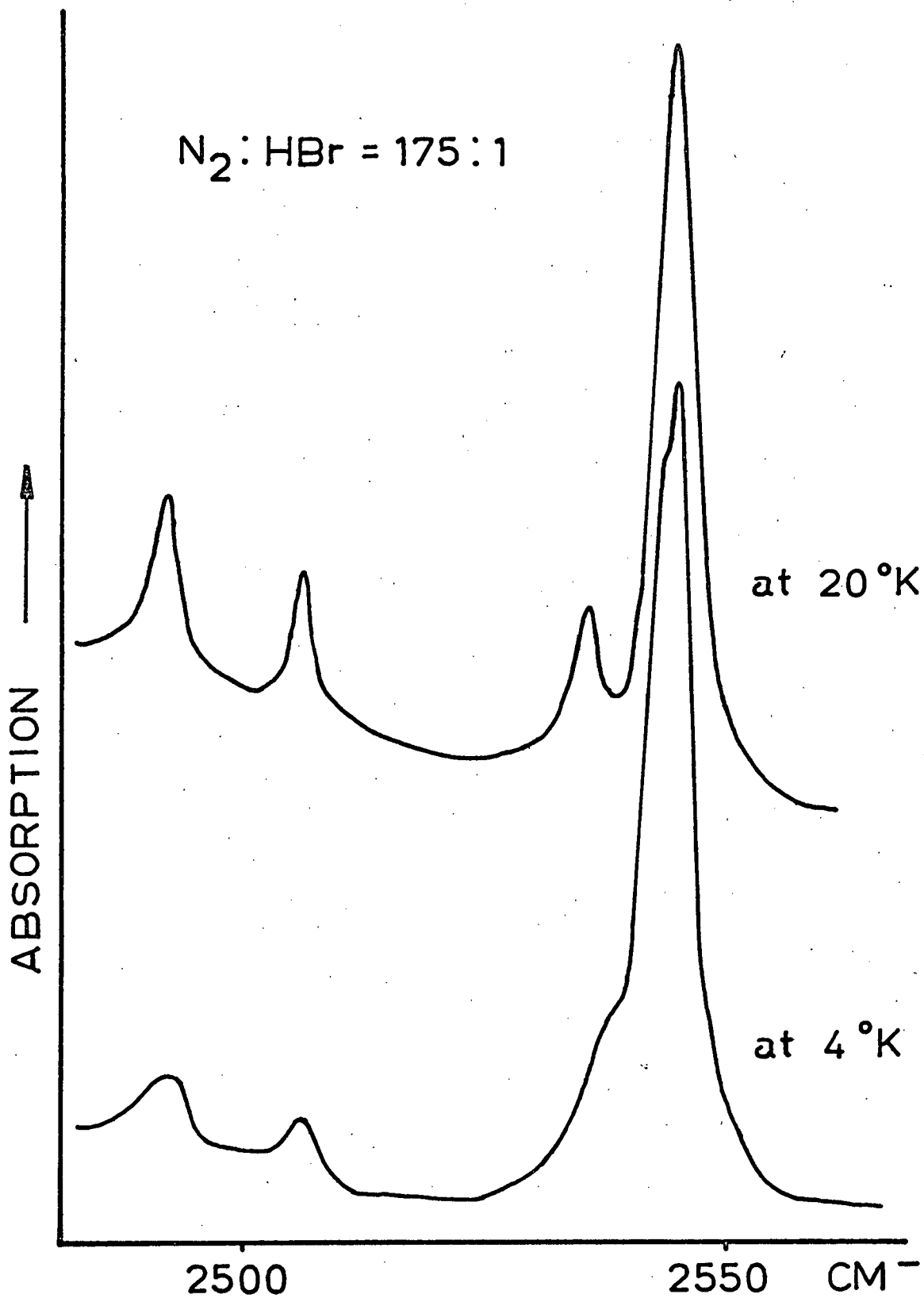

fig 13.

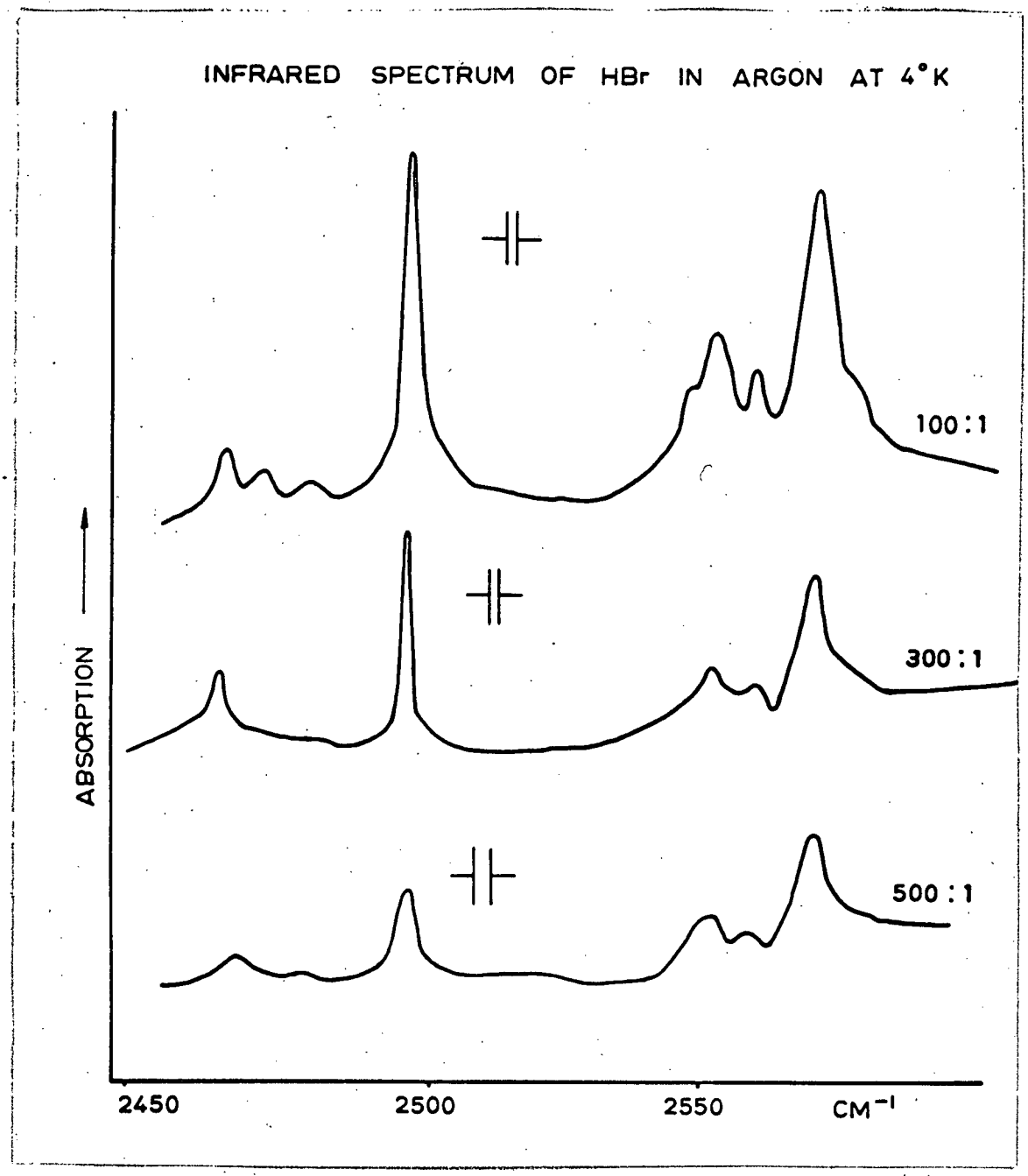
INFRARED SPECTRUM OF HBr IN ARGON AT 4°K
100 : 1
300 : 1
500 : 1
ABSORPTION
2450
2500
2550
CM⁻¹

fig 14.

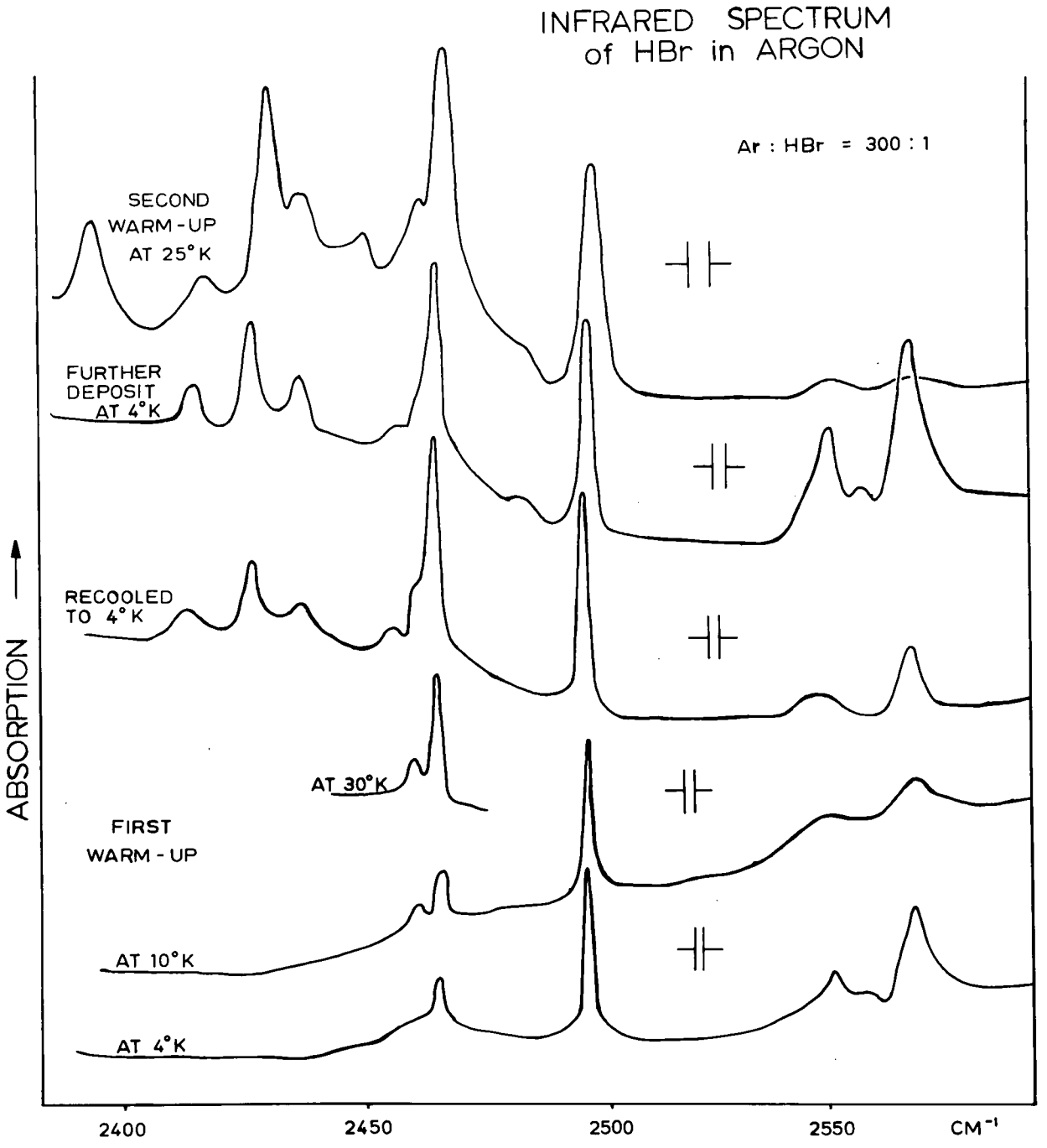
INFRARED SPECTRUM
of HBr in ARGON
Ar : HBr = 300 : 1
SECOND
WARM-UP
AT 25°K
FURTHER
DEPOSIT
AT 4°K
RECOOLED
TO 4°K
AT 30°K
FIRST
WARM-UP
AT 10°K
AT 4°K
ABSORPTION
2400
2450
2500
2550
CM⁻¹

fig 15.

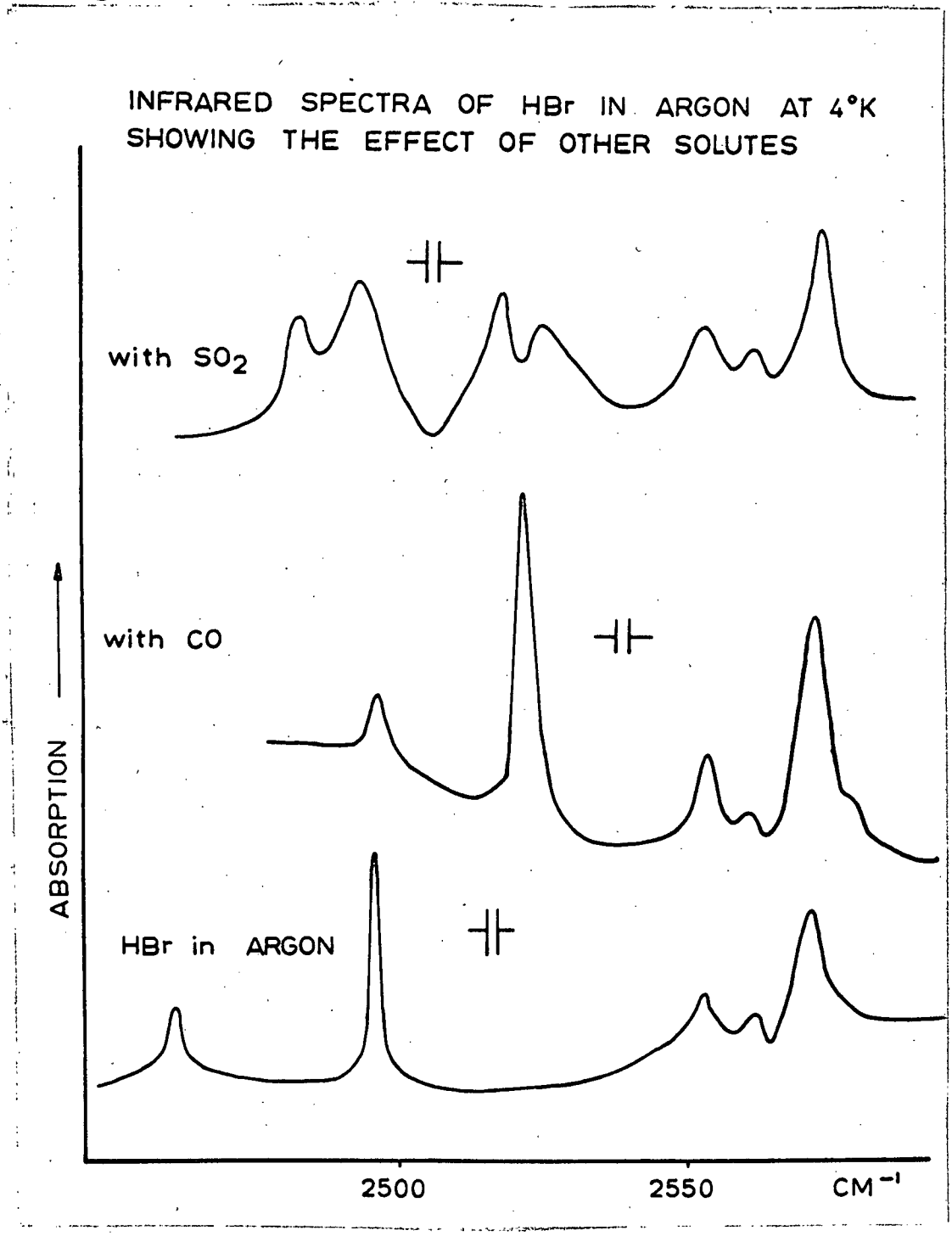
INFRARED SPECTRA OF HBr IN ARGON AT 4°K
SHOWING THE EFFECT OF OTHER SOLUTES
with SO_2
with CO
HBr in ARGON
ABSORPTION
2500
2550
CM^{-1}

3-4 Matrix Isolation Studies on CO and SO_2.

The spectrum of CO in argon (Fig. 16) consists of one very strong peak at 2138.5 cm^{-1}, with a peak of medium intensity at 2152 cm^{-1}. Three very weak satellites were also observed on the low frequency side of the main peak when very thick deposits were examined. No changes in the spectrum of CO were observed when some CO molecules were replaced by HCl or HBr. In the overtone region of CO, one weak peak at 4253 cm^{-1} was found. The observed frequencies together with results obtained by other workers for both solid and matrix isolated CO are included in Table 5.

TABLE 5.

Infrared Absorption of CO in Argon at 4°K, Compared with Results of Other Workers. (Frequencies in cm^{-1})

This Work CO/Ar at 4°K.		Maki (9) CO/Ar at 20°K.	Ewing and Pimentel (19) Solid CO at 20°K.
4253	w	-	4253.5
2152	m	2148.0	-
-		2142.4	-
2138.5	vs	2137.2	2138.1
2115	vw	-	2112.3
2091	w	-	2092.2
-		-	2088.4
2065	w	-	-

Infrared spectra in the regions of the symmetric and antisymmetric stretching fundamentals (ν_1 and ν_3) of SO_2 in argon and nitrogen matrices are presented in Fig. 17. A significant difference between the spectrum of SO_2 in the two matrices is observed. In argon, both the ν_1 and ν_3 bands consist of a strong doublet with a weak satellite. In nitrogen, however, only one strong peak is found in each region, again with a weak satellite. The doublets coalesce into a single peak during warm-up.

In Table 6 the observed frequencies are listed for gaseous SO_2, solid SO_2, SO_2 in argon and nitrogen matrices and SO_2 in the gas hydrate.

TABLE 6.

Infrared Absorption of SO_2 (frequencies in cm^{-1}).

SO_2 Gas reference (44)	Solid 80°K	Hydrate 80°K	In Argon 4°K	In Nitrogen 4°K
518	521 s	521 s	-	-
-	528 sh	-	-	-
-	-	1035 w	-	-
-	1141.8 m	-	1140.0 w	-
1151	1144.5 vs	1148.8 s	1147.3 s	1145.0 w
-	-	-	1152.1 s	1152.6 s
-	1305.5 s	-	-	-
-	1312.0 vs	-	-	-
-	1325.0 vs	1326 w	-	-
-	-	1336 sh	1334.3 w	1334.8 w
-	-	1342.5 vs	1351.4 vs	1346.7 sh
-	-	1349 sh	1355.6 vs	1351.8 vs
1362	-	-	-	-

fig 16.

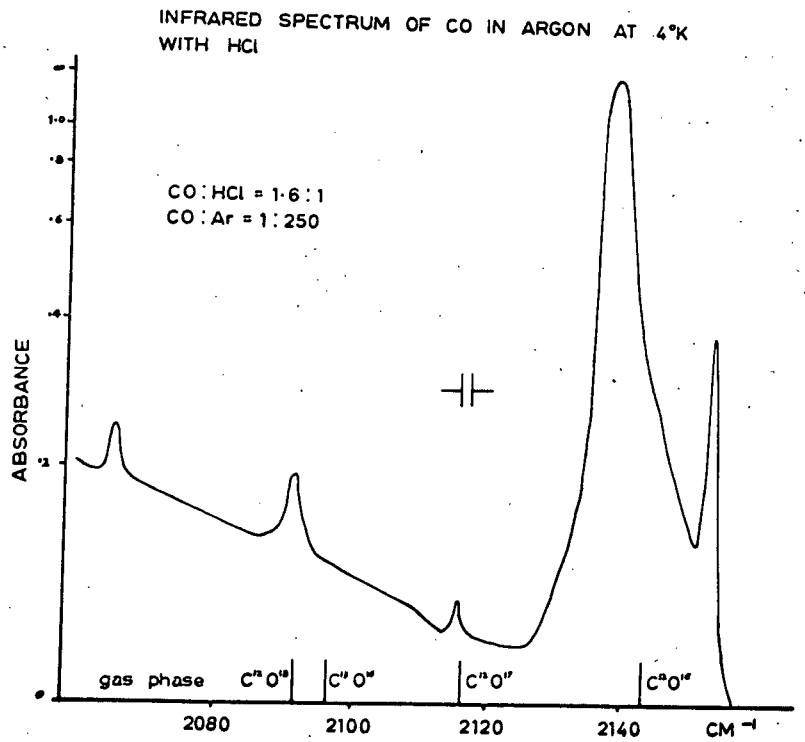
INFRARED SPECTRUM OF CO IN ARGON AT 4°K
WITH HCl
CO : HCl = 1·6 : 1
CO : Ar = 1 : 250
ABSORBANCE
gas phase
2080
2100
2120
2140
CM⁻¹

fig 17.

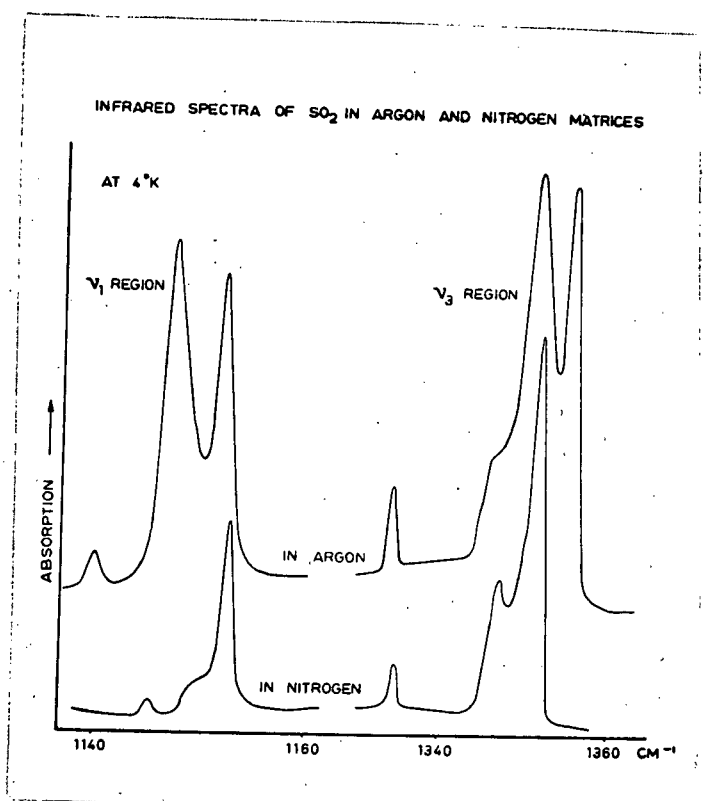
INFRARED SPECTRA OF SO2 IN ARGON AND NITROGEN MATRICES
AT 4°K
ν1 REGION
ν3 REGION
ABSORPTION
IN ARGON
IN NITROGEN
1140
1160
1340
1360 CM⁻¹

3-5 Gas Hydrates.

The skeletal water spectrum of SO_2 and krypton hydrates is compared with the spectrum of ice in Fig. 18. The corresponding frequencies, which are tabulated in Table 7, are the averages of several runs. Due to the uncertainty in locating the maxima of these broad bands, the frequencies in Table 7 are accurate only to $\pm$ 10 cm^{-1}. In spite of this however, Fig. 18 clearly shows shifts of the peaks at 820 and 1600 cm^{-1} in the spectrum of ice to 780 and 1640 cm^{-1} in the SO_2 hydrate, and a new peak at 2420 cm^{-1} in the krypton and SO_2 hydrates is also evident.

The frequencies associated with the SO_2 molecule in the hydrate and the solid are compared in Fig. 19. Significant differences are found for each of the three fundamentals. The ν_3 region of SO_2 during an experiment in which SO_2 hydrate was formed at 80°K cooled to 4°K and rewarmed to 120°K, is presented in Fig. 20. The central peak at 1340 cm^{-1} is seen to have two shoulders at 120°K, one of which is not present at 4°K.

TABLE 7.

Skeletal Water Spectrum in the Gas Hydrates at 80°K
(frequencies in cm^{-1}).

Ice	$SO_2.6H_2O$	$Kr.6H_2O$	$H_2S.6H_2O$	Assignment
820 s	780 s	820 s	815 s	ν_R
1600 m	1640 m	1610 m	1620 m	ν_2
2220 w	2220 w 2410 vw	2210 w 2420 w	2190 w -	$\nu_R + \nu_2$
3230 vs	3230 vs	3260 vs	-	ν_1 , ν_3

fig 18.

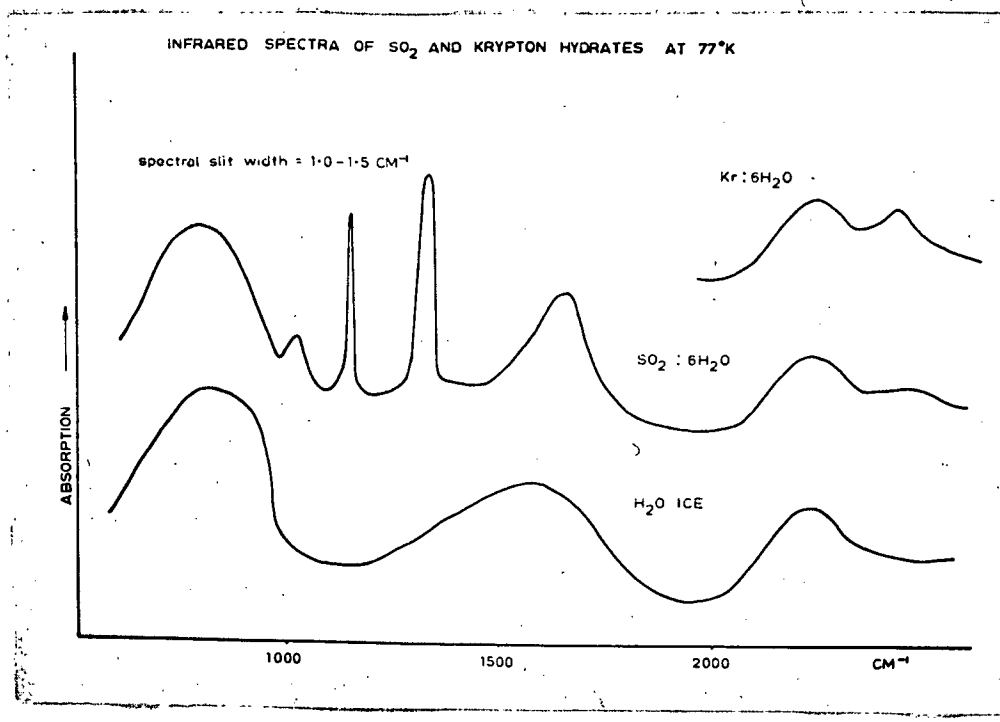
INFRARED SPECTRA OF SO_2 AND KRYPTON HYDRATES AT 77°K
spectral slit width = 1·0 - 1·5 CM^{-1}
$Kr:6H_2O$
$SO_2:6H_2O$
H_2O ICE
ABSORPTION
1000
1500
2000
CM^{-1}

fig 19.

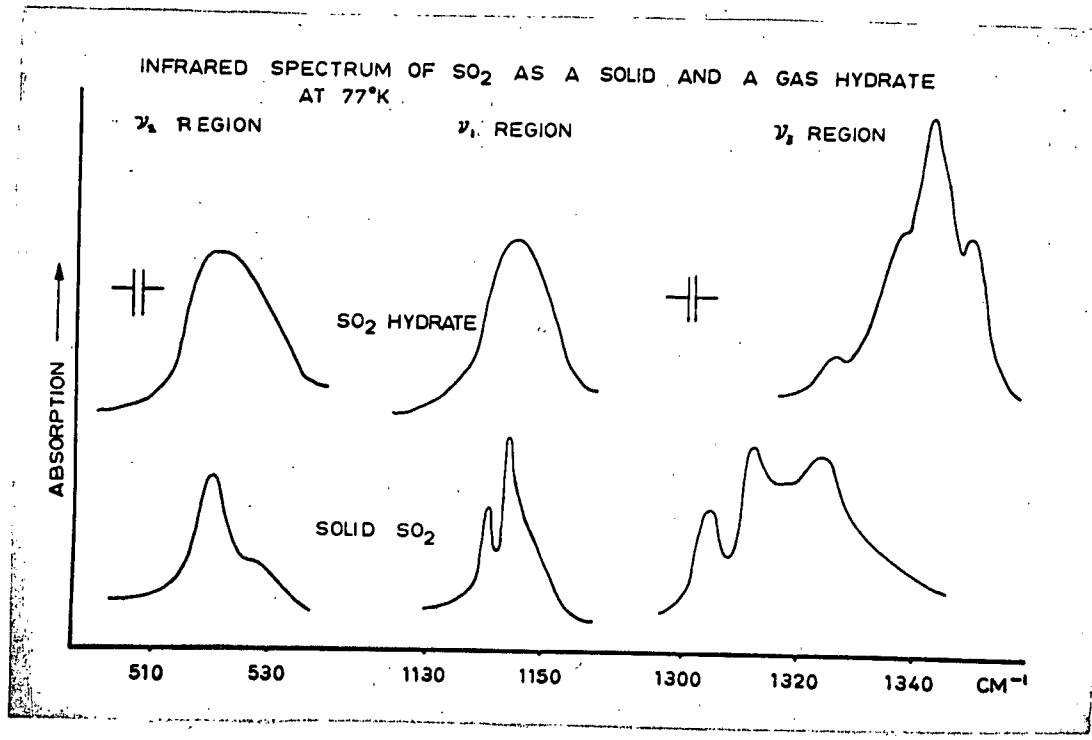
INFRARED SPECTRUM OF SO_2 AS A SOLID AND A GAS HYDRATE AT 77°K
ν_2 REGION
ν_1 REGION
ν_3 REGION
SO_2 HYDRATE
SOLID SO_2
ABSORPTION
510
530
1130
1150
1300
1320
1340
CM^{-1}

fig 20.

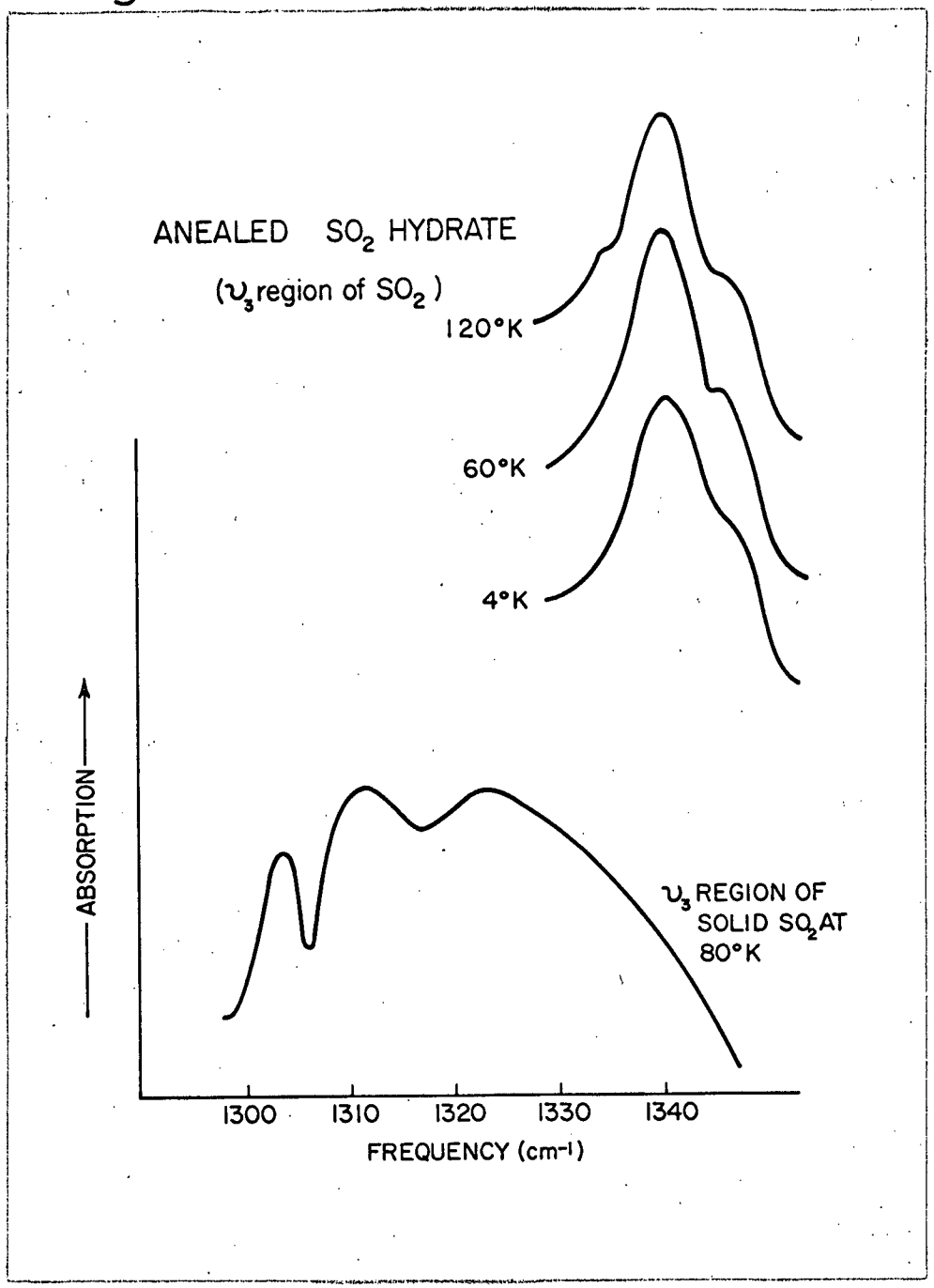
ANEALED SO2 HYDRATE
(υ3 region of SO2)
120°K
60°K
4°K
ABSORPTION
υ3 REGION OF SOLID SO2 AT 80°K
1300
1310
1320
1330
1340
FREQUENCY (cm-1)

CHAPTER 4. THEORETICAL.

4-1 Introductory Remarks.

The calculations described in this chapter fall into three categories:

(i) Calculation of shifts of vibrational frequency due to interactions between solute and matrix.

(ii) Calculations of perturbation energies for rotational levels of isolated solute molecules.

(iii) Calculation of shifts of vibrational frequency due to mutual interactions between pairs of solute molecules in nearest neighbour, next nearest neighbour, etc., sites in the lattice.

The formulae and results developed in this chapter will be applied in Chapter 5 to the interpretation of the observed spectra.

4-2 Shifts of Vibrational Frequencies Due to Matrix-Solute Interactions.

The energy of interaction between a solute molecule and the surrounding matrix is made up of the sum of three terms (45):

$$\phi = \phi\,(\text{ind}) + \phi\,(\text{dis}) + \phi\,(\text{es}) \qquad (1)$$

A fourth term should be added to Eq. (1) to take account of repulsive forces. However, this effect will be treated empirically later.

The induction energy ϕ (ind) may be estimated from the energy of interaction between the permanent charge distribution of one molecule and the moments induced in the other. The term ϕ (dis)

is the London dispersion energy and represents the interaction between the two induced charge distributions. The third term, ϕ (es) is the purely electrostatic interaction energy between the permanent charge distributions. The electrostatic energy is zero for the rare gas matrices, but is non-zero for nitrogen which has an electric quadrupole moment.

The induction potential in the case of the nitrogen or rare gas matrices is given by (45):

$$\phi \text{ (ind)} = -\mu_a^2 \alpha_b (3\cos^2\theta + 1)/2r^6 \qquad (2)$$

where: α_b is the polarizability of the matrix atom, μ_a is the dipole moment of the solute molecule, r is the internuclear distance in the solid rare gas, and θ is the angle between the z axis (chosen as a cube axis) and the axis of the dipole (the molecular axis).

By considering the average interaction, the angular part of Eq. (2) gives a contribution of +2 regardless of the orientation of the solute molecule. The rare gases crystallize with the cubic close-packed structure (46), and the Lennard-Jones' sum for an inverse sixth power potential for this lattice is 14.45 (47). This sum gives the effective number of nearest neighbours, and takes account of interactions between the isolated solute molecule and the rare gas atoms or nitrogen molecules in the whole lattice. Hence Eq. (2) becomes:

$$\phi \text{ (ind)} = \frac{-14.45\ \mu_a^2 \alpha_b}{r^6} \qquad (3)$$

which gives rise to a frequency shift given by:

$$\Delta\nu\,(\text{ind}) = \frac{-14.45\ \Delta(\mu_a^2)\ \alpha_b}{r^6\ hc} = C_1\ \Delta(\mu_a^2) \qquad (4)$$

where: $\Delta(\mu_a^2)$ is the change in the square of the dipole moment between the ground and first excited vibrational states.

For the nitrogen matrix, there will be additional terms in the potential involving the electric quadrupole of the nitrogen molecule; however, the contribution from these terms will be much smaller than Eq. (4) and they can be neglected.

An approximate expression for the dispersion energy is given by (45):

$$\phi\,(\text{dis}) = \frac{-3\alpha_a\alpha_b}{2r^6}\left(\frac{E_a E_b}{E_a + E_b}\right) \qquad (5)$$

where: α_a and α_b are the polarizabilities of the solute molecule and matrix atom or molecule, and E_a and E_b are approximately equal to their respective ionization energies.

Eq. (8) may be used to estimate the dispersion contribution to the shift in vibrational frequency of a solute molecule, in the following way. Both the polarizability and the ionization potential of the solute molecule change during a vibrational transition. Thus:

$$\phi'(\text{dis}) = -\frac{C_2\,\alpha_a'\,E_a'}{E_a' + E_b} \qquad (6)$$

$$\phi''(\text{dis}) = -\frac{C_2\,\alpha_a''\,E_a''}{E_a'' + E_b} \qquad (7)$$

where: the double prime denotes the ground vibrational state and the single prime the first excited vibrational state. The constant $C_2 = 3\alpha_b E_b / 2r^6$

Subtracting Eq. (7) from Eq. (6) we get:

$$\phi' - \phi'' = -C_2 \left[\frac{\alpha_a' E_a'}{E_a' + E_b} - \frac{\alpha_a'' E_a''}{E_a'' + E_b} \right] \qquad (8)$$

We again introduce a factor of 14.45 to account for the interaction of the solute molecule with the entire matrix. The dispersion contribution to the shift of vibrational frequency is given by:

$$\Delta \nu (dis) = -14.45\, C_2 \left[\frac{\alpha_a' E_a'}{E_a' + E_b} - \frac{\alpha_a'' E_a''}{E_a'' + E_b} \right] \qquad (9)$$

In the case of the nitrogen matrix the electrostatic term consists of a dipole-quadrupole interaction given by (45):

$$\phi(es) = \frac{3\mu_a Q_b}{4r^4} \left[\cos\theta_a (3\cos^2\theta_b - 1) - 2\sin\theta_a \sin\theta_b \cos(\phi_a - \phi_b) \right] \qquad (10)$$

where: Q_b is the quadrupole moment of N_2, μ_a is the dipole moment of the solute molecule, θ_a, θ_b, ϕ_a, ϕ_b, are the polar angles associated with the dipole (HCl or HBr) and the quadrupole (N_2), and r is the nearest neighbour distance in the solid matrix.

The average of the angular terms in Eq. (10) is zero; however, in the case of nitrogen, the symmetry of the substitutional site is not spherical and the electrostatic interaction is not expected to vanish. An estimate of the order of magnitude of ϕ(es) may be obtained by assuming maximum interaction which leads to a value of $-2/\sqrt{5}$ per nitrogen molecule regardless of the

orientation of the solute molecule (20). Nitrogen below 35°K crystallizes in a cubic close-packed structure (48), and the Lennard-Jones' sum for an inverse fourth power potential in this lattice is 25.34 (47). Eq. (10) now becomes:

$$\phi(es) = - \frac{3 \mu_a Q_b (25.34)}{4 r^4} \left(\sqrt{\frac{2}{5}} \right) \qquad (11)$$

and the shift in vibrational frequency of the solute is given by:

$$\Delta \nu (es) = - \frac{17.00 \, \Delta \mu_a Q_b}{r^4 \, hc} = - C_3 \, \Delta \mu_a \qquad (12)$$

where: $\Delta \mu_a$ is the change in dipole moment between the ground and first excited vibrational states.

In Table 8, the constants in Eqs. (4), (9) and (12) are evaluated for argon, krypton and nitrogen matrices, using the values of polarizability, internuclear distance, etc., from Appendix I.

TABLE 8.

Values of Constants in Calculations of Matrix Shifts.

Formula	$\Delta \nu (ind) = -C_1 \Delta (\mu_a^2)$	$\Delta \nu (dis) = -C_2 \left[\frac{\alpha_a' E_a'}{E_a' + E_b} - \frac{\alpha_a'' E_a''}{E_a'' + E_b} \right]$	$\Delta \nu (es) = -C_3 \Delta \mu_a$
Expression for the constant	$\frac{14.45 \ \alpha_b}{r^6 hc}$	$\frac{21.68 \ E_b \ \alpha_b}{r^6}$	$\frac{17.00 \ Q_b}{r^4 hc}$
Units of C	$cm^{-3} \ esu^{-2}$	cm^{-4}	$cm^{-2} \ esu^{-1}$
Ar	3.76 x 10	1.42 x 10	-
Kr	3.95 x 10	1.32 x 10	-
N_2	3.17 x 10	1.18 x 10	5.03 x 10

4-3 Rotation of Molecules Trapped in Solid Rare Gases.

Schoen et al (8) assumed that the solute molecule was confined in a field of cylindrical symmetry. The potential barrier to rotation was taken as $C^1(1-\cos^2\theta)$ where C^1 is the barrier height and θ the angle between the molecular axis and the cylinder axis. Using this model for HCl in argon, these workers predicted a three line spectrum corresponding to R(0), P(1) and R*(1), where R*(1) is due to a blend of transitions of the hindered rotator.

The potential function used by Schoen et al is essentially that used by Pauling (14); $V\ (1-\cos 2\theta)$† for a diatomic molecule rotating in a cylindrical well.

Armstrong (12) investigated the effect of electrostatic interactions on the rotational energy levels of an isolated solute molecule trapped in a rare gas lattice at low temperatures. He concluded that these interactions produce no effect on the rotational energy levels of the solute molecule, and his expression for the interaction energy is very similar to the sum of Eqs. (6) and (8) of the previous section. Armstrong also considered dipole-dipole interactions between the solute molecules. For a diatomic molecule in a solid rare-gas his results indicate that a slight mixing of rotational states occurs, the J = 2 level being the first level to be split.

More recently Flygare (11) presented a theory dealing with the same problem. This author agrees with Armstrong that the

---

† $V\ (1-\cos 2\theta) = 2V\ \sin^2\theta = C^1(1-\cos^2\theta)$

dipole-induced dipole term does not effect the rotational energy, but goes on to show that higher multi-polar interactions can be responsible for the rotational perturbations experienced by the solute molecules.

All the above authors ignore exchange interactions arising from overlap of electronic charge distributions of the solute molecule and surrounding matrix atoms. The repulsive exchange forces would give rise to a "blue" shift of the vibrational frequency, whereas a "red" shift is usually observed. However, it is possible that the effect of the repulsive interactions is undetected because the attractive electrostatic forces give rise to a large "red" shift of the vibrational frequency.

The following calculations are based on the assumption that the isolated solute molecule experiences repulsive forces in addition to attractive forces which perturb the rotational energy levels.

4-4 The Hindered Rotator Potential.

In this section a potential will be developed for the case of a hydrogen halide molecule surrounded by twelve nearest neighbour matrix atoms. The model used for the calculation assumes that the hydrogen halide molecule rotates about its centre of mass which is taken to be at the nucleus of the halogen atom.† We also assume that the molecular centre of mass is on a lattice point, which is not strictly true. In fact, the centre of volume of the molecule

† The actual C.O.M. of HCl is 0.035A from the chlorine nucleus; this may be compared with the internuclear distance in HCl 1.275A.

will more probably be on a lattice point. However, it may be shown (49) that regardless of the choice of origin, the angular dependence of the potential will be the same.

A useful mathematical form for an interaction potential which includes repulsive and attractive forces is the Lennard-Jones' (6-12) potential (50):

$$V(r) = \epsilon_o \left[\left(\frac{r_o}{r_{ji}} \right)^{12} - 2 \left(\frac{r_o}{r_{ji}} \right)^{6} \right] \qquad (14)$$

where: r_{ji} is the internuclear distance of the interacting atoms, r_o is the internuclear distance at which the potential is a minimum, and ϵ_o is the depth of the potential minimum.

Eq. (14) may be rewritten as:

$$V(r) = V_o r_{ji}^{-12} - V_o' r_{ji}^{-6} \qquad \begin{matrix} j = 1, 2. \\ i = 1, 2, \ldots, 12. \end{matrix} \qquad (15)$$

where: $V_o = \epsilon_o r_o^{-12}$ and $V_o' = 2\epsilon_o r_o^{6}$

The matrix-halogen interactions will be different from the matrix-hydrogen interactions, and V_o and V_o' will not be the same for the two cases.

The co-ordinate system used in the following calculation is illustrated in Fig. 21. The distance r_{2i} between the nucleus of the halogen atom and each of the twelve nearest neighbour matrix atoms is equal to the internuclear distance in the solid rare gas, and equation (15) gives:

$$V(r) = 12\ V_o\ r^{-12} - 12\ V_o'\ r^{-6} \qquad (16)$$

where: r is the internuclear distance in the solid rare gas.

fig 21.

CO-ORDINATE SYSTEM USED FOR THE HINDERED ROTATOR POTENTIAL

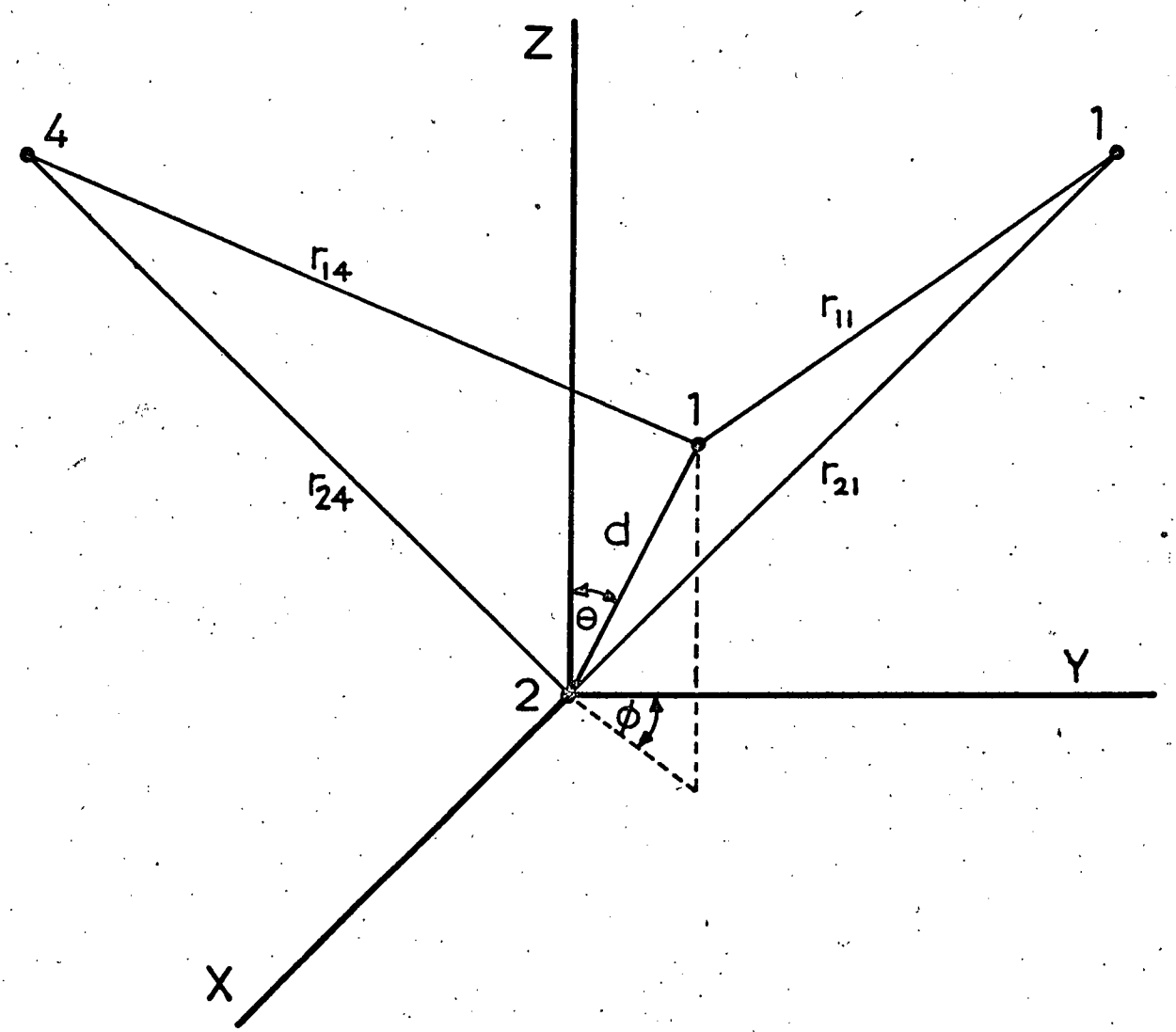

Thus, the halogen-matrix interactions give rise to an angle-independent term in the potential which we will call V .

For the hydrogen-matrix interactions the potential has an angular dependence, since the internuclear distances r_{1i} depend on θ and ϕ (see Fig. 21). The r_{1i} may be evaluated using the formula of analytical geometry:

$$r_{1i} = \sqrt{(x_1 - x_i)^2 + (y_1 - y_i)^2 + (z_1 - z_i)^2} \tag{17}$$

which leads to expressions of the form:

$$r_{1i} = r\sqrt{1 + \frac{d^2}{r^2} \pm \frac{\sqrt{2}\,d}{r} f(\theta,\phi)} \tag{18}$$

where: d is the internuclear distance in the solute molecule and $f(\theta,\phi)$ is a function of θ and ϕ.

A typical r_{1i} is:

$$r_{14} = r\sqrt{1 + \frac{d^2}{r^2} + \frac{\sqrt{2}\,d}{r}(\sin\theta \sin\phi - \cos\theta)} \tag{19}$$

Future calculations will be simplified if we neglect d^2/r^2 compared to 1. This is a poor approximation since d^2/r^2 for HCl in argon is 0.111. The square root may be expanded by the binomial theorem to give:

$$r_{1i} = r\left[1 + \frac{\sqrt{2}\,d}{2r} f(\theta,\phi) + \cdots\right] \tag{20}$$

Again we neglect terms in d^2/r^2, and higher powers. By this procedure the r_{1i} are found to be:

$$\begin{aligned} &\text{yz plane} \quad r(1 \pm c\cos\theta \pm c\sin\theta\cos\phi) \\ &\text{xz plane} \quad r(1 \pm c\cos\theta \pm c\sin\theta\sin\phi) \\ &\text{xy plane} \quad r(1 \pm c\sin\theta\cos\phi \pm c\sin\theta\sin\phi) \end{aligned} \tag{21}$$

where: $c = \dfrac{\sqrt{2}\,d}{2r}$

On substituting the values of r_{1i} into Eq. (15) we get twelve terms of the form:

$$V_0 r^{-12}(1 \pm x)^{-12} - V_0' r^{-6}(1 \pm x)^{-6} \tag{22}$$

where: $x = c f(\theta\phi)$

Expanding the inverse twelfth and inverse sixth power terms by the binomial theorem gives:

$$V_0 r^{-12}\left[1 \mp 12x + \frac{12\cdot13}{2!}x^2 \mp \frac{12\cdot13\cdot14}{3!}x^3 + \cdots\right]$$

$$-V_0' r^{-6}\left[1 \mp 6x + \frac{6\cdot7}{2!}x^2 \mp \frac{6\cdot7\cdot8}{3!}x^3 + \cdots\right] \tag{23}$$

It is necessary to take the inverse twelfth power expansion up to the sixth power of x because the binomial coeficients are large, and $(d/r)^n$ does not decrease rapidly enough with n. However, for the inverse sixth power expansion, only the terms up to the fourth power of x are important.

When the twelve expressions for x are substituted in Eq.23, and after much simplification, the expression for $V(\theta\phi)$ becomes:

$$V(\theta\phi) = V_1 + V_2 + V_3 \cos^2\theta \sin^2\theta + V_4 \sin^4\theta \cos^2\phi \sin^2\phi + V_5 \sin^6\theta \cos^2\phi \sin^2\phi \qquad (24)$$

where:

$$V_1 = 12 V_0 r^{-12} - 12 V_0' r^{-6}$$

$$V_2 = (12 + 4\alpha + 4\beta + 4\gamma) V_0 r^{-12} - (12 + 4\delta + 4\zeta) V_0' r^{-6}$$

$$V_3 = (4\beta + 18\gamma) V_0 r^{-12} - 4\zeta V_0' r^{-6}$$

$$V_4 = (4\beta - 60\gamma) V_0 r^{-12} - 4\zeta V_0' r^{-6}$$

$$V_5 = 78\gamma V_0 r^{-12}$$

with $\alpha = 78\ d^2/r^2$ $\qquad \delta = 21\ d^2/r^2$

$\beta = 682.5\ d^4/r^4$ $\qquad \zeta = 63\ d^4/r^4$

$\gamma = 1547\ d^6/r^6$

In Eq. (24), $V_1 + V_2$ will give rise to a constant perturbation which affects all rotational energy levels equally and thus will not effect the rotational structure of the spectrum of the solute molecule. Hence the angle dependent potential $V(\theta\phi)$ may be written:

$$V(\theta\phi) = V_3 \cos^2\theta \sin^2\theta + (V_4 \sin^4\theta + V_5 \sin^6\theta) \cos^2\phi \sin^2\phi \qquad (25)$$

The potential given by Eq. (25)† may be considered as a perturbation and may be used to calculate corrections to the energy levels of the hindered rotator.

---

† It has been pointed out (49) that the potential, Eq.24, does not have the symmetry of the octahedral site, due to the inclusion of sixth power terms. Although this is inconsistant with the treatments of previous workers (11,13) the results are expected to be qualitatively correct.

4-5 Calculation of Energy Levels of the Hindered Rotator.

From perturbation theory (51), the first order energies for a degenerate level $E_J^{(0)}$ are the roots of a secular determinant. The number of rows and columns of the determinant is 2J + 1, the degeneracy of the level $E_J^{(0)}$. Such a determinant may be written:

$$\begin{vmatrix} V_{11} - E_{JM}^{(1)} & V_{12} & \cdots & V_{1\alpha} \\ V_{21} & V_{22} - E_{JM}^{(1)} & \cdots & V_{2\alpha} \\ \vdots & \vdots & & \vdots \\ V_{\alpha 1} & & & V_{\alpha\alpha} - E_{JM}^{(1)} \end{vmatrix} = 0 \qquad (26)$$

with $V_{ik} = \langle \psi_i | V | \psi_k \rangle$, where V is the perturbation and ψ_i, ψ_k are normalized orthogonal wave functions belonging to the unperturbed degenerate level $E_J^{(0)}$. The corrected energy levels are given by:

$$E_{JM} = E_J^{(0)} + E_{JM}^{(1)} \qquad (27)$$

In the case of a diatomic molecule, the normalized spherical harmonics Y_J^M are the zero order rotational wave functions. The first order corrections are given by:

J = 0 $$E_{00}^{(1)} = \langle Y_0^0 | V(\theta\phi) | Y_0^0 \rangle \qquad (28)$$

J = 1 $$\begin{vmatrix} (V_{11} - E_{1M}) & V_{12} & V_{13} \\ V_{21} & (V_{22} - E_{1M}) & V_{23} \\ V_{31} & V_{32} & (V_{33} - E_{1M}) \end{vmatrix} = 0 \qquad (29)$$

where: $$V_{ik} = \langle Y_1^{M_i} | V(\theta\phi) | Y_1^{M_k} \rangle \qquad (30)$$

with $M_i, M_k = 1, 0, -1$

$J = 2$

$$\begin{vmatrix} (V_{11} - E_{2m}) & V_{12} & V_{13} & V_{14} & V_{15} \\ V_{21} & (V_{22} - E_{2m}) & V_{23} & V_{24} & V_{25} \\ V_{31} & V_{32} & (V_{33} - E_{2m}) & V_{34} & V_{35} \\ V_{41} & V_{42} & V_{43} & (V_{44} - E_{2m}) & V_{45} \\ V_{51} & V_{52} & V_{53} & V_{54} & (V_{55} - E_{2m}) \end{vmatrix} = 0 \qquad (31)$$

where: $$V_{ik} = \langle Y_2^{M_i} | V(\theta\phi) | Y_2^{M_k} \rangle \qquad (32)$$

with $M_i, M_k = 2, 1, 0, -1, -2.$

All off diagonal terms in Eqs. (29) and (31) vanish because they all involve integrals of the form:

$$\int_0^{2\pi} \exp \pm i\, n\, \phi\, d\phi = 0 \quad (n = \text{a real non-zero integer})$$

A further simplification results from the property $(Y_J^M)^* = \pm (Y_J^{-M})$, so that Eqs. (29) and (31) give:

$$\begin{aligned} E_{1,1}^{(1)} &= E_{1,-1}^{(1)} = \langle Y_1^1 | V(\theta\phi) | Y_1^1 \rangle \\ E_{1,0}^{(1)} &= \langle Y_1^0 | V(\theta\phi) | Y_1^0 \rangle \\ E_{2,2}^{(1)} &= E_{2,-2}^{(1)} = \langle Y_2^2 | V(\theta\phi) | Y_2^2 \rangle \\ E_{2,1}^{(1)} &= E_{2,-1}^{(1)} = \langle Y_2^1 | V(\theta\phi) | Y_2^1 \rangle \\ E_{2,0}^{(1)} &= \langle Y_2^0 | V(\theta\phi) | Y_2^0 \rangle \end{aligned} \qquad (33)$$

The normalized spherical harmonics for J = 0, 1 and 2, are (51):

$$
\begin{aligned}
Y_0^0 &= \left(\frac{1}{4\pi}\right)^{\frac{1}{2}} \\
Y_1^1 &= -\left(\frac{3}{8\pi}\right)^{\frac{1}{2}} \sin\theta\, e^{i\phi} \\
Y_1^0 &= \left(\frac{3}{4\pi}\right)^{\frac{1}{2}} \cos\theta \\
Y_2^2 &= \left(\frac{15}{32\pi}\right)^{\frac{1}{2}} \sin^2\theta\, e^{2i\phi} \qquad (34) \\
Y_2^1 &= -\left(\frac{15}{8\pi}\right)^{\frac{1}{2}} \cos\theta \sin\theta\, e^{i\phi} \\
Y_2^0 &= \left(\frac{5}{16\pi}\right)^{\frac{1}{2}} (3\cos^2\theta - 1)
\end{aligned}
$$

The Y_J^M and the perturbing potential V (θ ϕ) from Eq. (25) were substituted into the expressions for $E_{JM}^{(1)}$ from Eqs. (33) and the resulting integrals evaluated. Use was made of tables of standard integrals (52) in the evaluation of the $E_{JM}^{(1)}$.

The first order energies were found to be identical for the J = 0 and J = 1 levels, but small splittings of the J = 2 levels were found. Numerical results were obtained using accepted values for the constants r and d. r = 3.83 A for solid argon (45), d = 1.275 A for HCl (38) and d = 1.420 A for HBr (39). The results are tabulated in Table 9.

To calculate the rotational energy levels for HCl and HBr, values must be assigned to the constants K_1 and K_2 of Table 9. Reasonable first order corrections to the rotational energy levels are obtained by giving r/r_0 the value 0.85 and ϵ_0 the value 10cm^{-1}.

TABLE 9.

First Order Energies for the Hindered Rotator.

(J,M)	$E'(J,M)$ HCl	HBr
(00)		
(1,0)	$12.7K_1 - 0.62K_2$	$21.8K_1 - 0.95\ K_2$
(1,± 1)		
(2,0)	$9.50K_1 - 0.44K_2$	$16.4K_1 - 0.68K_2$
(2,± 1)	$14.8K_1 - 0.73K_2$	$25.5K_1 - 1.13K_2$
(2,± 2)	$12.2K_1 - 0.59K_2$	$20.9K_1 - 0.91K_2$

where $K_1 = V_o\ r^{-12}$ and $K_2 = V_o'\ r^{-6}$

Using these arbitrary values the constants K_1 and K_2 were found to be 1.42 cm^{-1} and 3.77 cm^{-1} respectively. The first order energies were calculated, and are listed in column two of Table 10. Since we are only interested in energy differences, $E'(0,0)$ is set equal to zero, and the other first order energies are given relative to $E'(0,0)$. The unperturbed rotational energies for the ground vibrational state are given by:

$$E''_J = B'' J(J+1) - D'' J (J+1) \qquad (35)$$

where: B'' and D'' are the rotational constants for the ground vibrational state,

and have been tabulated in references (38) and (39) for HCl and HBr respectively. The hindered rotational levels are listed in column three of Table 10 and the last three columns give the relative populations of the energy levels at 5°, 10° and 20°K

using the formula:

$$N(J,M) = N(0,0)\ g \exp - E(J,M)/kT \qquad (36)$$

where: $N(J,M)$ is the number of molecules in the level (J,M), $N(0,0)$ is arbitrarily set equal to one ; g is the degeneracy of the level; k, the Boltzmann constant, and T, the absolute temperature.

It should be noted that the results of the above calculation are only qualitative in nature, owing to the many assumptions and approximations made.

TABLE 10.

Hindered Rotational Energy Levels and Populations for HCl and HBr in Argon.

(a) HCl

Level J,M	1st Order Energy $E'(J,M)$ cm^{-1}	Corrected Energy Level cm^{-1}	Relative Population 5°K	10°K	20°K
0,0	0.0	0.0	1	1	1
1,0	0.0	20.9	.002	.05	.22
1,±1	0.0	20.9	.004	.10	.44
2,0	-3.8	58.8	-	-	.01
2,±1	+2.6	65.2	-	-	.02
2,±2	-0.6	62.0	-	-	.02

(b) HBr

Level J,M	1st Order Energy $E'(J,M)$ cm^{-1}	Corrected Energy Level cm^{-1}	Relative Population 5°K	10°K	20°K
0,0	0.0	0.0	1	1	1
1,0	0.0	16.7	0.008	0.09	0.30
1,±1	0.0	16.7	0.016	0.18	0.61
2,0	-6.6	43.6	-	0.001	0.03
2,±1	+4.6	54.8	-	0.002	0.06
2,±2	-1.1	49.1	-	0.002	0.06

4-6 Shifts Due to Solute-Solute Interactions.

In this section, interactions between solute molecules in nearest neighbour, next nearest neighbour, etc. sites will be considered.

The potential energy of interaction between two ideal dipoles is given by (45):

$$\phi_{ab} = \frac{\mu_a \mu_b}{r_{ab}^3} \left[-2\cos\theta_a \cos\theta_b - \sin\theta_a \sin\theta_b \cos(\phi_b - \phi_a) \right] \quad (37)$$

At low temperatures, where ϕ_{ab} is greater than kT, the dipoles are assumed to be aligned to give maximum attraction. That is, $\phi_b = \phi_a$ and $\theta_b = \theta_a$; Eq. (37) then becomes:

$$\phi_{ab} = \frac{\mu_a \mu_b}{r_{ab}^3} (1 - 3\cos^2\theta) \quad (38)$$

The maximum value of Eq. (38) is obtained when $\theta = 0$, hence

$$\phi_{ab} = -\frac{2\mu_a \mu_b}{r_{ab}^3} \quad (39)$$

The shift in vibrational frequency for the case of interaction between like dipoles is then given by:

$$\Delta\nu = \frac{-2\,\Delta(\mu^2)}{r_{ab}^3\, hc} = -C_4\,\Delta(\mu^2) \quad (40)$$

where: $\Delta(\mu^2)$ is the change in the square of the dipole moment during a transition from the ground state to the first excited vibrational state.

For the case of interaction between unlike dipoles:

$$\Delta \nu_a = - C_4 \mu_b \Delta \mu_a \qquad (41)$$

Values of the constant C_4 in Eqs. (40) and (41) are tabulated in Table 11 for various values of r_{ab} encountered in the cubic lattices of argon, krypton and nitrogen, assuming that the dipoles are trapped on substitutional sites in the lattice.

Other terms in the interaction energy between pairs of dipoles could be included. These arise from induction and dispersion forces. However, the intermolecular potentials due to these effects both involve the inverse sixth power of the intermolecular distance, and even for the case of contiguous solute molecules, the contribution to the shift of vibrational frequency is negligible.

TABLE 11.

Values of the constant C_4 in Eq.(40) in units of 10^{37} esu^{-2} cm^{-3}.

r_{ab}	Argon	Krypton	Nitrogen
r	17.92	15.27	15.85
$\sqrt{2}$ r	6.34	5.40	5.60
$\sqrt{3}$ r	3.45	2.94	3.05
2 r	2.24	1.91	1.98

CHAPTER 5. DISCUSSION.

5-1 Classification of Peaks in the Matrix Spectra of HCl and HBr.

The observed peaks in the matrix spectra can be classified according to their behaviour under various conditions. Closer examination of the spectra of HCl (Figs. 5-7) and HBr (Figs. 13-15) reveals that the observed peaks fall into four groups:

(i) Peaks which are present at all matrix to solute ratios, whose intensities relative to other peaks in the spectrum increase with dilution.

(ii) Peaks which are present at low matrix to solute ratios whose intensities relative to group (i) decrease with dilution.

(iii) Peaks which appear during warm-up studies.

(iv) Peaks which are only present when other solutes are included in the mixtures.

Division of peaks in the spectra of HCl and HBr among the first three categories is made in Table 12.

The behaviour with dilution of the four most important peaks in the spectra of HBr and HCl in argon, is illustrated graphically in Fig. 22. In the case of HBr, it is seen that, relative to the peak at 2569 cm^{-1}, the intensity of the peak at 2550 cm^{-1} remains constant, while those at 2496 and 2465 cm^{-1} decrease with dilution. A similar situation is found for HCl where the intensity of the peak at 2853 cm^{-1} relative to the peak at 2889 cm^{-1} remains constant, while those at 2817 and 2787.5 cm^{-1}

TABLE 12.

Classification of Observed Peaks in the Spectra of HCl and HBr in argon.

	Group (i)	Group (ii)	Group (iii)
HCl			2749*
			2761*
		2787	2787
		2817	
	2853		
		2863	
		2867	
	2889		
	2900 sh		
HBr			2426*
			2436*
			2450*
		2465	
		2496	
	2550		
		2558	
	2569		
	2575 sh		

*These peaks were only observed during warm-up and were not previously included in Table 1.

fig 22.

CHANGE OF PEAK INTENSITY WITH DILUTION

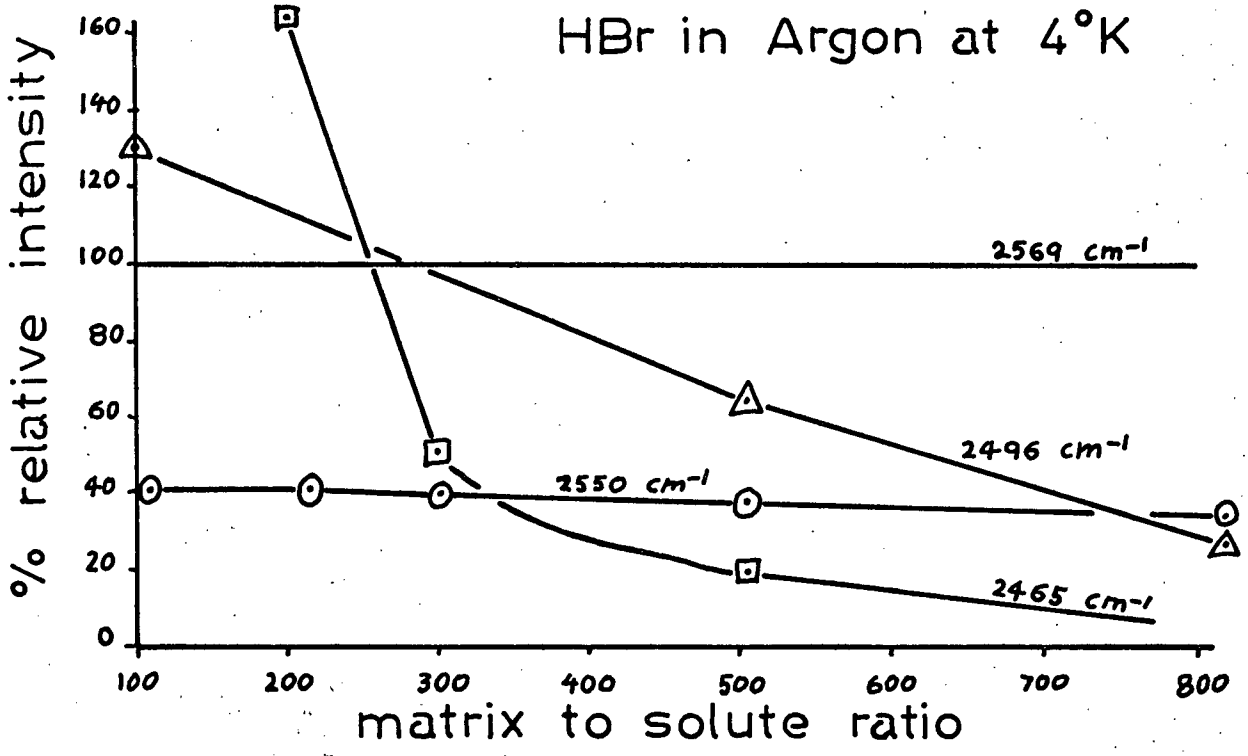

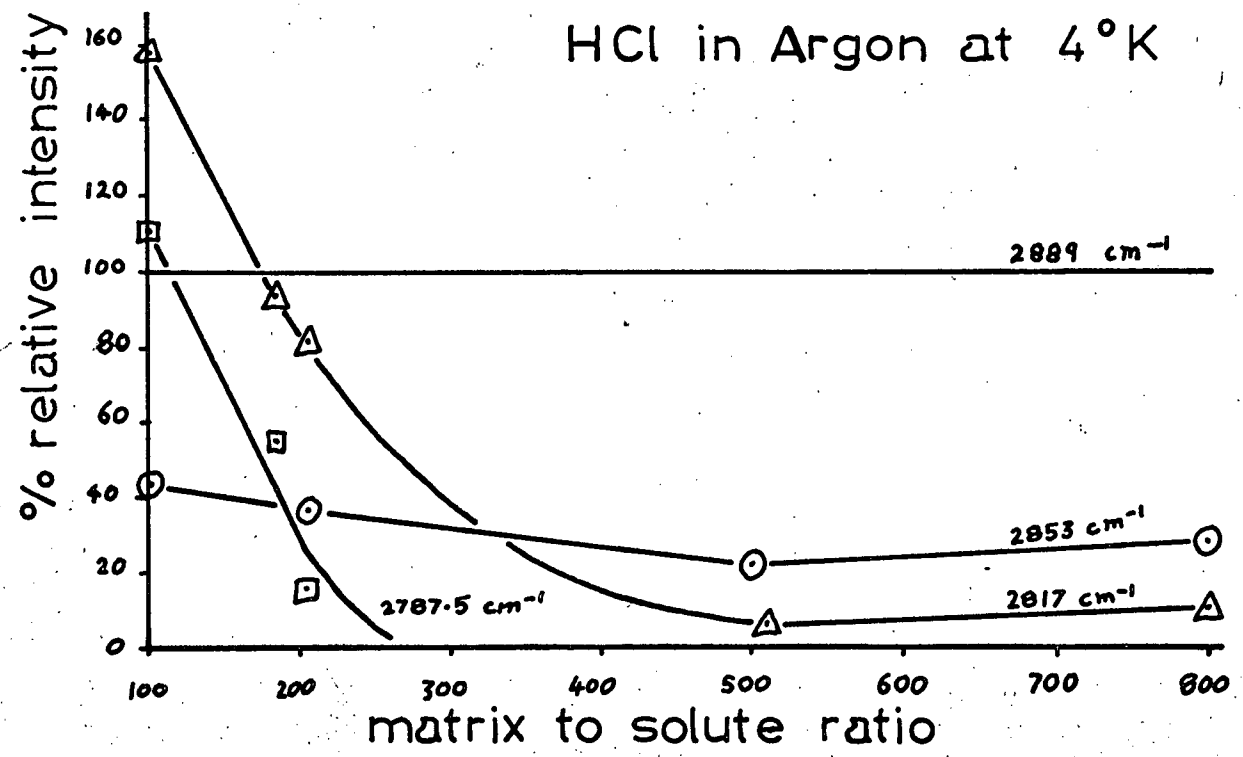

decrease rapidly on dilution.

It seems reasonable to assume that peaks in the first category are due to isolated HCl or HBr molecules. These peaks would be the only ones observed in studies of very dilute mixtures carefully deposited to minimize the possibility of diffusion of solute molecules. It is suggested that interactions between pairs of solute molecules in contiguous and other adjacent sites, as illustrated in Fig. 23, account for the peaks which decrease in intensity with dilution. Probabilities for finding such pairs at various matrix to solute ratios have been calculated (53) assuming a random distribution of solute molecules on substitutional sites in a cubic close-packed crystal.

For the peaks which only appear during warm-up, a similar explanation is offered. In this case, however, interactions between more than two solute molecules are suggested. Such interactions are expected to be important during warm-up, since diffusion of the trapped molecules would enable triple and larger clusters to be formed. At temperatures close to the melting point of the matrix, peaks appear in the region of solid HCl or HBr. From the work of Hornig and his co-workers (54,55,56), it is reasonable to assume that these peaks are due to hydrogen-bonded chains of varying length.

In many cases it was possible to resolve peaks in the spectrum of HCl into doublets due to the HCl^{35} and HCl^{37} isotopic molecules. It is perhaps significant that certain other peaks in the same spectrum remained unresolved under the same conditions of high resolution. These peaks were usually broader than the

fig 23.

CLOSE - PACKED - CUBIC STRUCTURE

showing first, second, third & fourth nearest neighbour positions

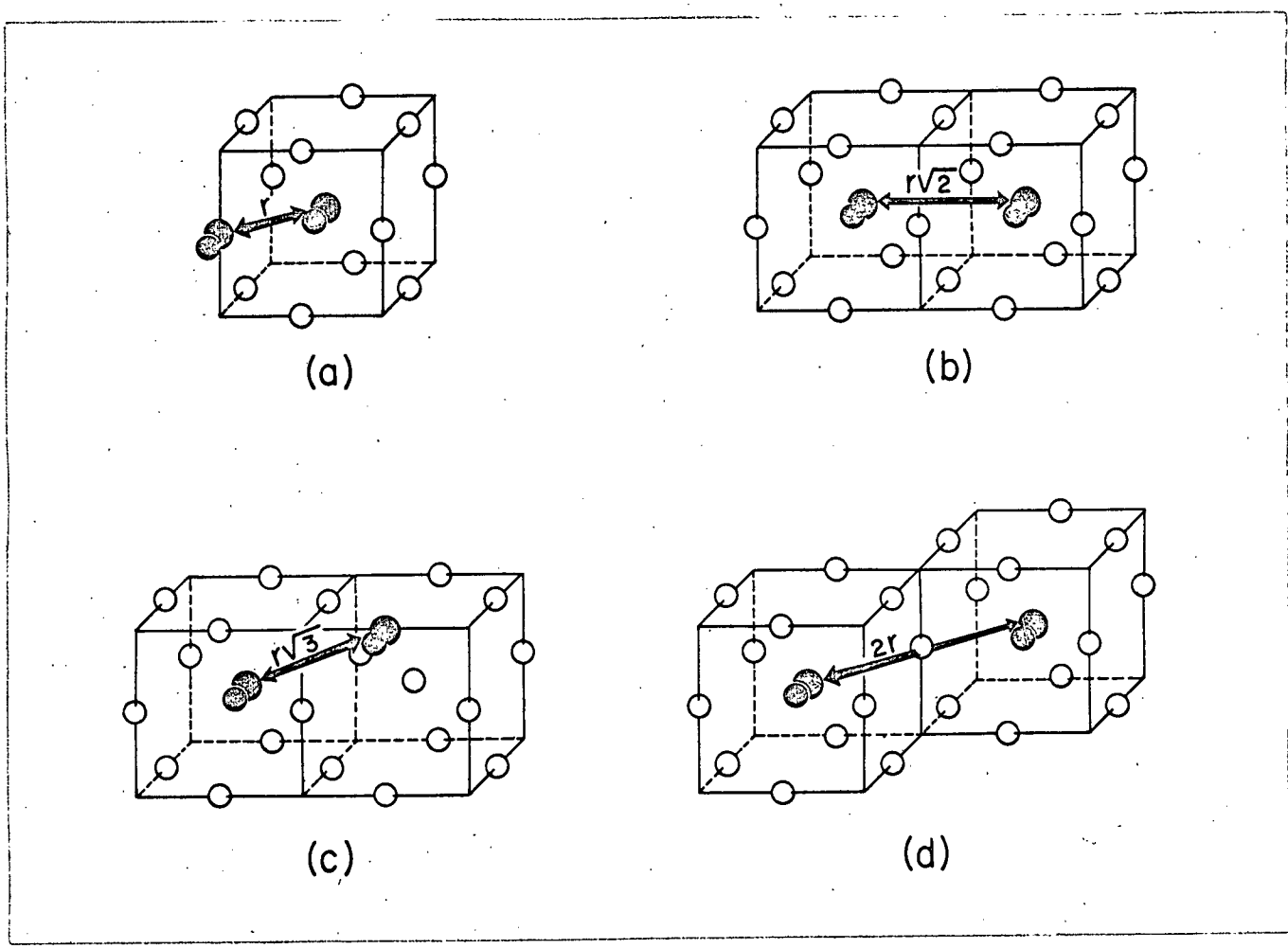

resolvable ones and often corresponded to the group (i) peaks. However, the problem of scattering with the consequent loss of resolution makes this latter classification uncertain.

5-2 Isolated Solute Molecules.

The observed infrared spectra of HCl and HBr in solid matrices, indicate that the statistically predicted isolation of solute molecules (57) was never achieved under the experimented conditions employed in this work. However, isolation approaching the statistical values was usually obtained when high matrix to solute ratios were used.

The three peaks which are assigned to HCl molecules isolated in argon are: the very strong peak at 2889 cm^{-1}, the shoulder at 2900 cm^{-1} and the peak of medium intensity at 2853 cm^{-1}. These three peaks make up a vibration-rotation band centred at 2871 cm^{-1} which is shifted by -13.5 cm^{-1} from the gas phase. A similar situation holds for HBr in argon where the observed frequencies are: 2550, 2569 and 2575 cm^{-1}. The corresponding band centre is at 2559.5 cm^{-1}, which represents a shift from the gas phase of +1 cm^{-1}.

In a discussion of the behaviour of isolated solute molecules in inert matrices it is necessary to consider several effects which, for the purpose of interpreting the observed infrared spectra, will be considered separately under the headings of vibration and rotation. In the first case, we examine the causes and effects of perturbations of the vibrational potential function of the molecule. Under the second heading, we consider the hindered rotation of the isolated

solute molecule.

One could circumvent the problem of the observed gas-matrix shift of the vibration-rotation band centre by invoking a change in the force constant of the solute molecule. Hornig and Osberg (54) estimated that the force constant of HCl decreases from 4.81 md/A in the gas to 4.31 md/A in the solid state. A smaller change is expected going from gas to matrix, and for HCl in argon the calculated value is 4.73 md/A. However, for HBr in argon, a slight increase in the force constant is necessary to account for the observed frequency shift. Force constants for HBr and HCl in various matrices are compared in Table 13 using the expression:

$$f(\text{matrix}) = f\ (\text{gas}) \left[\frac{\nu(\text{matrix})}{\nu(\text{gas})}\right]^2$$

TABLE 13.

Force constants of HBr and HCl in various matrices.

State	Force Constant (md/A) HBr	HCl
gas	3.85	4.81
solid	3.45	4.31
argon matrix	3.85	4.77
krypton matrix	3.80	4.72
nitrogen matrix	3.75	4.64

One might also consider the anharmonicity of the vibration of the solute molecule in a discussion of the shift of the vibrational frequency. An increase in the anharmonicity constant $\omega_e x_e$ would result in a shift to lower wave numbers, in agreement with experiment. However, Vodar et al (31) note that $\omega_e x_e$ for HCl or HBr decreases considerably in the solid state and as a result, the change of We is larger than the observed shift. It is not possible, however, to discuss changes in the anharmonicity of a matrix isolated solute molecule without knowledge of frequency shifts of overtone bands. The intensity of the overtones of HCl and HBr were too weak to be observed in the matrix work, because of the small amounts of material in the deposits studied.

In the event that changes of force constants or anharmonicities could account for the observed vibrational shifts in a consistant way, the question of the origin of these effects would still remain unanswered. A far more satisfactory approach is to consider the perturbing forces which could effect the potential function of the solute molecule.

5-3 Intermolecular Forces Between Solute and Matrix.

In section 4-2 we considered induction, dispersion and electrostatic effects, all of which give rise to a "red" shift of the vibrational frequency. To these three attractive interactions we must add the repulsive forces which produce a shift in the opposite direction. Repulsive forces are usually ignored (11, 12, 20), but Maki and Decius (58), van der Elsken (59) and Bryant and Turrell (60) considered these forces in their inter-

pretation of spectra of ions isolated in alkali halide lattices.

The observed shifts of band centres for matrix isolated HCl and HBr, which are tabulated in Table 14, can be expressed as a sum of four terms:

$$\Delta\nu(obs) \doteq \Delta\nu(ind) + \Delta\nu(dis) + \Delta\nu(es) + \Delta\nu(rep) \qquad (42)$$

($\Delta\nu$ (es) being zero for the rare gases.)

TABLE 14.

Observed Band Centres of Matrix-Isolated HCl and HBr.

Molecule	Gas Phase	In Argon	In Krypton	In Nitrogen
HCl band centre*	2884.5	2871	2856	2833
shift	-	-13.5	-28.5	-51.5
HBr band centre	2558.5	2559.5	2541	2525.5
shift	-	+1	-17.5	-33

*mean value for HCl^{35} and HCl^{37}.

We will now consider shifts of the band centre of HCl in the various matrices. The first term in Eq. (42) is given by Eq.4:

$$\Delta\nu(ind) = -C_1 \Delta(\mu_a^2)$$

Values of the constant C_1 have been tabulated in Table 8, so to evaluate $\Delta\nu$ (ind) we need a value for the change in the square of the dipole moment during the vibrational transition. Benedict et al (61) have given a dipole moment function for HCl:

$$\mu = M_0 + M_1(r-r_e) + M_2(r-r_e)^2 + \cdots \qquad (43)$$

where: $M_0 = 1.085$ Debye
$M_1 = 0.880$ D/A
$M_2 = 0.082$ D/A^2

Values of $d\mu/dr$ for the crystalline hydrogen halides have been reported by Friedrich and Person (62) and for HCl, $d\mu/dr = 2.12$ D/A. Neglecting the quadratic term in Eq. (43), we obtain an expression for $\Delta(\mu^2)$

$$\mu_1^2 - \mu_0^2 = M_1^2 \left[(r_1 - r_e)^2 - (r_0 - r_e)^2 \right] + 2 M_0 M_1 (r_1 - r_0) \qquad (44)$$

where: r_0 and r_1 are the internuclear distances in HCl for the ground and first excited vibrational states, and r_e is the equilibrium internuclear distance.

For HCl gas $r_e = 1.275$ A and $r_0 = 1.284$ A from reference (38). To obtain an estimate of $\Delta(\mu^2)$ in the matrix, we use the observed splitting of the R(0) and P(1) peaks to calculate r_1, assuming:

$$\nu R(0) - \nu P(1) = 4 B_1 \qquad (45)$$

where: B_1 is the rotational constant for the first excited vibrational state.

This is a poor approximation since:

$$\nu R(0) - \nu P(1) = 2(B_0 + B_1) \qquad (46)$$

where: B_0 is the rotational constant for the ground state, and probably also changes in the matrix. However, using Eq.(45) we can obtain an order of magnitude for the induction shift. The observed value of $\nu R(0) - \nu P(1)$ was 36 cm^{-1} for HCl in both argon and krypton, and 38 cm^{-1} in the nitrogen matrix. Now r_1 is given by:

$$r_1 = \sqrt{\frac{h}{8\pi^2 c m B_1}} \qquad (47)$$

In a private communication from D. F. Eggers Jr., it was pointed out that in the above calculation, $\Delta\nu$ (ind) vanishes in the harmonic approximation (i.e. when $r_1 = r_0 = r_e$). However, the approach used by Maki and Decius (58) gives a non zero value for $\Delta\nu$ (ind) in any approximation. These workers follow the treatment adopted in chapter 4-2 as far as Eq. (3).

$$\phi(ind) = -\frac{14.45\,\mu_a^2\,\alpha_b}{r^6}$$

Then, to estimate the effect upon the vibrational frequencies μ_a is replaced by : $(\partial\mu_a/\partial Q)_0 Q$. In this case the change in the square of the dipole moment between the ground and first excited vibrational states is given by:

$$\left(\frac{\partial\mu_a}{\partial Q}\right)_0 \left\langle Q_1^2 \right\rangle - \left\langle Q_0^2 \right\rangle \qquad (42a)$$

where: $\langle\ \rangle$ denotes a quantum mechanical mean value.

Using the harmonic oscillator wave functions we find:

$$\left\langle Q_1^2 \right\rangle - \left\langle Q_0^2 \right\rangle = \frac{h}{4\pi^2 c\,\nu_0} \qquad (42b)$$

where: ν_0 is the gas phase vibrational frequency in cm^{-1}.

By substitution of Eq. (42b) and Eq. (42a) into Eq. (3), the shift of vibrational frequency is given by:

$$\Delta\nu(ind) = -\left(\frac{\partial\mu_a}{\partial Q}\right)^2 \frac{C_1 h}{4\pi^2 c\,\nu_0} \qquad (42c)$$

where: C_1 is the value in Table 8.

Now $$\left(\frac{\partial \mu_a}{\partial Q}\right)_0^2 = \left(\frac{\partial \mu_a}{\partial r}\right)_0^2 \frac{1}{m} \qquad (42d)$$

where: m is the reduced mass.

Hence, using the previous value for $\partial \mu_a / \partial r$ we find for HCl:

$$\left(\frac{\partial \mu_a}{\partial Q}\right)^2 = 2.01 \times 10^4 \text{ esu}^2 \text{ g}^{-1}$$

Finally, the vibrational shifts were found to be:

$$\Delta\nu(ind) = -1.5 \text{ cm}^{-1} \quad \text{for Ar and Kr,}$$

$$\text{and } \Delta\nu(ind) = -1.2 \text{ cm}^{-1} \quad \text{for } N_2.$$

It is seen that these shifts are an order of magnitude less than those calculated in the anharmonic approximation. The two treatments would appear to supplement each other, and in spite of the inaccuracy of the present calculation, it seems that the anharmonic contribution is the most important term. It is unfortunate that no data on the overtone bands of HCl in the matrix is available at this time since this would give valuable information on the anharmonicity of the potential function.

where: h is Planck's constant, c is the velocity of light and m the reduced mass for HCl.

Hence r_i = 1.38 A in the rare gas matrices and r_i = 1.35 A in nitrogen. Substituting the values of r_e, r_o and r_i into Eq. (44) together with a value for M_1 of 1.8 D/A for HCl in the matrix, we find

$\Delta(\mu^2) = 4.2 \times 10^{-37}$ esu^2 cm^2 for HCl in argon or krypton and

$\Delta(\mu^2) = 2.6 \times 10^{-37}$ for HCl in nitrogen. Now, using the results of Table 8, we may calculate the shifts due to the induction forces:

$\Delta\nu$ (ind) = -16 cm^{-1} in argon

$\Delta\nu$ (ind) = -17 cm^{-1} in krypton

$\Delta\nu$ (ind) = -8 cm^{-1} in nitrogen.

The second term in Eq. (42) can be evaluated if we can estimate the change in α_a and E_a in Eq. (9):

$$\Delta\nu(dis) = -C_2\left[\frac{\alpha_a' E_a'}{E_a' + E_b} - \frac{\alpha_a'' E_a''}{E_a'' + E_b}\right]$$

where: two primes denote the ground state and one prime the first excited vibrational state.

The ionization potentials E_b for argon, krypton and nitrogen are 126,475 cm^{-1}, 112,359 cm^{-1} and 125,104 cm^{-1}, respectively (63). The ionization potential of HCl in the ground state E_a'' is 111,311 cm^{-1} (63) and the difference between the ground and first excited vibrational state is taken as the vibrational frequency in the matrix. Hence E_a' is 108,440 cm^{-1} in argon, 108,455 cm^{-1} in krypton and 108,478 cm^{-1} in nitrogen.

To estimate the change in polarizability, we expand α in

terms of the change in internuclear distance ($r - r_e$):

$$\alpha = \alpha_0 + \alpha_1 (r - r_e) + \cdots \qquad (48)$$

Values of α_1 for various molecules have been estimated by Stansbury et al (64) from intensity measurements of Raman spectra. For HCl the value was 1.0 A^2. Taking α_0 as 2.63 A^3 (65) and α_1 as 1.0 A^2 in Eq. (48) we get $\alpha_a' = 2.74$ A^3 for HCl in argon and krypton matrices, and $\alpha_a' = 2.70$ A^3 in nitrogen. Using these values, together with E_a'', E_a', and E_b, the shifts due to the dispersion forces were calculated:

$\Delta\nu$ (dis) = -48 cm^{-1} for argon,
$\Delta\nu$ (dis) = -49 cm^{-1} for krypton,
$\Delta\nu$ (dis) = -18 cm^{-1} for nitrogen.

Thus, the shifts due to dispersion forces are larger than those due to induction forces, in agreement with the work of Ben Reuven et al (66). These workers used an approach similar to the present one, to calculate pressure-induced shifts of HCl lines due to noble gases.

In the case of HCl in nitrogen, there is a contribution from the third term in Eq. (42). The expression for $\Delta\nu$ (es) was given by Eq. (12):

$$\Delta\nu(es) = -C_3 \Delta\mu_a$$

Using Eq. (43) the change in dipole moment of HCl during a vibrational transition is:

$$\Delta\mu = M_1 (r_1 - r_0) \qquad (49)$$

Using the same values of r_o and r_1 as before, Eq. (49) gives $\Delta\mu$ = 0.11 D for HCl in nitrogen, and the corresponding shift $\Delta\nu$(es) = -56 cm^{-1}.

The results of the above calculations for HCl in argon, krypton and nitrogen matrices are listed in Table 15 together with the observed gas-matrix shifts. Although the accuracy of these calculations is undoubtedly questionable, they do consistently predict a greater "red" shift than was observed. Thus, it is reasonable to assume that repulsive forces contribute to the overall shift.

Since repulsive forces arise from overlap of charge clouds, it is instructive to compare the relative sizes of HCl, argon, krypton and nitrogen. This is done in Fig. 24, where it is seen that the HCl molecule is larger than a substitutional site in any of the three matrices. On spatial grounds one would expect the repulsive interaction to increase in the order krypton, nitrogen, argon, but from Table 15 the apparent order obtained by subtracting $\Delta\nu$ (obs) from $\Delta\nu$ (calc) is nitrogen, krypton, argon. The explanation for this may well lie in the value taken for r_1, the internuclear distance in the excited vibrational state. The value estimated for this quantity was very approximate, and a smaller value of r_1 would result in smaller values of $\Delta\nu$ (ind) and $\Delta\nu$ (disp). Thus the contribution from the repulsive forces for HCl in nitrogen could be between the values for the argon and krypton matrices.

It should be emphasised that the numerical results of this section are orders of magnitude only, since many assumptions and

TABLE 15.

Vibrational Shifts in cm^{-1} for HCl in Various Matrices.

Matrix	$\Delta\nu$ (total) observed.	$\Delta\nu$ (es) calc.	$\Delta\nu$ (ind) calc.	$\Delta\nu$ (disp) calc.
Ar	-13.5	-	-16	-48
Kr	-28.5	-	-17	-49
N_2	-51.5	-56	-8	-18

fig 24.
RELATIVE SIZES OF SOME MOLECULES

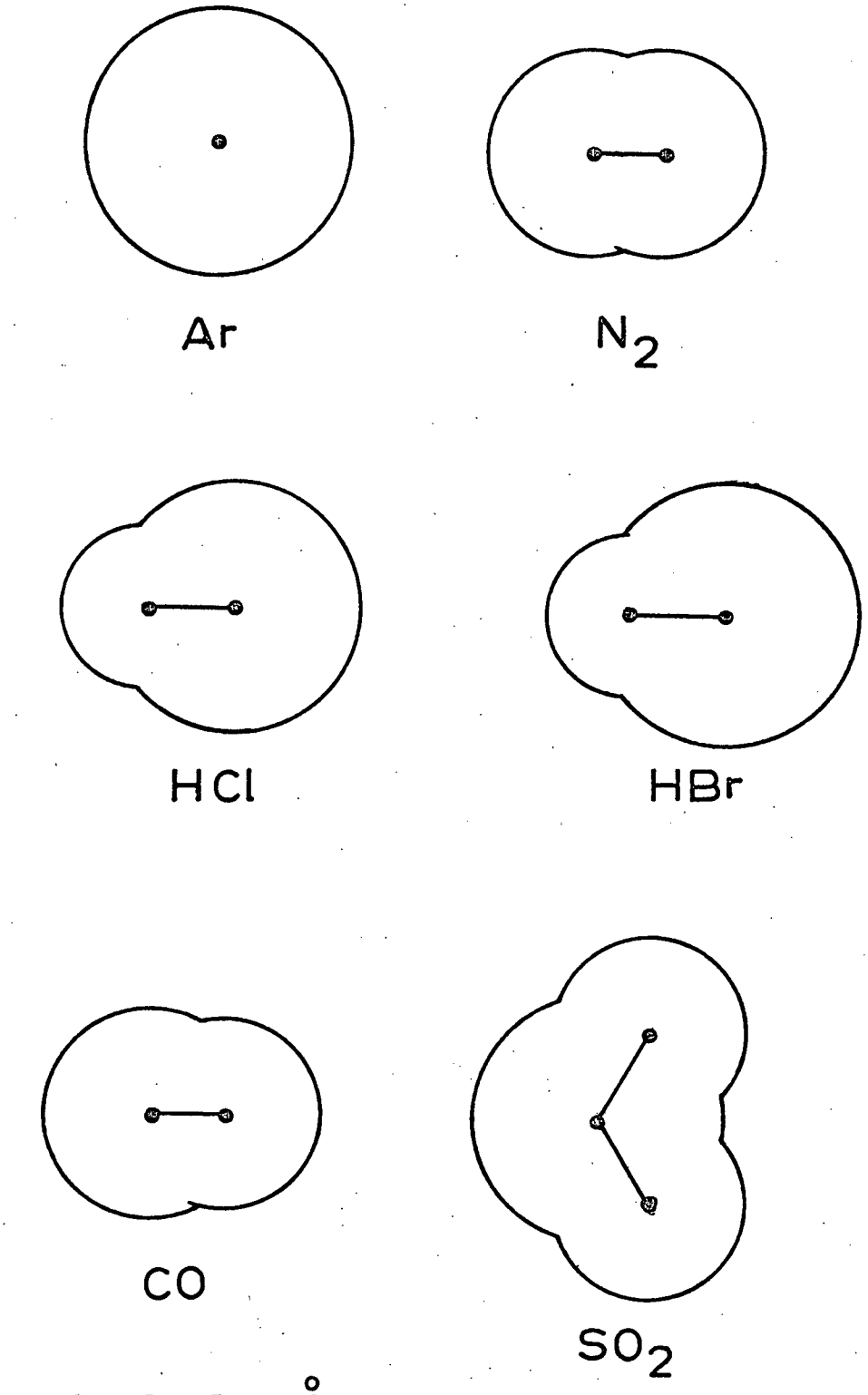

approximations were made in the calculations.

Calculations of the gas-matrix shifts for HBr could be carried out in the same way as for HCl. This has not been done here because the value of r, calculated from the observed splitting between R(0) and P(1) peaks is not reasonable. However, an idea of the magnitudes of the shifts relative to those calculated for HCl can be obtained by comparing the dipole moments, polarizabilities and ionization potentials of HCl and HBr, listed in Appendix 2.

The dipole moment of HBr is smaller than that of HCl, which suggests a smaller dipole derivative. The value of $d\mu/dr$ quoted by Friedrich and Person (62) for solid HBr was 1.72 D/A compared with 2.12 D/A for solid HCl. A similar gas-matrix change in r, is expected for HBr as for HCl. Thus, the value of $\Delta(\mu^2)$ in Eq. (44) is expected to be smaller for HBr than for HCl, hence the value of $\Delta\nu$ (ind) for HBr will be smaller.

The dispersion shift depends on the polarizability and ionization potential in the ground and first excited vibrational states Eq. (12). In Appendix 2, the ionization potential of HBr is seen to be less than that of HCl, while the polarizability is considerably larger for HBr than for HCl. It is expected, therefore, that $\Delta\nu$ (dis) for HBr in the matrix will be larger than the values for HCl. The overall attractive effects compared with HCl may well be similar or perhaps larger for HBr.

On spatial grounds, one would expect the repulsive forces to be greater in HBr than in HCl, since the HBr molecule is larger

than HCl (see Fig. 24). Repulsive forces usually give rise to an upward shift of vibrational frequency, thus an increase in repulsive interaction could account for the smaller "red" shifts observed for HBr in the matrix compared to the HCl case.

5-4 Rotation of Isolated Solute Molecules.

There is considerable evidence in the literature supporting free or nearly free rotation of small molecules in inert matrices. In the present study, groups of absorption peaks in the spectra of HCl and HBr in argon, krypton and nitrogen matrices, are assigned to vibration-rotation bands. However, several features must be explained before the issue is finally settled.

The first problem is the observed splitting of the R(0) and P(1) peaks in the matrix spectra of HCl and HBr, which gives rise to rotational constants smaller than the gas phase values. No theoretical treatment to date has predicted a change of $\nu R(0) - \nu P(1)$ in the matrix. However, very recently, Gebbie and Stone (67) measured widths and shifts of pure rotation lines of HCl perturbed by rare gases and found that the only line for which there was any measurable shift was the J(0-1) line. This corresponds to R(0) of the vibration-rotation spectrum. A perturbation which affects R(0) more than P(1) could account for the observed change in $4B$[†] if both shifts were to the "red". Ben-Reuven et al (66) report "red" shifts of vibration-rotation lines of HCl perturbed by noble gases, except R(0) in argon and krypton which

---

† Actually, the separation of R(0) and P(1) is $2(B_1+B_0)$, and both B_1 and B_0 may change in the matrix.

is shifted to the "blue". These workers also note that for low J numbers the shifts of corresponding lines are greater in the P branch than in the R branch. In other words, the observed splitting between R(0) and P(1) is increased by addition of noble gases, contrary to the observations for HCl in solid rare gases.

An interesting feature of the spectrum of HCl in nitrogen was the small change in the separations between R(1), R(0) and P(1), going from gas to matrix. On this basis it would appear that the HCl molecule experiences less perturbation of its rotational levels in nitrogen than in the rare gas matrices, in spite of the greater shift of the band centre. This could be due to smaller repulsive forces in the nitrogen matrix, in agreement with the calculations of the previous section.

The perturbation treatment of the previous chapter predicts a splitting of the R(1) peak of HCl or HBr into three components. The calculated frequencies are listed in Table 16 for these molecules in argon. For these calculations the selection rules $J = \pm 1$ and $M = 0, \pm 1$ apply, and no violations of these selection rules are predicted by first order perturbation theory (69). The frequencies of the allowed transitions are given by:

$$\nu R^{0}(0) = \nu_{o}' R(0) + E'(1,0)$$
$$\nu R^{0}(1) = \nu_{o}' R(1) + E'(2,0) - E'(1,0)$$
$$\nu R^{\pm}(1) = \nu_{o}' R(1) + E'(2,\pm 1) - E'(1,\pm 1)$$
$$\nu P^{0}(1) = \nu_{o}' P(1) - E'(1,0)$$
$$\nu R^{\pm}(1) = \nu_{o}' R(1) + E'(2,\pm 2) - E'(1,\pm 1)$$

where: $E'(0,0)$ has been arbitrarily set equal to zero. The ν_{o}' are the gas phase frequencies corrected for the shift of the band centre in the matrix. The superscript on the symbol $\nu R^{m}(0)$ refers to the value of the quantum number M, of the lower level.

TABLE 16.

Predicted Spectrum of HCl and HBr in Argon, Compared With Observed and Gas Phase Spectrum.

(a) HCl

Peak		Frequencies in cm^{-1} Calculated	Observed	Gas Phase
P^{o}	(1)	2850.5	2853	2864
R^{o}	(0)	2891.5	2889	2905
R^{o}	(1)	2907.5	2900	2925
$R^{\pm 1}$	(1)	2914 2911	-	-

(b) HBr

Peak		Frequencies in cm^{-1} Calculated	Observed	Gas Phase
P^{o}	(1)	2543	2550	2542
R^{o}	(0)	2576	2569	2575
R^{o}	(1)	2585	2575	2591
$R^{\pm 1}$	(1)	2596.5 2591	-	-

Splitting of the R(1) peak was not observed in either the present work or the work of Schoen et al (8). Previous hindered rotational calculations (8, 12, 13, 14) also predicted a splitting of the R(1) peak. Thus, it appears that a theory is needed which will predict perturbations of all rotational energy levels of the solute molecule, but which does not remove the degeneracy of these levels.

It has been suggested (69) that in an octahedral field with a barrier height of about 10 cm^{-1}, the J = 0 level ($E = 0.0\ cm^{-1}$) of HCl would be perturbed considerably more than the J = 1 level ($E = 20.9\ cm^{-1}$). The physical interpretation of this (69) is that a molecule in the J = 0 level does not rotate, but executes oscillations about some mean position, whereas a molecule in the J = 1 level can undergo more or less free rotation. Such a model would predict a spectrum in agreement with the observed spectrum.

A second major problem is the observed relative intensities in the matrix spectra. In Table 17, the observed intensity ratios of the R(0) and P(1) peaks of HCl and HBr in various matrices, are compared with calculated ratios at several temperatures. A simple explanation for the observed intensities is that the temperature of the deposit during the recording of the spectrum may not have been $4^{\circ}K$, but in fact, several degrees higher. The very poor thermal conductivity of the solid rare gases (70) could enable a thermal gradient to be established in the deposit, with the surface layers at a higher temperature than the layers near the caesium

iodide plate. This idea is supported by the intensity ratios for HCl and HBr in nitrogen which are much closer to the 5°K figure (see Table 17). The thermal conductivity of nitrogen (71) is 2.5 times that of argon and 7 times that of krypton at 5°K, thus the warming of the deposit by the incident radiation should be less important in the nitrogen matrix. Further evidence for the warming of the rare gas deposits was provided by the warm-up study of HCl in nitrogen (see Fig. 12). At 15°K the intensity of P(1) relative to R(0) was the same as that observed for HCl in the rare gas matrices at the lowest temperature, when the thermocouple recorded 4°K.

TABLE 17.

Intensities of the P(1) peak of HCl and HBr Relative to R(0) = 100, in Various Matrices.

(a) HCl

Matrix	Observed 4°K*	Calculated 5°K	10°K	20°K
Ar	30	0.6	15	66
Kr	30	0.6	15	66
N_2	4	0.6	15	66

(b) HBr

Matrix	Observed 4°K*	Calculated 5°K	10°K	20°K
Ar	40	2.4	27	91
Kr	35	2.4	27	91
N_2	3	2.4	27	91

*It is believed that in the noble gas matrices the temperature was several degrees above 4°K. See text for discussion of this point.

One further intensity anomaly is found in the spectra of HBr and HCl in the rare gas matrices. The shoulder on the high frequency side of R(0), which is assigned to R(1), is much weaker than the P(1) peak. The intensities of these peaks should be comparable since they both originate from the J = 1 level. In fact, in the gas phase, R(1) is somewhat stronger than P(1), due to the difference in absorption frequencies and transition moments for these two lines. The energy absorbed during a transition from the mth to the nth energy level is given by (68):

$$dE = K N_m \nu_{mn} \left| \mu_{mn} \right|^2 \tag{51}$$

where: K is a constant, Nm is the population of the mth level, ν mn is the absorption frequency, and $\left| \mu_{mn} \right|$ is the transition moment.

From Eq. (51) the ratio of the intensities of R(1) and P(1) is:

$$I_{R(1)} / I_{P(1)} = \frac{\nu_{R(1)} \left| \mu_{R(1)} \right|^2}{\nu_{P(1)} \left| \mu_{P(1)} \right|^2} \tag{52}$$

In the gas phase $I_{R(1)}/I_{P(1)}$ is found to be 1.5 for HCl and 1.3 for HBr, while in the matrix, the ratio is of the order of 0.3. The explanation may be that the R(1) peak in the matrix is close to the relatively broad R(0) peak and some of the R(1) intensity is included in this very strong peak. However, it seems doubtful that this could account for the factor of five between the gas and matrix intensities.

5-5 Interactions Between Solute Molecules.

It is suggested that interactions between non-isolated solute molecules give rise to the peaks classified in section 5-1 into groups ii, iii and iv. Such pairs, triple clusters, etc., could be formed by diffusion of solute molecules in the lattice. The thermal conductivity of the solid rare gases is very small (70), and it is quite possible that the new layers of deposit are not cooled to $4^{\circ}K$ rapidly enough to prevent diffusion entirely. This is supported by experiments in which a mixture was deposited at the normal rate, and very rapidly, and the resulting spectra compared. In the case of rapid deposit, additional peaks were observed, many of which were only observed during warm-up of the slowly deposited mixture.

Statistically (53), the most probable pair of solute molecules is the third nearest neighbour pair (see Fig. 23). However, when diffusion occurs, the nearest neighbour pair (i.e. the dimer) is energetically more favourable. Shifts of vibrational frequencies due to dipole-dipole interaction between pairs of solute molecules may be calculated using the values of $\Delta(\mu^2)$ for HCl estimated in section 5-2, and Eq. (40) developed in section 4-6:

$$\Delta\nu = -C_4 \Delta(\mu^2)$$

The shifts calculated from this equation are added to the matrix shifts from Table 14, and the results compared with the observed spectra in Table 18.

TABLE 18.

Calculated Shifts* in cm^{-1} for Interactions Between Pairs of HCl Molecules.

Internuclear Distance	Ar calc.	Ar obs.	Kr calc.	Kr obs.	N_2 calc.	N_2 obs.
r	-89	-67.5	-88.5	-84.5	-92.5	-
$\sqrt{2}$ r	-40	-	-51	-	-67	-
$\sqrt{3}$ r	-28	-21.5	-41	-30.5	-59.5	-42.5
2 r	-23	-17	-36.5	-	-56.5	-

*These shifts include the matrix shifts from Table 14.

In the case of interactions between solute molecules in sites other than nearest neighbour sites, the observed shifts will be less than predicted in Table 18, because screening by the matrix atoms will tend to reduce the intermolecular forces. With this in mind, the agreement between observed and calculated shifts in Table 18 is remarkably good. It is also significant that in the case of HCl in nitrogen, no peak is found near 2790 cm^{-1}, the predicted frequency for HCl molecules in nearest neighbour sites in this matrix. The only observed peak corresponds to the statistically favourable second nearest neighbour pair. These observations are compatible with the higher thermal conductivity and smaller heat of sublimation (see Appendix 1) of nitrogen at 4°K compared with the rare gases, since if diffusion is minimized a statistical distribution of solute molecules in the lattice would

be expected.

Peaks at frequencies lower than the "nearest neighbour" frequency must be due to interactions between three or more solute molecules. Many of these peaks are found only during warm-up (see Figs. 6 and 14) and the others are only found at low matrix to solute ratios (see Figs. 5 and 13).

The effect of solute-solute interaction was also demonstrated in experiments where other solute molecules were added to the gas mixtures. Several new features were introduced into the spectra of HCl and HBr (see Figs. 7 and 15), which can be explained qualitatively on the basis of dipole-dipole interactions between the hydrogen halide and the other solute molecule.

5-6 Matrix Isolation Studies of CO and SO_2.

The observed spectra of CO and SO_2 in the matrix are simpler than the HCl or HBr spectra. In the case of SO_2, the large dimensions of the molecule compared to argon or nitrogen (see Fig. 24) make rotation very unlikely. Shifts of band centres from the gas phase are surprisingly small for these molecules. In the case of SO_2, this could be due to the balancing of repulsive and attractive forces, with a small net effect, as was found for HBr in argon. CO, on the other hand, has a very small dipole moment and a smaller polarizability than the hydrogen halides, thus interactions with the matrix are expected to be less.

On spatial grounds, CO should be able to rotate in an

argon matrix. Nevertheless, it is difficult to correlate the observed matrix spectrum with the gas phase vibration-rotation spectrum. It is interesting to note that a calculation by Ewing (72) predicts a Q branch in the vibration-hindered rotation spectrum of liquid CO. If Ewing's theory could be carried over into the present matrix situation, the very strong peak at 2138.5 cm^{-1} could be assigned to an unresolved triplet due to the P(1), Q(0) and R(0) transitions. The peak at 2152 cm^{-1} would then be assigned to R(1). However, it is very doubtful that such an explanation could be correct. The rotational constant for CO is about 2 cm^{-1} (40) and the expected separation of P(1) and Q(0) or Q(0) and R(0) would be approximately 4 cm^{-1}. The 112 G spectrometer should be capable of resolving these peaks, whereas the 2138.5 cm^{-1} peak was unresolved. Furthermore, no violation of the $\Delta J = \pm 1$ selection rule is expected in the matrix environment (69).

The very weak peaks at 2115 and 2091 cm^{-1} are undoubtedly due to isotopic CO molecules (19). In the spectrum of CO perturbed by HCl (see Fig. 17), if we assign the peak at 2065 cm^{-1} to CO molecules interacting with HCl molecules in nearest neighbour sites, then the change in dipole moment of CO during a vibrational transition may be calculated from Eq. (41):

$$\Delta\nu = -C_4 \mu_b \Delta\mu_a$$

The calculated value for $\Delta\mu_a$ is 0.38D which is of the same order of magnitude as that estimated for HCl in the matrix in section 5-3.

In the gas phase spectrum of SO_2 the band centres are at

1151.4 cm^{-1} and 1361.8 cm^{-1} for ν_1 and ν_3 respectively (44). The shifts in the nitrogen matrix for ν_1 and ν_3 were + 1.2 cm^{-1} and -10 cm^{-1}, and in argon, -1.7 cm^{-1} and -8.3 cm^{-1} respectively. These shifts are small compared with the gas-solid shifts of -8 cm^{-1} and -46 cm^{-1} for these bands. It may be noted also that the gas-solid shifts are much smaller for SO_2 than for HCl or HBr, because there is no hydrogen bonding in solid SO_2.

Rotation of the SO_2 molecule is unlikely on spatial grounds, and the appearance of the matrix spectrum supports this conclusion. The SO_2 molecule has rotational constants: A = 2.03 cm^{-1}, B = 0.34 cm^{-1} and C = 0.29 cm^{-1} (73). It is therefore a nearly prolate symmetric top with asymmetry parameter K = -0.94. Using the formulae given in reference (68) the lower rotational levels were calculated and are tabulated in Table 19 together with relative populations at 5°, 10°, and 20°K.

At 5 K, all levels up to 3-1 are appreciably populated, and at 10°K, higher levels will also be important. Thus, the rotation-vibration bands even at 5°K would be very complex, consisting of several groups of unresolved lines. The simple appearance of the spectrum of SO_2 in argon and nitrogen matrices, therefore, indicates that rotation of the trapped molecule does not occur.

It is interesting to note that in the argon matrix both the ν_1 and ν_3 bands consist of strong doublets, while in nitrogen, the main feature in each of these bands is a single strong peak. One might put forward an explanation analogous to inversion doubling (74) based on the following argument.

TABLE 19.

Rotational Energy Levels of the SO_2 Molecule.

J_τ	cm^{-1}	Populations Relative to 0_0		
		5°K	10°K	20°K
0_0	0.00	1	1	1
1-1	0.64	.84	.91	.96
1_0	2.32	.51	.72	.84
1_1	2.37	.51	.71	.84
2-2	1.63	.63	.79	.89
2-1	3.55	.36	.60	.78
2_0	3.70	.35	.59	.77
2_1	8.75	.08	.28	.52
2_2	9.03	.07	.27	.52
3-3	3.77	.34	.58	.76
3-2	5.34	.21	.46	.68
3-1	5.65	.20	.44	.67
3_0	10.63	.05	.21	.46
3_1	10.65	.05	.21	.46
3_2	19.22	.004	.06	.25
3_3	19.21	.004	.06	.25

Assuming that the SO_2 molecule is prevented from rotating by the surrounding matrix atoms, then the molecule can only execute vibrations in an equilibrium position in the cavity. If the sulphur atom passes between the oxygen atoms to an equivalent position on the other side, an inverted configuration is obtained. This situation could not occur in the free molecule because the equivalent position could be obtained by a simple rotation. The two equilibrium positions may be described mathematically by a double minimum potential, which gives rise to a doubling of the vibrational energy levels of the molecule (74). This phenomenon has been observed for the ammonia molecule in the gas phase, and more recently it has been suggested that inversion doubling may occur in solid phosphine (75).

The splitting in the ground state is very small, but as the energy levels approach the barrier height the separation increases rapidly (74). Thus, if the observed splittings for ν_1 and ν_3 of SO_2 are due to the type of inversion doubling described above, then the splittings for the overtones $2\nu_1$ and $2\nu_3$ should be much larger. Also, it is expected that the bending mode ν_2 should exhibit greater splitting (74). Unfortunately, it was not possible to study these bands in the present work because the overtones are too weak, and the region of the bending mode was inaccessible.

Arguments against the above explanation are: the absence of doubling in nitrogen, and the large reduced mass of SO_2, which would be expected to limit the splittings to very small values, unless the barrier to inversion was low (74). In view of this,

the observed splittings of 4.8 cm^{-1} for ν_1 and 4.2 cm^{-1} for ν_3 would appear to be too large to arise from inversion doubling.

Another explanation involving multiple trapping sites could be considered. Harvey and Ogilvie (76) in their work on formaldehyde in an argon matrix, suggested that the formaldehyde molecule could be trapped in a substitutional site, or in larger holes in which two or three argon atoms were displaced. Applying this suggestion to the SO_2/argon spectrum, one can account for the doublets observed for the ν_1 and ν_3 bands.

5-7 Gas Hydrates.

The hydrates studied in the present work have the composition $M \cdot 6H_2O$ and have been classified as type I hydrates by von Stackelberg (21). In these compounds the hydrate former M is trapped in hydrogen bonded cages of water molecules. The structure of the type I gas hydrates has been worked out by von Stackelberg (21), Pauling and Marsh (77) and Claussen (78), and is illustrated in Fig. 25.

Two types of cages are formed in the type I hydrates, pentagonal dodecahedra enclosing nearly spherical cavities of diameter 5.1 A, and tetrakaidecahedra enclosing slightly oblate cavities of diameter 5.8 A (79). These cavities should be large enough to allow rotation of small molecules, and X-ray diffraction data (21,77) for SO_2, H_2S and Cl_2 could be interpreted as indicating free rotation of these molecules in the cages.

The physical properties of some of these compounds are listed in Table 20.

TABLE 20.

Properties of Some Gas Hydrates.

M	M.P. of M °C	diss. press. atm. at 0°C	decomp. temp. °C at latm.
Ar	-190	105	-42.8
Kr	-152	14.5	-27.8
Xe	-107	1.5	- 3.4
Cl_2	- 34	0.33	9.6
H_2S	- 60	0.96	0.35
SO_2	- 10	0.39	7.0

Discussion of the spectra of the gas hydrates can be considered in two parts. The spectrum of the skeletal water vibrations, and the spectrum of the hydrate former (where it exists).

The skeletal water spectrum has several points of interest. In the SO_2 hydrate, the librational frequency of H_2O is shifted by -40 cm^{-1}, while the peak at 1600 cm^{-1} in ice is shifted in the opposite direction by 40 cm^{-1}, confirming its assignment to ν_2 rather than $2\nu_R$, as has been suggested (80). The peak at 2230 cm^{-1} in ice, usually assigned to $\nu_2 + \nu_R$, has almost the same frequency in the hydrate, in agreement with the above conclusion.

A new feature in the skeletal water spectrum at 2410 cm^{-1} is observed in all the hydrates studied in this work. This may

fig 25.

STRUCTURE OF TYPE I GAS HYDRATES

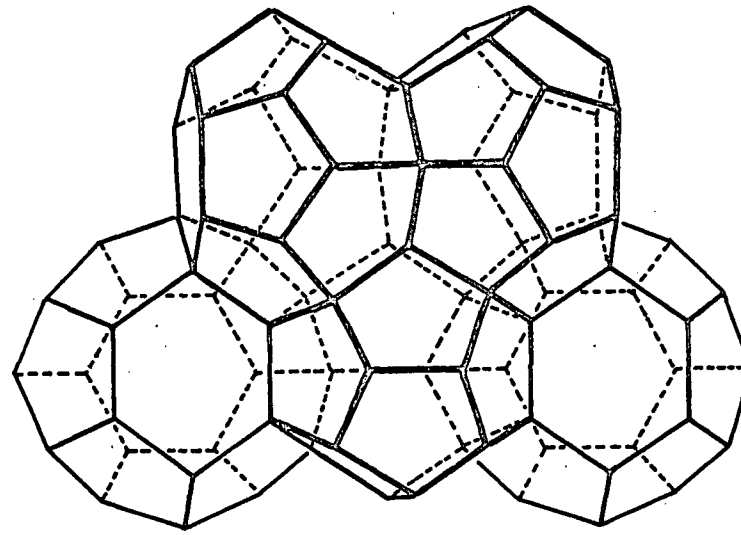

a. A portion of the hydrogen-bond framework, oxygen atoms are at the corners of tetrakaidecahedra and dodecahedra.

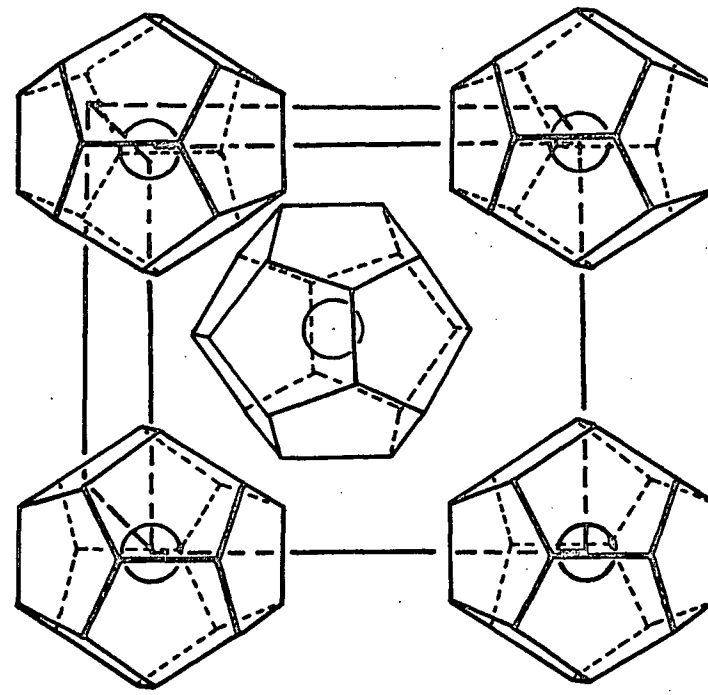

b. The arrangement of the dodecahedra in the gas hydrate crystal. The open circles denote centres of cavities.

be a second component of the combination band $\nu_2 + \nu_R$. The shift of the librational frequency in the SO_2 hydrate precludes the possibility that the new peak is an overtone of ν_R .

The SO_2 peaks in the hydrate are generally broader than in the solid (see Fig. 19) which may be due to unresolved rotational structure or intermolecular forces. The splitting of peaks observed in solid SO_2 is not found in the hydrate, since the SO_2 molecules are isolated in this environment and crystal effects (81) are absent. The weak peak at 1035 cm^{-1} is assigned to $2\nu_2$. This overtone peak was not reported in previous work on solid SO_2 (82,83).

An anealed deposit of SO_2 hydrate was studied over the temperature range 4°-120°K. In Fig. 20, the ν_3 peak was seen to have two shoulders at 120°K spaced at 6.5 cm^{-1} above and below the principal peak at 1342.5 cm^{-1}. The intensity of the low frequency shoulder decreases as the temperature is lowered. This observation is explained by a sum and differences of the ν_3 fundamental with a rotatory or translatory lattice mode, the decrease in intensity of the difference peak with lowering of the temperature would result from depopulation of the upper level in the ground state.

It might be interesting to examine the spectrum of the SO_2-hydroquinone clathrate compound (84) since the cavity size is much smaller (79) than in the case of the hydrate, and motion of the SO_2 molecule would be even more restricted than it appears to be in the SO_2 hydrate.

5-8 Conclusions.

It is concluded that hydrogen halide molecules isolated in solid rare gases and nitrogen are able to execute hindered rotations. At the same time, the vibrational potential function of the solute molecule is perturbed by interactions with the surrounding matrix. It has been possible to correlate the shift of the vibrational frequency with various intermolecular forces and it was found that the repulsive forces play an important role in determining the magnitude and direction of the shift.

Thus, the main features of the matrix spectra of HCl and HBr may be interpreted as a vibration-rotation band. Other peaks in the observed spectra are attributed to mutual interactions between clusters of solute molecules in contiguous and other neighbouring sites. At the lowest temperatures, only isolated solute molecules and pairs of solute molecules are present in significant concentrations.

Arguments against rotation of isolated hydrogen halide molecules may be rationalized. In the spectra of HCl and HBr in solid argon, three of the peaks observed were assigned to R(0), R(1) and P(1), but at $4^{\circ}K$ only the R(0) should have an observable intensity. The explanation is probably that the argon matrix warms slightly during the recording of the spectrum, due to poor thermal conductivity of solid argon. The temperature rise allows the $J = 1$ level to become appreciably populated, and thus the R(1) and P(1) transitions are observed. In nitrogen, the R(0) peak predominates and it may be concluded that the temperature in this

matrix remains near 4°K. This is reasonable because solid nitrogen has a higher thermal conductivity than solid argon. A second argument against rotation is the failure to observe changes in relative intensity of peaks in the spectra of HCl and HBr in argon, as the temperature rises during warm-up. The explanation for this may be that diffusion sets in rapidly enough to reduce the concentration of isolated solute molecules before the changes in the vibration-rotation band are observed. This is supported by the warm-up studies on HBr and HCl in nitrogen, where the R(1) and P(1) peaks do increase in intensity relative to R(0) in the early part of the warm-up. The intensities of R(2) and P(2) are negligible below 20°K and are therefore not observed.

It would be interesting to observe the spectra of DCl and DBr under the same conditions as in this work, since the bond lengths, force constants and dipole moments are the same as for HCl and HBr, to a good approximation (85,86). The expected vibrational shifts should be the same for the heavy hydrogen halides as for the normal halides. The vibration-rotation lines, on the other hand, should be closer together since the rotational constants are smaller. There is also the possibility that the R(2) and P(2) transitions could be observed during the early part of a warm-up study. Thus, the matrix spectra of DCl and DBr could provide supporting evidence for the interpretation given in this thesis of the observed spectra of HCl and HBr. It is also possible that further information could be obtained on the causes of the reduced separation of the R(0) and P(1) peaks.

Problems arising from diffusion of solute molecules during deposition can be reduced by using dilute mixtures and forming the deposits slowly. The problem of warming of the sample by the incident radiation could be eliminated by arranging the spectrometer optics so that the infrared beam is dispersed before passing through the sample. By this means, the total intensity of the radiation falling on the deposit will be a fraction of its value in this work.

The observed spectra of CO in argon is generally in good agreement with previous work. However, a different interpretation involving rotation of the CO molecule is put forward. A new peak in the CO spectrum when HCl was added to the gas mixtures is explained on the basis of a dipole-dipole interaction between CO and HCl molecules in nearest neighbour sites.

An interesting difference in the spectrum of SO_2 in argon and nitrogen matrices was found. In the argon matrix both the ν_1 and ν_3 bands consist of strong doublets, while in nitrogen the main feature of each band is a single strong peak. The shifts from the gas phase in both cases were small, from which it is concluded that repulsive and attractive forces are nearly balanced. Two possible explanations for the doubling in the SO_2/argon spectrum have been suggested. The first was based on a type of inversion doubling, arising from restriction of rotational freedom of the trapped molecule. The second explanation involved multiple trapping sites in solid argon in which the SO_2 molecule replaces one or two argon atoms. It would be useful to be able to observe the bending

mode ν_2 of SO_2 in the two matrices. There is a small upward shift of vibrational frequency (+3 cm^{-1}) going from gaseous to solid SO_2, so one would expect little or no shift in the matrix. It would be interesting to see if splitting of the ν_2 peak in the argon matrix occurs. The magnitude of the splitting might give some indication of the origin of the effect since, if inversion doubling occurs, the bending mode is expected to show the greatest splitting (74). Further work with SO_2 in various matrices might provide additional information on intermolecular forces and restriction of rotation.

The work on the gas hydrates has provided confirmation of the assignment of the 1600 cm^{-1} peak in the spectrum of ice, to the bending mode ν_2 . A new peak in the skeletal water spectrum has been observed which may be a second component of the combination mode $\nu_2 + \nu_R$. Evidence for restricted motion of the SO_2 molecule in the hydrate was found from variations with temperature of the spectrum. Further studies on the gas hydrates by infrared spectroscopic methods are contemplated to study the motion of molecules in the cages, and to investigate the origin of the new peak in the water spectrum.

APPENDIX 1.

Physical Properties of Matrix Materials.

Properties		Ar	Kr	N_2	References
melting point	^{o}K	83.9	116.6	63.3	(61)
boiling point	^{o}K	87.5	120.3	77.4	(61)
heat of fusion	cal/mole	284	392	85.3	(87) (88)
heat of vaporization	cal/mole	1555	2162	667	
thermal conductivity	at $5^{o}K$	20	7	50	
milliwatts/cm ^{o}K	at $10^{o}K$	40	15	26	(68) (69)
	at $20^{o}K$	15	10	4	
cell constant	A	5.43	5.71	5.64	(45) (47)
internuclear distance (r)	A	3.83	4.04	3.99	
polarizability	10^{24} cm^3	1.63	2.36	1.76*	(63)
ionization potential	e.v.	15.68	13.93	15.51	(61)

* mean polarizability $\alpha = \frac{1}{3}(\alpha_1 + \alpha_2 + \alpha_3)$

where: $\alpha_1, \alpha_2, \alpha_3$ are the three principal components of the polarizability tensor.

APPENDIX 2.

Properties of Some Diatomic Molecules.

Property	Units	HCl	HBr	CO	References
melting point	^{o}K	161	184.5	66	(61)
boiling point	^{o}K	189.5	206	83	
(gas)	cm^{-1}	2884.5	2558.5	2143	(41)
R(0) (gas)	cm^{-1}	2905	2575	2147	(41)
ionization potential	e.v.	13.8	13.2	14.1	(61)
dipole moment	D	1.085	0.78	0.112	(89)(44)(90)
polarizability* 10^{-24}	cm^3	2.63	3.61	1.95	(63)
molecular dimensions		4.27	4.57	3.73	(91)
	A	3.60	3.90	2.80	
internuclear distance (r) A		1.275	1.42	1.13	(38)(39)(40)

*mean polarizability

BIBLIOGRAPHY

1. E.D. Becker and G.C. Pimentel, J. Chem. Phys. 25, 224 (1956).

2. M. Van Thiel, E.D. Becker and G.C. Pimentel, Ibid., 27, 95, 486 (1957).

3. G.C. Pimentel, M.O. Bulanin and M. Van Thiel, Ibid., 36, 500 (1962).

4. E. Catalano and D.E. Milligan, Ibid., 30, 45 (1959).

5. R.L. Redington and D.E. Milligan, Ibid., 37., 2162 (1962); Ibid., 39, 1276 (1963).

6. D.E. Milligan, R.M. Hexter and K. Dressler, Ibid., 34, 1009 (1961).

7. J.A. Glasel, Ibid., 33, 252 (1960).

8. L.J. Schoen, D.E. Mann, C. Knobler and D. White, Ibid., 37, 1146, (1962).

9. A. Maki, Ibid., 35, 931 (1961).

10. H.F. Shurvell, M.Sc. Thesis, U.B.C. (1962).

11. W. H. Flygare, J. Chem. Phys. 39, 2263 (1963).

12. R.L. Armstrong, Ibid., 36, 2429 (1962).

13. A.F. Devonshire, Proc. Roy. Soc. (London) A 153, 601 (1963).

14. L. Pauling, Phys. Rev. 36, 430 (1930).

15. W. West and R. T. Edwards, J. Chem. Phys. 5, 14 (1937).

16. E. Bauer and M. Magat, J. Phys. rad. 9, 319 (1938); Physica, 5, 718 (1938).

17. A.D.E. Pullin, Spectrochimica Acta, 13, 125 (1958).

18. A.D. Buckingham, Proc. Roy. Soc. (London), A 248, 169 (1958).

19. G.E. Ewing and G.C. Pimentel, J. Chem. Phys. 35, 925 (1961).

20. M.J. Linevsky, Ibid., 34, 507 (1961).

21. M. von Stackelberg et al, Z. Electrochem. 58, 25, 40, 99, 104, 162 (1954).

22. F. McCourt, B.Sc. Thesis, U.B.C. (1962).

23. G.C. Turrell, H. Vu and B. Vodar, J. Chem. Phys. 33, 315 (1960).

24. D.H. Rank, B.S. Rao and T.A. Wiggins, Ibid., 37, 2511 (1962).

25. A. Ben-Reuven, S. Kimel, M.A. Hirshfeld and J.A. Jaffe, Ibid., 35, 955 (1961).

26. J. Kwok and G.W. Robinson, Ibid., 36, 3137 (1962).

27. J. Lascombe, P.V. Huong and M.L. Josien, Bull. Soc. Chim., France, 1175 (1959).

28. M.O. Bulanin and N.D. Orlova, Optika i Spectroskopiya, 4, 569, (1958).

29. N.J. Jones and N. Sheppard, Trans. Far. Soc. 56, 625 (1960).

30. H. Vu, M.R. Atwood and B. Vodar, J. Chem. Phys., 38, 2671 (1963).

31. H. Vu, M.R. Atwood and B. Vodar, Intern. Symp. Mol. Struct. Specty. Tokyo, Japan (1962).

32. D.F. Hornig and W.E. Osberg, J. Chem. Phys. 23, 662 (1955).

33. D.F. Hornig and G.L. Hiebert, Ibid., 27, 752 (1957).

34. E. Whittle, D.A. Dows, and G.C. Pimentel, Ibid., 22, 1943 (1954).

35. A.M. Bass and H.P. Broida, "Formation and Trapping of Free Radicals", Academic Press, N.Y. (1960).

36. W.H. Duerig and I.L. Mador, Rev. Sci. Instr. 23, 421 (1952).

37. B.J. Fontana, J. Appl. Phys. 29, 668 (1958).

38. E.K. Plyler and E.D. Tidwell, Z. Electrochem. 64, 717 (1960).

39. E.K. Plyler, J. Res. Natl. Bur. Stand., 64A, 377 (1960).

40. E.K. Plyler, J. Opt. Soc. Am., 45, 102 (1955).

41. "Tables of Wave Numbers for the Calibration of Infrared Spectrometers", Butterworths, London (1961).

42. E.H. Siegler, Engineering report no. 563, Perkin-Elmer Corpn., Norwalk (1959).

43. J.M. Roche, Engineering report no. 601, Perkin-Elmer Corpn., Norwalk (1962).

44. R.D. Shelton, A.H. Nielsen and W.H. Fletcher, J. Chem. Phys. 21, 2178 (1953).

45. J.O. Hirschfelder, C.F. Curtiss and R.B. Bird, "Molecular Theory of Gases and Liquids", John Wiley & Sons, New York (1954).

46. R.G. Wyckoff, "Crystal Structures", Interscience Publishers, New York (1948), Vol. 1.

47. J.E. Lennard-Jones and A.E. Ingham, Proc. Roy. Soc. A 107, 636 (1925).

48. L.H. Bolz, M.E. Boyd, F.A. Mauer and H.S. Pieser, Acta Cryst. 12, 247 (1959).

49. R.F. Snider - Private Communication.

50. K.S. Pitzer, "Quantum Chemistry", Prentice-Hall, Englewood Cliffs, N.J. (1953).

51. L. Pauling and E.B. Wilson, Jr., "Introduction to Quantum Mechanics", McGraw-Hill, New York (1935).

52. G. Petit Bois, "Tables of Indefinite Integrals", Dover, New York, (1961).

53. K.B. Harvey, J.R. Henderson and H.F. Shurvell, Can. J. Chem. 42, (1964).

54. D.F. Hornig and W.E. Osberg, J. Chem. Phys. 23, 662 (1955).

55. D.F. Hornig and G.L. Hiebert, Ibid., 27, 752 (1957).

56. G.L. Hiebert and D.F. Hornig, Ibid., 28, 316 (1958).

57. R.E. Behringer, Ibid., 29, 537 (1958).

58. A. Maki and J.C. Decius, Ibid., 31, 772 (1959).

59. J. van der Elsken, Ph.D. Thesis, University of Amsterdam (1959).

60. J. L Bryant and G.C. Turrell, J. Chem. Phys. 37, 1069 (1962).

61. W.S. Benedict, R. Herman, G.E. Moore and S. Silverman, Ibid., 26, 1671 (1957).

62. H.B. Friedrich and W.B. Person, J. Chem. Phys. 39, 811 (1963).

63. "Handbook of Chemistry", 44th Ed. (1962-63), Chemical Rubber Publishing Co., Cleveland, Ohio.

64. E.J. Stansbury, M.F. Crawford and H.L. Welsh, Can. J. Phys. 31, 954 (1953).

65. "Landolt-Bornstein Tables", Springer-Verlag, Berlin 1950, Vol. 1.

66. A. Ben-Reuven, S. Kimel, M.A. Hirshfeld and J.H. Jaffe, J. Chem. Phys. 35, 955 (1961).

67. H.A. Gebbie and N.W.B. Stone, Proc. Phys. Soc. 82, 309 (1963).

68. G.M. Barrow, "Introduction to Molecular Spectroscopy", McGraw-Hill, New York (1962).

69. J.A.R. Coope - Private Communication.

70. G.K. White and S.B. Woods, Phil May 3, 785 (1958).

71. H.M. Roder, Cryogenics 2, 302 (1962).

72. G.E. Ewing, J. Chem. Phys. 37, 2250 (1962).

73. M.H. Sirvetz, Ibid., 19, 938 (1951).

74. G. Herzberg, "Infrared and Raman Spectra", Van Nostrand, Princeton, N.J., (1945).

75. A.H. Hardin and K.B. Harvey, Can. J. Chem. 42, 84 (1964).

76. K.B. Harvey and J.F. Ogilvie, Ibid., 40, 85 (1962).

77. L. Pauling and R.E. Marsh, Proc. Nat. Acad. Sci., 38, 112 (1952).

78. W.F. Claussen, J. Chem. Phys. 19, 259, 662, 1425 (1951).

79. J.H. van der Waals and J.C. Platteeuw, "Advances in Chemical Physics", Interscience, New York (1959), vol. 2, p.1.

80. D.F. Hornig, H.F. White and F.P. Reding, Spectrochimica Acta 12, 338 (1958).

81. W. Vedder and D.F. Hornig, "Advances in Spectroscopy", Interscience, New York (1961), Vol. 2, p.189.

82. P.A. Giguère and M. Falk, Can. J. Chem. 34, 1833 (1956).

83. R.N. Wiener and E.R. Nixon, J. Chem. Phys. 25, 175 (1956).

84. D.E. Palin and H.M. Powell, J. Chem. Soc. 208, (1947).

85. E.B. Wilson, J.C. Decius and P.C. Cross, "Molecular Vibrations", McGraw-Hill, New York (1955).

86. G. Herzberg, "Spectra of Diatomic Molecules", Van Nostrand, Princeton, N.J. (1950).

87. P. Flubacher, A.J. Leadbetter and J.A. Morrison, Proc. Phys. Soc. 78, 1449 (1961).

88. R.H. Beaumont, H. Chihara and J.A. Morrison, Ibid., 78, 1462 (1962).

89. R.P. Bell and I.E. Coop, Trans. Faraday Soc. 34, 1209 (1938).

90. C.A. Burrus, J. Chem. Phys. 28, 427 (1958).

91. L. Pauling, "The Nature of the Chemical Bond", Cornell, Ithaca, N.Y. (1960).